BRNO UNIVERSITY OF TECHNOLOGY

VYSOKÉ UČENÍ TECHNICKÉ V BRNĚ

FACULTY OF MECHANICAL ENGINEERING

FAKULTA STROJNÍHO INŽENÝRSTVÍ

INSTITUTE OF MATERIALS SCIENCE AND ENGINEERING

ÚSTAV MATERIÁLOVÝCH VĚD A INŽENÝRSTVÍ

DEVELOPMENT OF CERAMIC FILTER EQUIPMENT FOR ELECTRO-INSULATING LIQUIDS

VÝVOJ KERAMICKÉHO FILTRAČNÍHO ZAŘÍZENÍ PRO ELEKTROIZOLAČNÍ KAPALINY

MASTER'S THESIS

DIPLOMOVÁ PRÁCE

AUTHOR Bc. Tereza Havlíková

AUTOR PRÁCE

SUPERVISOR prof. RNDr. Karel Maca, Dr.

VEDOUCÍ PRÁCE

BRNO 2024

BRNO UNIVERSITY OF TECHNOLOGY FACULTY OF MECHANICAL ENGINEERING

Assignment Master's Thesis

Institut:	Institute of Materials Science and Engineering
Student:	**Bc. Tereza Havlíková**
Degree programm:	Materials Engineering
Branch:	no specialisation
Supervisor:	**prof. RNDr. Karel Maca, Dr.**
Academic year:	2023/24

As provided for by the Act No. 111/98 Coll. on higher education institutions and the BUT Study and Examination Regulations, the director of the Institute hereby assigns the following topic of Master's Thesis:

Development of ceramic filter equipment for electro–insulating liquids

Brief Description:

The student will prepare a literature review on the topic of different methods of preparing ceramic filters. As part of the experimental work, he/ will learn about selected filter preparation methods (replication method, foaming of ceramic suspension,…) and prepare ceramic filters using them. The prepared filters will be evaluated for their microstructure and filtering capacity.

Master's Thesis goals:

The aim of the work will be to assess the possibility of using ceramic filters for filtering electro–insulating liquids in distribution transformers, and thus replace the paper filters with a short lifespan used up to now. The work will be supported by TAČR project FW06010300.

Recommended bibliography:

1. CHEN, Yu, Nannan WANG, Oluwafunmilola OLA, Yongde XIA a Yanqiu ZHU. Porous ceramics: Light in weight but heavy in energy and environment technologies. Materials Science and Engineering: R: Reports [online]. 2021, 143. ISSN 0927796X. Dostupné z: doi:10.1016/j.mser.2020.100589

2. NAZAROVA, Elena A., Diana S. ALIMOVA, Vasily I. MIKHAYLOV, Elena F. KRIVOSHAPKINA a Pavel V. KRIVOSHAPKIN. Macroporous ceramic filters from mineral raw materials for machine oils filtration. Ceramics International [online]. 2019, 45(7), 8767-8773. ISSN 02728842. Dostupné z: doi:10.1016/j.ceramint.2019.01.201

3. OHJI, T a M FUKUSHIMA. Macro-porous ceramics: processing and properties. International Materials Reviews [online]. 2013, 57(2), 115-131. ISSN 0950-6608. Dostupné z: doi:10.1179/1743280411Y.0000000006

Deadline for submission Master's Thesis is given by the Schedule of the Academic year 2023/24

In Brno,

L. S.

prof. Ing. Ivo Dlouhý, CSc. Director of the Institute	doc. Ing. Jiří Hlinka, Ph.D. FME dean

ABSTRACT

The aim of this master's thesis was to prepare macroporous ceramic filters based on mullite and silica, suitable for the filtration of electro-insulating liquids in distribution transformers. The first part of this thesis is a literature review, which addresses the topic of electro-insulating liquids and their degradation, processing techniques of macroporous ceramics and their use in filtration, including an overview of the materials used. The experimental part describes the preparation of porous filters using two selected methods, the replica template method and direct foaming. Filters prepared with optimised processing parameters were evaluated for phase composition, microstructure and compressive strength. Filters prepared using the replica template method consisted of open interconnected pores ranging from 150 to 350 µm, achieved a porosity of around 80 % and compressive strength up to 2.4 MPa. Ceramic foams obtained using direct foaming achieved a porosity of 68–73 % and open interconnected pores up to 100 µm. Due to the requirements of the filtration equipment, the dimensions of the filters had to be scaled up. Direct foaming was found to be unsuitable for the large-scale preparation of filters, however, filters prepared by the replica template method were successfully scaled up and are ready for the testing of their filtration capacity. These filters with open interconnected pores, unimodal pore size distribution and sufficient mechanical strength are potential candidates for use in the first stage of filtration of electro-insulating liquids, offering a more sustainable alternative to the currently used paper filters.

Key words
macroporous ceramics, ceramic filters, mullite, silica, replica template method, direct foaming, electro-insulating liquid

ROZŠÍŘENÝ ABSTRAKT

V rámci této diplomové práce byla studována příprava makroporézních keramických filtrů na bázi mullitu a oxidu křemičitého, za účelem jejich potenciálního využití pro filtraci elektroizolačních kapalin v distribučních transformátorech.

Elektroizolační kapalina je důležitou součástí distribučního transformátoru, zajišťující jeho chlazení a izolaci. Během provozu se v ní však mohou hromadit nečistoty, které degradují její izolační schopnost a snižují životnost transformátoru. Proto je nutné elektroizolační kapalinu pravidelně čistit, k čemuž se dnes běžně využívají jednorázové papírové filtry. Tyto filtry ale mohou být samy zdrojem kontaminace v podobě celulózových vláken a produkují odpad po každém provedeném filtračním cyklu. Z tohoto důvodu lze uvažovat o jejich nahrazení odolnější a udržitelnější alternativou.

Jako vhodný kandidát se nabízejí keramické filtry, které jsou v dnešní době hojně využívány díky své chemické odolnosti, tepelné stabilitě či otěruvzdornosti. Mezi jejich nepopiratelné výhody patří také možnost jejich regenerace pomocí mechanického a chemického čištění či opětovné použití materiálu po vyřazení filtru z funkce, což významně přispívá k jejich udržitelnosti.

Mezi hlavní technologie přípravy porézních keramických pěn využitelných pro filtraci se řadí částečné slinování, metoda obětované šablony, replikační metoda, přímé pěnění a aditivní technologie, lišící se od sebe především dosažitelnou porozitou, charakterem a velikostí pórů. Při volbě materiálu se bere ohled na konkrétní podmínky filtrace. Pro nízkoteplotní

aplikace se běžně využívají filtry z oxidu hlinitého, oxidu křemičitého nebo mullitu. Vzhledem k relativně vysoké ceně pokročilých keramických materiálu se výzkum zaměřuje i na přípravu filtrů z levnějších přírodních alternativ nebo keramického odpadu.

V rámci experimentální části této diplomové práce byly připraveny keramické filtry pomocí dvou metod, replikační metody a přímého pěnění. Pro zajištění konkurenceschopnosti připraveného filtru původnímu papírovému filtru byl jako výchozí keramický materiál zvolen Molochite^{TM}, relativně levný keramický prášek na bázi mullitu a oxidu křemičitého vzniklý kalcinací kaolinu. Příprava filtrů byla optimalizována vzhledem k požadované otevřené porézní struktuře a dostatečné pevnosti. Filtry byly v první fázi hodnoceny z pohledu jejich fázového složení a mikrostruktury, u vybraných vzorků byla také testována jejich mechanická pevnost v tlaku.

Příprava filtrů pomocí replikační metody spočívala v impregnaci retikulované polymerní pěny na bázi polyuretanu keramickou suspenzí obsahující 63 hm.% keramického prášku v koloidním roztoku oxidu křemičitého. Finální porézní struktura, získána vypálením polymerní šablony a slinutím na 1400 °C, vykazovala stejnou morfologii jako původní pěna. Byla tvořena otevřenými, vzájemně propojenými póry o velikosti 150–350 µm, s průměrnou porozitou 80 % a pevností v tlaku až 2,4 MPa. Z hlediska fázového složení byl hlavní fází mullit, doplněný oxidem křemičitým ve formě cristobalitu v zastoupení přibližně 7 %. Jednou z hlavních limitací porézní keramiky připravené pomocí replikační metody je přítomnost dutých trámců vzniklých vypalováním polymerní šablony, snižujících její mechanickou pevnost. Část filtrů tak byla infiltrována suspenzí bohatou na oxid křemičitý za účelem vyplnění těchto dutin. Ačkoliv byla infiltrací snížena celková porozita filtrů i velikost pórů, došlo ke snížení jejich mechanické pevnosti, pravděpodobně v důsledku zvýšeného podílu oxidu křemičitého ve formě cristobalitu.

Druhou studovanou metodou bylo přímé pěnění, které spočívá v inkorporaci keramického materiálu přímo do polyuretanové pěny vzniklé *in situ* reakcí mezi diisokyanátem a polyolem. Keramické pěny získané vypálením organických složek z kompozitní pěny a slinutím na 1400 °C vykazovaly porozitu 68–73 % a otevřené póry o velikosti až 100 µm.

Vzorky připravené v laboratorním měřítku bylo nutné zvětšit na rozměry dané pouzdrem, ve kterém je filtr při procesu filtrace uložen (válec o průměru 100 mm a výšce 100 mm). Filtry připravené přímým pěněním se vzhledem k obtížnému řízení jejich finální struktury ukázaly jako nevhodné pro výrobu ve větším měřítku. Filtry připravené replikační metodou byly úspěšně zvětšeny na požadovanou velikost, a jsou připravené k testování jejich filtrační schopnosti. Díky jejich struktuře s otevřenými, vzájemně propojenými póry, unimodální distribuci velikosti pórů a dostatečné mechanické pevnosti se připravené filtry zdají být vhodnými kandidáty pro potenciální využití v prvním stupni filtrace elektroizolačních kapalin za účelem odstranění hrubých nečistot z kontaminované kapaliny.

Klíčová slova
makroporézní keramika, keramické filtry, mullit, oxid křemičitý, replikační metoda, přímé pěnění, elektroizolační kapalina

BIBLIOGRAPHIC CITATION

HAVLÍKOVÁ, Tereza. *Development of ceramic filter equipment for electro-insulating liquids*. Brno, 2024. Available also at: https://www.vut.cz/studenti/zav-prace/detail/157480. Master's Thesis. Brno University of Technology, Faculty of Mechanical Engineering, Institute of Materials Science and Engineering. Supervisor Karel Maca.

BIBLIOGRAFICKÁ CITACE

HAVLÍKOVÁ, Tereza. *Vývoj keramického filtračního zařízení pro elektroizolační kapaliny.* Brno, 2024. Dostupné také z: https://www.vut.cz/studenti/zav-prace/detail/157480. Diplomová práce. Vysoké učení technické v Brně, Fakulta strojního inženýrství, Ústav materiálových věd a inženýrství. Vedoucí práce Karel Maca.

DECLARATION

I hereby declare that I have written this master's thesis entitled "Development of ceramic filter equipment for electro-insulating liquids" on my own, according to the objectives set by my supervisor prof. RNDr. Karel Maca, Dr., using the literature sources listed in the references.

Brno, 24th of May 2024

……..

Bc. Tereza Havlíková

ACKNOWLEDGEMENTS

First, I would like to express my gratitude to my supervisor, prof. RNDr. Karel Maca, Dr., for his advice and patience during the work on this thesis. I would also like to thank Ing. Lenka Novotná, Ph.D., for her assistance in the experimental work and her valuable advice throughout our entire collaboration. My gratitude also extends to Ing. Zdeněk Chlup, Ph.D. from IPM ASCR, for the measurement of mechanical properties, as well as to other employees of CEITEC BUT for their help with the analysis of the samples, namely Ing. Daniel Drdlík, Ph.D., for the SEM and XRD analysis, Ing. Přemysl Šťastný, Ph.D., for the TG analysis and Ing. Zdenka Skálová, for the porosimetry analysis.

This work was carried out with the support of the research infrastructure CzechNanoLab (ID LM2023051, MŠMT, 2023-2026), CEITEC BUT, and with the support of project TAČR FW06010300.

CONTENT

1 INTRODUCTION 11
2 LITERATURE REVIEW 12
2.1 Insulating oil in distribution transformer 12
2.1.1 Deterioration of insulating oil 12
2.1.2 Maintenance of insulating oil 12
2.2 Macroporous ceramics 14
2.3 Processing techniques for macroporous ceramic foams 15
2.3.1 Partial sintering 15
2.3.2 Sacrificial template method 16
2.3.3 Replica template method 17
2.3.4 Direct foaming 20
2.3.5 Additive manufacturing 22
2.4 Application of macroporous ceramics in filtration 23
2.4.1 Hot gas filters 24
2.4.2 Molten metal filters 25
2.4.3 Water filters 26
2.4.4 Oil filters 26
2.5 Ceramic materials used in filtration 27
2.5.1 Alumina 27
2.5.2 Silica 28
2.5.3 Mullite 28
2.5.4 Kaolin clay 29
3 AIMS OF THE EXPERIMENTAL PART 30
4 EXPERIMENTAL PART 31
4.1 Materials 31
4.1.1 Replica template method 31
4.1.2 Direct foaming 31
4.2 Methodology 31
4.2.1 Replica template method 31
4.2.2 Direct foaming 34
4.3 Characterisation of powders and foams 36
4.3.1 Particle size distribution 36
4.3.2 Thermogravimetric analysis 36
4.3.3 Phase composition 36
4.3.4 Microstructure analysis 36
4.3.5 Compressive strength 38
4.3.6 Filtration capacity 39

5 REPLICA TEMPLATE METHOD – RESULTS AND DISCUSSION 41
5.1 Optimisation of processing parameters 41
5.1.1 Preparation of the suspension 41
5.1.2 Impregnation of PU foams with the suspension 43
5.1.3 Heat treatment 44
5.1.4 Filling the hollow struts by infiltration 47
5.1.5 Scale up 48
5.2 Characterisation of filters 49
5.2.1 Phase composition 49
5.2.2 Microstructure analysis 50
5.2.3 Compressive strength 53
5.2.4 Filtration capacity 55
6 DIRECT FOAMING – RESULTS AND DISCUSSION 57
6.1 Optimisation of processing parameters 57
6.1.1 Composite foams composition 57
6.1.2 Composite foams processing 59
6.1.3 Heat treatment 60
6.1.4 Scale up 61
6.2 Characterisation of filters 62
6.2.1 Phase composition 62
6.2.2 Microstructure analysis 63
7 CONCLUSION 66

1 INTRODUCTION

The global market for electric vehicles is growing every year and this trend is expected to continue even further. In 2023, over 250 000 electric cars were sold worldwide each week, which is more than the annual total a decade ago [1]. This growth is driven by many countries adopting policies to switch to zero-emission vehicles and ban fossil fuels. Among the various challenges associated with the transition to electro-mobility, a key factor is to provide a reliable electrical distribution infrastructure.

The distribution transformer is an integral part of power conversion and transmission systems. The presence of an electro-insulating liquid, which acts both as a coolant and an insulant, is essential to ensure its good operation. However, during service, humidity and contaminants can accumulate in the liquid, reducing its insulating and cooling properties. This can lead to a failure of the transformer or a significant shortening of its lifetime. Therefore, the electro-insulating oil needs to be regularly purified. Currently, disposable paper filters are used for this purpose, raising concerns about the sustainability and environmental impact of this solution.

Ceramic filters are nowadays being used more and more often due to their unique properties and durability in harsh conditions. Porous ceramics can achieve porosity of up to 96 % and contain pores ranging in size from 3 nm to 3 mm [2], enabling their use in a wide range of different filtration processes. Another big advantage of ceramic filters is the possibility of their repeated use thanks to regeneration and possible reuse of the material at the end of their service life. The use of macroporous ceramics for filtration and purification presents great potential for sustainable development and environmental applications, as presented in recent reviews by Chen et al. [2] and Fukushima et al. [3]. Nevertheless, a common limitation of the implementation of ceramic filters in operation is their higher cost. In reaction to this, more researchers have recently been exploring the possibility of preparing them from cheaper alternatives, such as kaolin clay, dolomite or fly ash [4].

The aim of this thesis is to assess the possibility of employing ceramic filters for the filtration of electro-insulating liquids in distribution transformers and thus offer an alternative to the paper filters with a short lifespan used to date. The work is divided into two parts, a theoretical part and an experimental part. The theoretical part includes a literature review that first addresses the topic of electro-insulating oils and their degradation, followed by the processing techniques of macroporous ceramics and their use in filtration, including an overview of ceramic materials used. The experimental part of the work focuses on the preparation of filters from a relatively low-cost kaolin-based ceramic material, using two different processing methods. Porous ceramics prepared by the replica template method and direct foaming were analysed in terms of their phase composition, microstructure and compressive strength. Finally, they were evaluated for their suitability for use in filtration of electro-insulating liquids based on the determined properties.

2 LITERATURE REVIEW

2.1 Insulating oil in distribution transformer

Most distribution transformers used nowadays are the oil-immersed type, with mineral oil and cellulosic paper being used as the liquid and solid insulation, respectively. The role of insulating liquid is critical for the reliable operation of the transformer, it provides electrical insulation, acts as a cooling medium for heat dissipation and helps to suppress the formation of electric arcs. The liquid should have certain properties, such as high dielectric strength, low viscosity or good oxidation resistance. [5]

Mineral oils have been the most widely used insulating liquid since the 1900s due to their low viscosity, good ageing behaviour and low cost. Nowadays, these are complex blends of more than 3000 hydrocarbons composed mainly of paraffinic, naphthenic and aromatic chains, produced by fractional distillation of crude petroleum. Synthetic oils are used when special properties are required, for instance in transformers with high fire security standards. As examples, halogenated hydrocarbons, high-molecular-weight hydrocarbons, silicone oils or vegetable oils can be cited. [6, 7]

2.1.1 Deterioration of insulating oil

Insulating oil is exposed to thermal, electrical and chemical stresses during its service life, leading to its deterioration over time. Water contamination can originate from residual moisture from production, atmospheric moisture or as a product of ageing of the solid cellulose insulation, which is itself accelerated by the presence of water. Exposure to the atmosphere also causes the oil to undergo oxidation, resulting in colour change of the oil, formation of acidic compounds or precipitation of sludge. In addition, other types of contamination can accumulate in the oil during its service life, for instance, cellulose fibres or metallic particles, which may also be present from manufacturing processes or component wear. The presence of these impurities, especially conductive ones like metal, carbon or wet fibres, can lead to a significant loss of dielectric strength of the oil. [8]

Maintenance of the oil is essential to prevent transformer failure and its overall condition is assessed by conducting physical, chemical and electrical tests on regularly collected samples. Acidity, water content, interfacial tension, dielectric dissipation factor or breakdown voltage are among the most important monitored parameters. The specific requirements vary according to the type of equipment and voltage class. There are no strict limits, but reference values can be found in the literature. [9] When the condition of the oil is found to be unacceptable, it can no longer function reliably and must be replaced or treated to restore its properties [10].

2.1.2 Maintenance of insulating oil

Guidance for the maintenance procedure of insulating oil is covered by standard ČSN EN 60422. Two processes can extend the useful life of service-aged insulating oil by improving its properties. Reconditioning is defined as a „process that eliminates or reduces gases, water and solid particles and contaminants by physical processing only". Reclamation is a „process that eliminates or reduces soluble and insoluble polar contaminants from the oil by chemical and physical processing". The purpose of reconditioning is to improve the dielectric properties of the oil by reducing the content of water and solid particles, while reclamation involves more extensive treatment with the aim of restoring the oil's original properties. [5]

Purification practices that can be included to recondition or reclaim service-aged oil to an acceptable level are summarised in Tab. 1, along with the type of contamination removable by each respective technique.

Tab. 1: Oil purification practices employed during reconditioning or reclamation of insulating oil [10].

Oil purification practices	Type of contamination removed					
	Solids	Free water	Soluble water	Air and gas	Volatile acids	Other
Vacuum dehydrator	x	✓	✓	✓	Most	x
Mechanical filter (blotter or filter press)	✓	Partial	Partial	x	x	x
Centrifuge	✓	✓	x	x	x	x
Coalescing filter	✓	✓	x	x	x	x
Precipitation settling	✓	✓	✓	x	x	x
Contact process	✓	✓	✓	x	✓	✓
Percolation by gravity	✓	✓	Partial	x	✓	✓
Percolation by pressure	✓	✓	Partial	x	✓	✓
Activated carbon sodium silicate process	✓	x	x	x	✓	✓
Trisodium phosphate process	✓	x	x	x	✓	✓

The flow diagram of a typical modern oil treatment plant can be seen in Fig. 1. The most common process used in the industry is reclamation by percolation, typically consisting of three major steps. First, the oil is pumped from the bottom of the transformer, heated and passed through a filter to remove particles and insoluble contamination. Then, the oil is circulated through one or more cartridges filled with fuller's earth or other absorbent material in order to remove soluble polar contaminants. Finally, the oil reaches a reconditioning device (vacuum dehydrator or centrifuge) to remove moisture and gases. The reclamation can be done in multiple passes, usually not less than three until the oil reaches the desired properties. [5]

The filtration system of the oil treatment plant is usually multi-staged and various filters may be included to effectively remove particle contamination [10–12]:

- ***Coarse filter*** is usually used as the first stage, its purpose is to protect the inlet of the plant from potential damage. It retains magnetic particles and larger particles above 1 mm in size.
- ***Blotter or filter press*** consists usually of paper filters held between metallic discs and is suitable for removal of particles bigger than 50 µm.
- ***Cartridge filter*** consists of cylindrical housing containing a disposable filter from hygroscopic material (usually paper). Its purpose is to ensure fine filtration and remove smaller particles of around 1 µm.

A paper filter itself can be a source of additional contamination, as it can release fibres into the oil when reused and therefore it must be regularly changed [8]. Most filters are disposable and once they become clogged, they are thrown away and produce waste [5].

For this reason, replacing them with more sustainable and reusable filters can be considered. The use of macroporous ceramics seems to be a promising solution in the field of filtration and purification in terms of sustainability, as presented in recent reviews by Chen et al. [2] and Fukushima et al. [3].

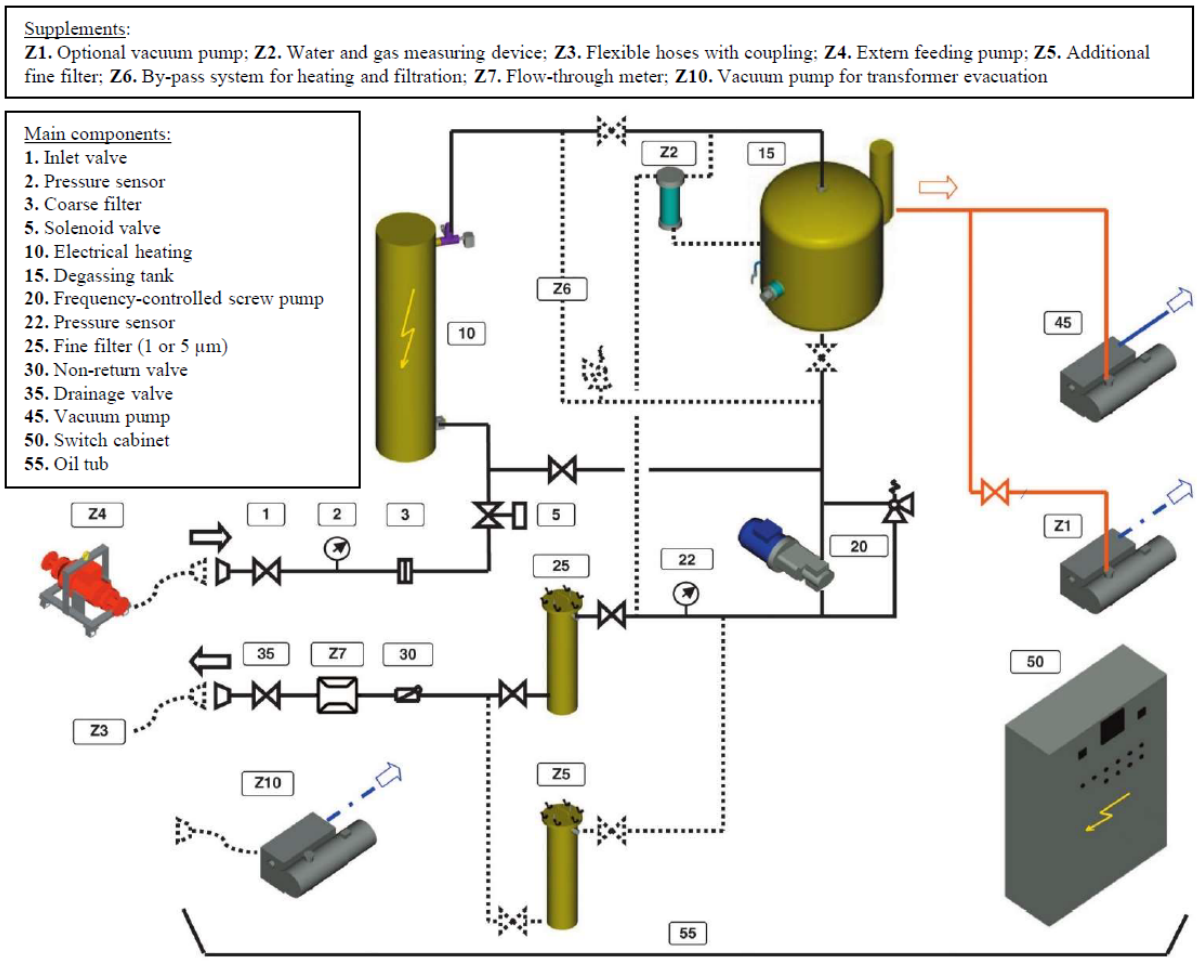

Fig. 1: Flow diagram of a typical modern oil treatment plant [11].

2.2 Macroporous ceramics

For most engineering applications, a high porosity of ceramic materials is undesirable due to inferior mechanical properties, especially brittleness. However, the intentional incorporation of pores may be of interest in some cases because unique properties can be achieved by a suitable combination of their size, shape, distribution and degree of interconnectivity. These materials benefit from the advantages typical for ceramics, for instance, chemical stability, resistance in corrosive environment, stability at high temperatures or wear resistance, whereas an increase in porosity can result in lower density, high specific surface area, low thermal conductivity, permeability or low dielectric constant. Porous ceramics are nowadays widely used as filters, catalyst supports, heat exchangers or scaffolds for biomedical implants. [13]

Conventionally, porous materials can be defined according to their pore size as macroporous ($d > 50$ nm), mesoporous (50 nm $> d >$ 2 nm) and microporous ($d < 2$ nm), where d represents the width of the pore [14]. This terminology, established by the International Union of Pure and Applied Chemistry (IUPAC), was later complemented with additional parameters and experimental techniques used to characterise porous solids, for example, pore size distribution, shape and volume [15]. Solids commonly contain pores in a wider size range and are referred to as materials with hierarchical porosity, which may additionally be graded or oriented [16].

Cellular ceramics are porous ceramics with porosity higher than 60 %. They are composed of cells, which can be classified according to the accessibility to an external fluid as open or closed. Open cells have pores in their walls, also referred to as cell windows, which ensure interconnection between cells and allow the flow of fluids from one cell to another. Therefore, an open-cell structure is suitable for applications involving fluid transport such as filtration. In contrast, a closed-cell structure is composed of polyhedral cells connected via solid faces with no possibility of fluid flow, making it relevant for insulation applications. Cellular ceramics can be defined by their overall morphology and structure, the two most common being honeycombs with prismatic cells and foams composed of randomly oriented cells. [17, 18]

2.3 Processing techniques for macroporous ceramic foams

The choice of processing technique has a great influence on the microstructural features of the foam, such as porosity, interconnectivity of cells, pore size and shape. This consequently affects the mechanical properties and functionality of the material and can be tailored based on a particular application, as shown in Fig. 2. The main methods used to fabricate a macroporous ceramic foam are partial sintering, sacrificial template, replica template, direct foaming and additive manufacturing.

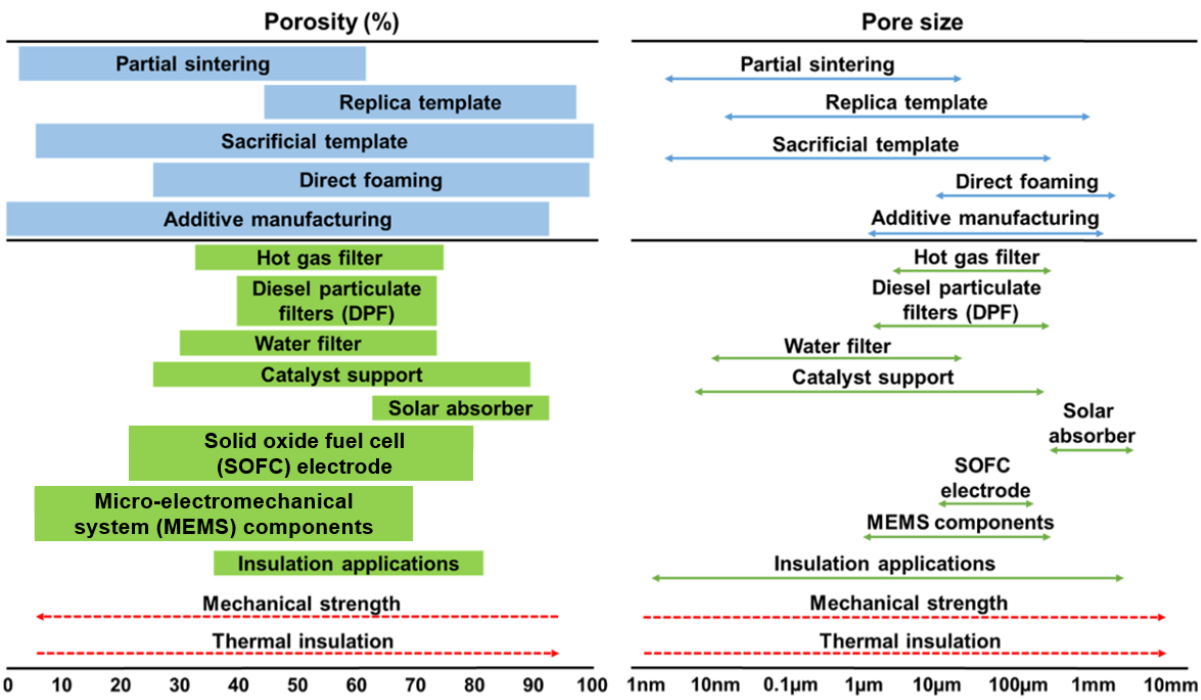

Fig. 2: Processing techniques and applications of porous ceramics according to porosity and pore size [2].

2.3.1 Partial sintering

The simplest method to prepare macroporous ceramic materials is partial sintering (Fig. 3). Cold-pressed powder, otherwise known as green body, is sintered at lower temperatures or for a shorter time than is required to obtain the corresponding fully densified material. At elevated temperatures, there is no chemical phase transformation, only a change in microstructure. A neck is formed between individual powder particles through the process of surface diffusion, evaporation-condensation, recrystallisation or solution-reprecipitation.

A porous network is constituted by the cavities remaining between the bonded powder particles. The main advantage of this process is the possible control over the resulting structure, which is homogeneous and consists of open interconnected pores with a narrow size distribution. On the contrary, the use of this method is limited by a lower achievable porosity (< 60 %) and the pore size constraint imposed by the sinterability of raw powders. [17, 19]

The raw powder particle size should be 2–5 times bigger than the required pore size [17]. The porosity can be controlled by many factors, such as powder particle size, additives [20] or degree of partial sintering which depends on the compaction pressure, sintering temperature, and time [17]. Advanced sintering techniques like spark plasma sintering [21] or partial hot pressing [22] can be employed for better control over the final microstructure and improved mechanical properties.

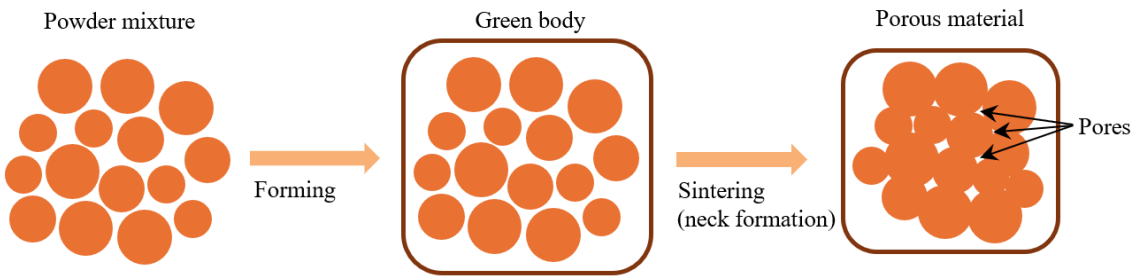

Fig. 3: Scheme of partial sintering [23].

2.3.2 Sacrificial template method

An appropriate amount of pore-forming agent is uniformly dispersed in a ceramic raw powder or precursor. The sacrificial phase is subsequently removed by evaporation, burn-off, thermal decomposition, etching or leaching and leaves pores in the structure that reflect its initial form. Ceramic foams with open or closed porosity in the range of 20–90 % and pore size 1–700 µm can be usually produced by this technique, although the lower limit of pore size can be shifted into the nanometre scale if nanoparticles are used as the pore-forming agent. Generally, porosity is controlled by the ratio of the sacrificial phase to the powder. Pore size and shape also depend on the choice of the pore-forming agent, hence the main advantage of this method, which is its versatility. The main drawback is a low interconnectivity between pores. [2, 19]

Pore-forming agents can be in solid or liquid form of various origins [17]:

- Synthetic organic matter – polymer beads, organic fibres,
- Natural organic matter – potato starch, cellulose, cotton,
- Metallic and inorganic matter – nickel, carbon, fly ash, glass particles,
- Liquid – water, camphene, tert-butyl alcohol, naphthalene-camphor, emulsion.

The type of pore-forming agent defines the way of its extraction. The matrix must be partially consolidated before the extraction to avoid the collapse of the structure. Inorganic materials like metallic or ceramic particles are usually removed chemically, for instance by acidic leaching [24]. When organic fugitives are used, the removal is usually carried out by pyrolysis and can produce harmful substances and be power-consuming (long thermal treatment between 200 and 600 °C). This can be avoided by using liquid fugitives that can be evaporated without shrinkage cracking and formation of toxic products [25].

An example of this is freeze-casting, a promising technique highly studied in the last two decades. The fabrication process is shown in Fig. 4. It consists of freezing a liquid ceramic

suspension, followed by sublimation of the solidified pore-forming agent under reduced pressure. After sintering, uniquely tailored microstructure with highly oriented dendritic channels can be obtained. [26]

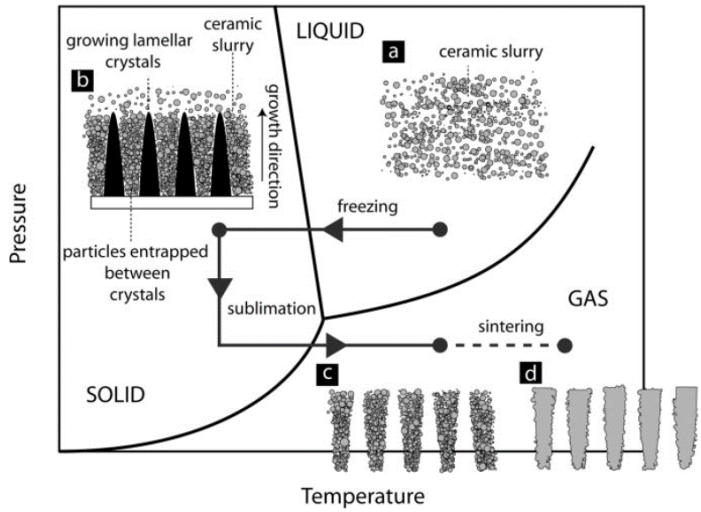

Fig. 4: Process of freeze casting: a) slurry preparation, b) solidification, c) sublimation, d) sintering [26].

2.3.3 Replica template method

Firstly introduced by Schwartzwalder and Somers in the 1960s [27], the replica template method is still widely used nowadays for its simplicity and flexibility. A porous cellular structure (template) is impregnated with a ceramic suspension (slurry) or a precursor solution. After the coating process, the excess slurry is removed and the sample is dried. During a subsequent thermal treatment, the template is burned and the remaining ceramic particles are sintered, retaining the original morphology of the template. The scheme of the process can be seen in Fig. 5. Producing porous foams by the replica method has the advantage of precise control over the pore shape and size based on the template used. When using a polymeric sponge, a macroporous ceramic foam with interconnected open pores can be obtained, with porosity going from 40 to 95 % and pore size in the range from 200 µm up to 3 mm. The size of pores formed by replication of a wooden template is lower, usually 10–300 µm with a porosity of 25–95 %. [19].

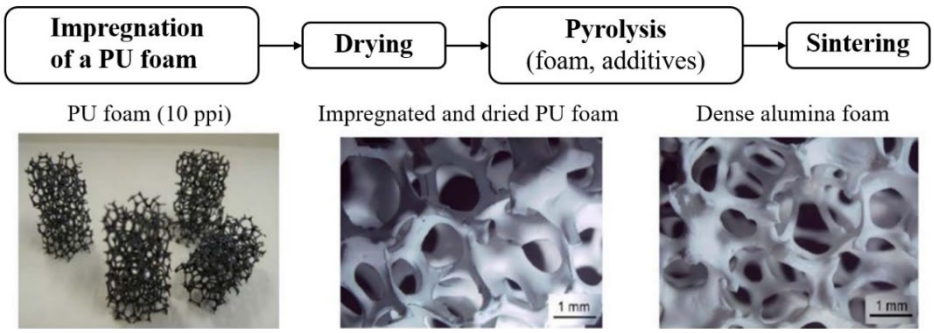

Fig. 5: Scheme of alumina foam preparation by the replica template method using polyurethane (PU) foam as a template [28].

Template

The template is selected according to required properties like permeability, pore size or shape. Many synthetic or natural structures can be used. Examples of synthetic organic materials include polyvinyl chloride, cellulose, carbon foam and the most common is a polymeric sponge from polyurethane [27]. Natural templates such as wood, coral or sea sponge are usually employed for their unique morphology, which can hardly be produced synthetically [17]. For instance, macroporous ceramics fabricated by replication of wood are characteristic for their anisotropic aligned pores [29].

Ceramic suspension

Ceramic suspension used for the coating of the template is a dispersion system consisting of ceramic powder particles and a fluid phase. Its rheological properties, solid loading and stability are crucial for the outcome. The fluid phase contains a binder and eventually additives, such as thickeners, defoaming agents or dispersants [30–32]. Binders can be ceramic (colloidal silica, bentonite), organic (polyvinylalcohol, carboxymethyl cellulose) or so-called low-loss (preceramic polymers). [33]

A shear-thinning behaviour of the suspension is necessary to ensure its adhesion to the template. The suspension has to be sufficiently fluid to penetrate the template, but viscous enough to adhere to the template and avoid dripping once the shear stress applied during coating decreases. [19] For some slurries, an additional thixotropy must be considered [33]. Suspensions with viscosity decrease from 10–30 Pa·s at a shear rate of 5 s^{-1} down to 1–6 Pa·s at a shear rate of 100 s^{-1} have been shown to give good results [19]. However, the viscosity of the suspension must be adapted to the pore size of the cellular structure, less viscous suspension is preferred when the pore size of the template is decreased [34]. In general, higher viscosity results in struts with increased thickness [35].

Replica processing

The template must be homogenously covered with the slurry. The excess suspension can be removed by centrifugation [36] or by pressing the foam manually or with a roller press [37]. Compressed air or a defoaming agent can be used to promote the opening of the pore windows in the cell walls to enhance interconnectivity between the cells [33].

Thermal treatment

Once the slurry covering the foam is solidified and dried, all organic components are eliminated via an optimised thermal treatment. The majority of polyurethane (90 %) vanishes after heating to ~450 °C, a full decomposition is observed by firing at ~600 °C [38]. An appropriately slow heating rate, usually lower than 1 °C·min^{-1}, must be employed to prevent stress formation within the coated struts, which could result in their cracking or a collapse of the structure composed of non-sintered particles. Sintering at high temperatures ranging from 1100 to 1700 °C can be combined with the burn-out phase or carried out as a separate step, with parameters specific to each ceramic material. [19]

Improvement of the mechanical strength

The porous solid obtained is a positive replica of the burned template and its morphology consists of open cell pores (1st order pores) and struts as illustrated in Fig. 6. The struts are hollow with triangularly shaped voids (2nd order pores) with peak stress in the corners. Combined with the presence of cracks formed during pyrolysis of the template (3rd order pores)

and intrinsic materials porosity (4th order pores), it leads to poor mechanical strength, which is the main drawback of this method. [18, 19] However, many approaches have been developed to overcome this shortcoming.

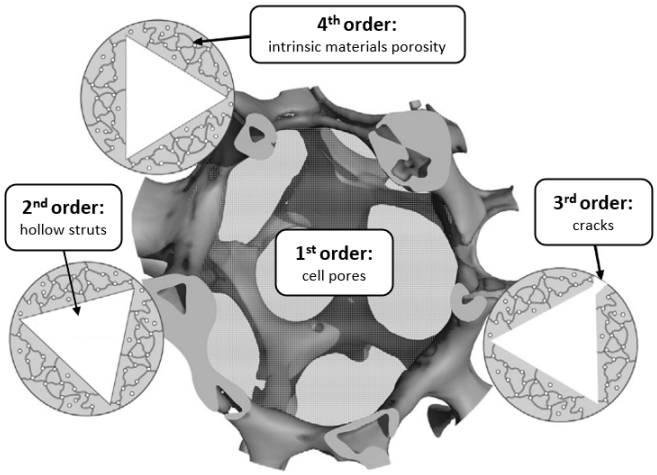

Fig. 6: Morphology of a ceramic foam prepared by the replica template method [39].

The polymeric template can be coated before the application of the suspension with a fugitive material to round off its sharp edges. For instance, zirconia foam, made from PU foam pre-coated with carbon black, achieved a higher mechanical strength by a factor of 1.8 due to rounder voids in the struts and the elimination of cracks [40].

Another possibility is to repeat the soaking of the template and drying step multiple times, which can increase the initial strut thickness without significantly decreasing the permeability of the foam [41]. It is also possible to deposit additional layers of a thinner slurry on a pre-sintered foam (after the firing of the template). The thickness of the struts is increased and flaws like longitudinal cracks and holes can be removed [37, 42].

Less viscous ceramic dispersion can also be used to eliminate hollow struts by infiltrating them under vacuum. Filling the cavities (Fig. 7) can significantly enhance the mechanical strength of the foams.

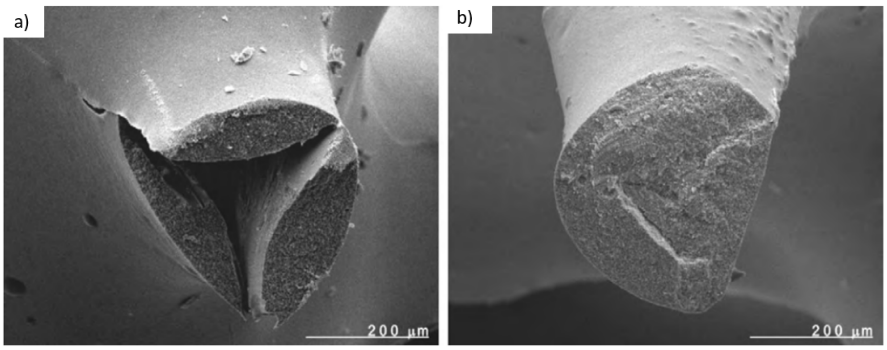

Fig. 7: SEM images of foam prepared by the replica template method, a detail of a) a hollow strut after firing the polyurethane template, b) a dense strut after vacuum infiltration [43].

Vogt et al. [43] infiltrated an alumina foam by alumina and zirconia, respectively, and in terms of mechanical strength, they achieved an increase by a factor of 2, respectively 3–4 for the zirconia-toughened alumina (with a decrease in porosity of 1 %). Even if the triangular cavities are not filled completely, the sharp corners, acting as stress concentrators, can be

partially rounded up from the inside and therefore the mechanical strength can be increased. For instance, in the work of Jun et al. [42], the initial compressive strength was successfully enhanced by partial infiltration of the struts (initial: ~0.4 MPa at a porosity of 93 %; recoating one layer: ~0.8 MPa at a porosity of 91 %; partial infiltration: ~1.6 MPa at a porosity of 91 %). Processing parameters and the suspension used for this purpose should always be optimised to achieve the best balance among mechanical strength, mass and strut thickness. Solid loading, particle size distribution, type of material and time of infiltration must be considered [44].

2.3.4 Direct foaming

By the direct foaming, a macroporous solid is produced by incorporating air or gas into ceramic slurry by physical or chemical blowing. The wet foam is then stabilised to keep the form of created bubbles which turn into cells of the ceramic foam after sintering. It is an easy, environmentally friendly and low-cost method that enables the preparation of solids with a porosity higher than 95 %. However, the control over the morphology can be often complex, anisotropy in the direction of foam expansion is possible, as well as the presence of both open and closed pores with a wide size distribution. [17, 18]

Gas incorporation

The gas phase can be dispersed through physical or chemical blowing. Chemical blowing is based on an *in situ* chemical reaction where the product is gaseous. A physical blowing agent can be a volatile liquid or solid which decomposes via heating, eventually, the gas (e.g. CO_2, H_2O) can be added into the slurry by mechanical stirring or gas injection [23]. The nucleated bubbles have a spherical shape and turn into polyhedral cells upon their growth. One of the main challenges is to stabilise the initially formed bubbles in the wet foam as they tend to coalesce to reduce the Gibbs free energy. [19].

Stabilisation of the wet foam

Having an amphiphilic character, surfactants prevent the destabilisation of the foam by reducing the gas-liquid surface tension by adsorbing at the interface. They are classified based on the hydrophilic group as ionic, cationic, non-ionic and amphoteric. Pore size and porosity depend on the used surfactant and its foaming ability [45], pore size within the range of 35 µm to 1.2 mm and porosity from 40 up to 97 % have been achieved [19].

Another option is to use colloidal particles. They exhibit great stability and tend to adsorb irreversibly at the interface, therefore foams stabilised by colloidal particles are not prone to collapse for several days (as opposed to several minutes for surfactant-stabilised foams). They do not always require a setting step and can be directly dried in air and sintered [46, 47]. Structures prepared by this method are usually close-celled with enhanced mechanical strength, however, ceramics with open porosity can be obtained by decreasing the concentration of stabilising particles or by adding a sacrificial phase (e.g. graphite). They usually have cells of smaller size (10–300 µm) with total porosity ranging from 45 to 95 % [17, 19].

Foam setting

Many different strategies can be employed to consolidate the stabilised foam to avoid its collapse. For instance, the conventional polymer foam preparation has been modified by Wood et al. [48] by incorporating ceramic particles directly into the organic solution containing

polyols and polyisocyanates that react together by thermosetting condensation to form polyurethane, as described by the following equation [49]:

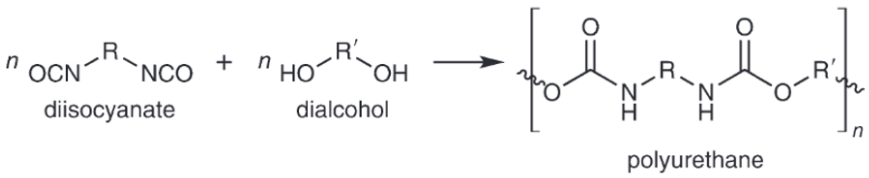

(1)

When water is added to the mixture, it reacts with the isocyanate groups and CO_2 is produced according to the reaction scheme (2), further encouraging pore formation.

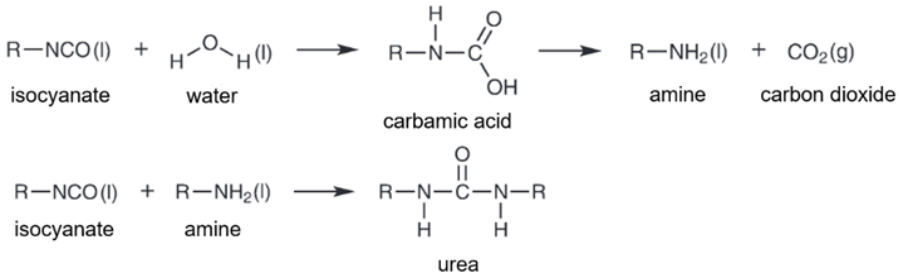

(2)

For a complete polymerisation, the amount of alcohol groups (OH) and isocyanate groups (NCO) must be equal. In practice, a slight excess of NCO groups is commonly used and the ratio between NCO and OH groups is given by the so-called NCO index (I_{NCO}). [49] Contrary to the replica template, the struts are dense after pyrolysis of the polyurethane and exhibit improved mechanical strength [19].

The ceramic powder can be replaced by polymeric precursors enabling the production of mainly Si-based ceramics [50]. Silica-based ceramics and other inorganic materials can also be set by sol-gel phase transition, an example of the microstructure is shown in Fig. 8 [51]. Another example is gel casting, a method based on *in situ* polymerisation of monomers dispersed in the foamed ceramic suspension. The initially used toxic materials were successfully replaced in the last years by cheaper and more environmentally friendly gelling agents (corn starch, glycols, agar, citric acid) and natural minerals and waste materials as raw material (kaolin, fly ash, dolomite) [52]. Graded structures with tailored microstructure can be produced by progressive evaporation of emulsified and dispersed alkane or air-alkane phases in a stabilised aqueous suspension [53].

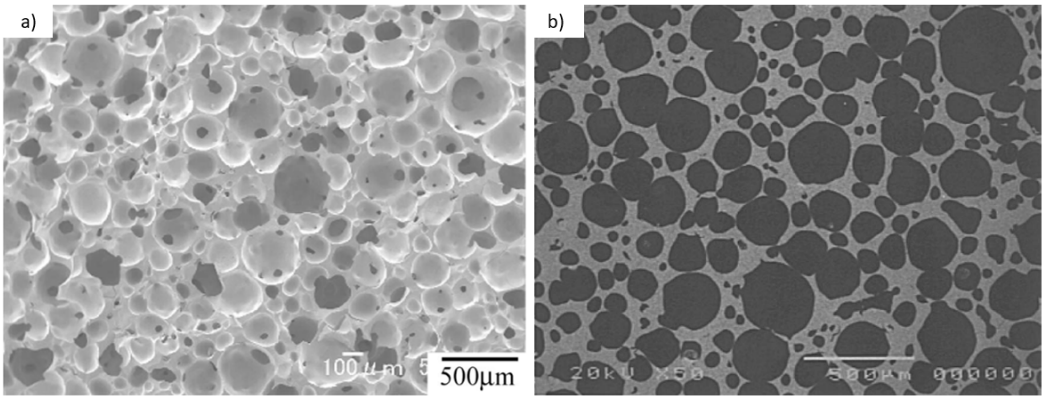

Fig. 8: SEM micrographs of silica foam prepared by sol-gel reaction and mechanical foaming, a) fractured cross-section, b) polished cross-section [51].

2.3.5 Additive manufacturing

Additive manufacturing (AM), also known as 3D printing, covers a wide range of processes that can create an object by adding material, typically layer by layer, based on a model provided by a computer-aided design. AM offers several advantages, in particular the ability to create complex, customised structures without the use of expensive tooling and machining. The microstructure and porosity can be tailored according to user requirements, an example of 3D printed filters with customisable pore size can be seen in Fig. 9. The pores can be of various shapes (square, cylindrical, spherical, etc.) and their size is determined by the printing parameters while being limited by the resolution of the specific printing technology. 3D printing of porous ceramics has great potential, especially for the production of artificial bone scaffolds and functionalised ceramics. However, it is not suitable for mass production and rather high cost, time and material constraints remain the major limiting factors of this technique. [2, 54]

Although almost all 3D printing technologies can be used to fabricate a porous solid, the most common technologies employed for this purpose are binder jetting (3DP), selective laser sintering (SLS), direct ink writing (DIW) and stereolithography (SL). 3DP involves a selective deposit of a liquid binder into a powder bed of ceramic material, followed by the solidification of the given layer [55]. SLS also uses dry powder as a starting material but the particles are fused by the energy delivered by a high-power laser [56]. In DIW, a continuous filament of ceramic slurry is extruded from the nozzle onto the support according to the path programmed by the model. This process, providing control over the macropores through the printing geometry, can be combined with conventional techniques such as direct foaming or sacrificial template method, which can introduce smaller pores into the extruded material and thus create hierarchical porosity. [57, 58] SL is also a slurry-based technique and uses a light source to selectively cure a suspension contained in a vat. The suspension consists of a photocurable liquid doped with ceramic particles and additives and undergoes a photo polymerisation process to turn into a solid. [54]

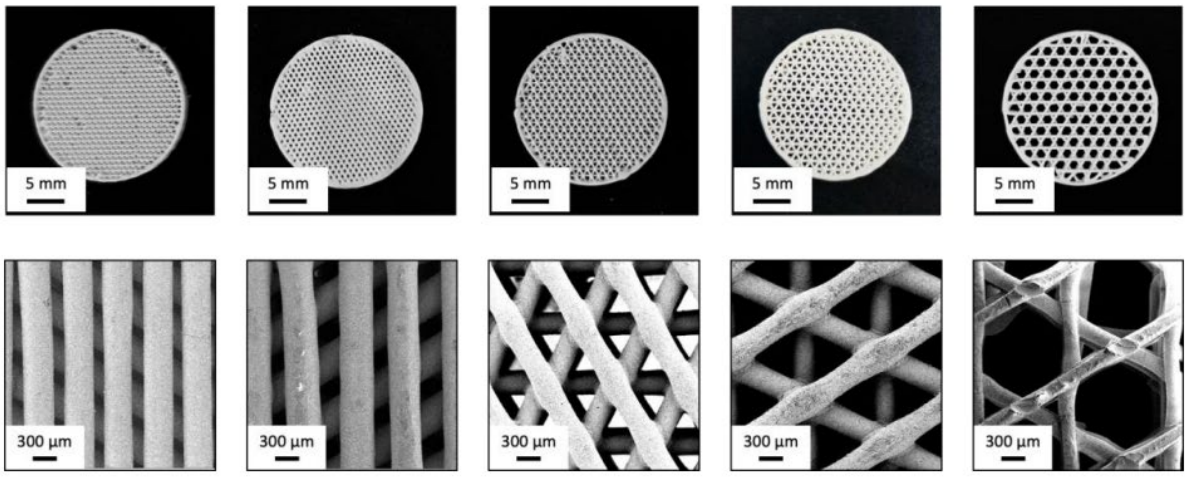

Fig. 9: 3D printed filters from silica, mesh spacing (from left to right) of 150 µm, 250 µm, 350 µm, 450 µm and 1300 µm [59].

2.4 Application of macroporous ceramics in filtration

Macroporous ceramics are often employed in filtration to separate contaminants from a fluid. Filtration can be classified into several categories according to the pore size *d*: filtration ($d > 10$ µm), microfiltration (MF, 10 µm > d > 100 nm), ultrafiltration (UF, 100 nm > d > 1 nm), nanofiltration (NF, d ~1 nm) and reverse osmosis (RO, $d < 1$ nm). In filtration and microfiltration, the separation is principally ensured by the sieving effect (i.e. the separation is based on the size of particles); for smaller pores, the fluid permeability also depends on the affinity of the solute/solvent with the porous material [17]. Filters with pores smaller than 10 µm are often designated as membranes. They are usually composed of two or three layers (see Fig. 10) of different porosity and pore size, (1) the outer layer serving as macroporous support, (2) the binding intermediate layer and (3) the inner layer ensuring the filtration [4].

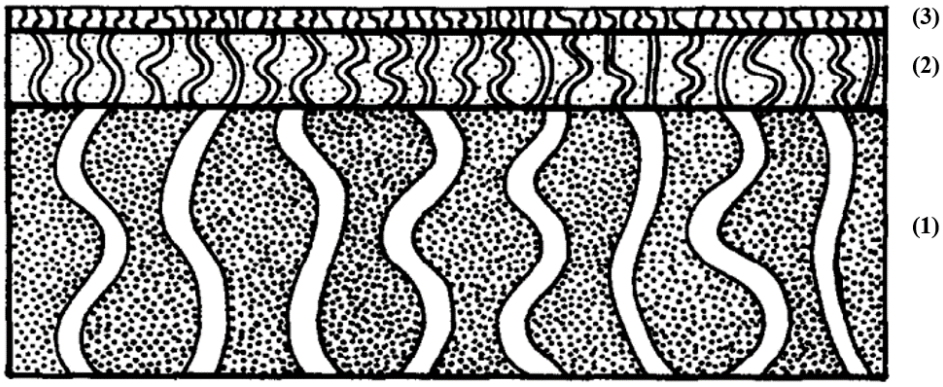

Fig. 10: Schematic representation of a membrane, (1) the outer layer, (2) the binding layer, (3) the inner layer [4].

Ceramic filters should have a specific morphology with high porosity, consisting of open interconnected pores with a narrow size distribution. The pores should be preferentially oriented in the flow direction to enhance a high flow rate and permeability, which are important factors in evaluating the effectivity of a filter. However, microstructural features should be optimised to still maintain a sufficient mechanical strength of the filter. [60]

They can operate in three modes (surface filtration, cake filtration and depth filtration), as represented in Fig. 11. Depth filtration, where the impurities are trapped in the interior of the filter, is usually preferred as it provides a larger surface area available for filtration [61].

In terms of properties, ceramic filters are favoured for their thermal stability, chemical durability and wear resistance, which leads to their longer lifetime compared to other materials. Another undeniable advantage is the possibility of their repeated use thanks to regeneration. During the filtration process, the impurities are retained by the active surface of the filter, causing a build-up of contaminants that can cause an unwanted pressure drop and decreased permeate flow. Based on the nature of the contaminants, multiple approaches can be used to clean the fouled filter and restore its removal efficiency, for instance physical, chemical, electrical or ultrasonic cleaning [62].

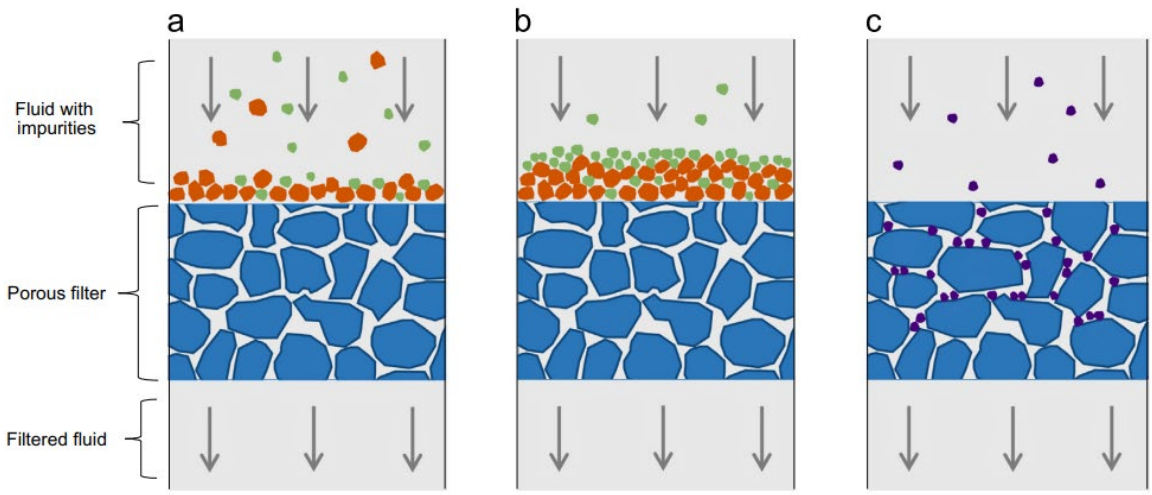

Fig. 11: Representation of the three modes of filtration: a) surface filtration, b) cake filtration, c) depth filtration [61].

In the following subchapters, the main applications of ceramic filters are presented. Since this work is devoted to the preparation of ceramic filters from a relatively low-cost material, the focus is mainly on filters from cheaper alternatives. Nevertheless, examples of filters made from advanced ceramic materials can be found in the literature and industrial applications [2].

2.4.1 Hot gas filters

Hot gas filters are necessary to remove particles harmful to human health and the environment contained in waste gases produced by the chemical industry, oil refineries or power plants. They are used at high temperatures (260–900 °C) and are often exposed to chemically aggressive environment (both oxidising and reducing atmospheres), so there are typically increased demands on the material selection, and therefore ceramic filters are preferred for this application. [63]

Ceramic filters are one of the most efficient diesel particulate filters (DPFs), where carbon-based particulate matter needs to be trapped. A filter with 40–60 % porosity, pore size around 10 µm and thickness of 400 µm is suited to filter more than 90 % of particles [64].

DPFs are usually extruded in the form of honeycombs because ceramics with unidirectionally aligned pores in the direction of flow have been demonstrated to have higher permeability compared to those with randomly distributed pores [65]. However, the traditional extrusion can be also replaced by alternative processing techniques. For instance, porous mullite supports with gradient unidirectional pores fabricated by tert-butyl alcohol-based freeze-casting were shown to have improved gas flux, moreover, the effect of solid loading, powder particle size and freezing temperature on the microstructure have been also investigated in this study [66]. Filters from silicon carbide exhibiting anisotropy have been also prepared by Gómez-Martín et al. [29], who replicated 5 different wood templates with porosities between 45 and 72 % and evaluated the dependence of gas permeability and mechanical strength on microstructural parameters, obtaining the best results for a filter with the narrowest radial pore size distribution (3–30 µm) and 49 % porosity.

Foam-type filters were also reported for this application. Park et al. [67] prepared various-shaped porous cordierite filters by gel-casting (porosity 80 %, pore size 100–200 µm) with removal efficiency above 99 % for dust particles finer than 10 µm. Gel-casting can also be used to fabricate layered structures, as reported by Takahashi et al. [68], who employed

natural gelation agents to fabricate alumina filters with double-layered structure (Fig. 12) and cordierite filters with added non-through holes to minimise the pressure drop.

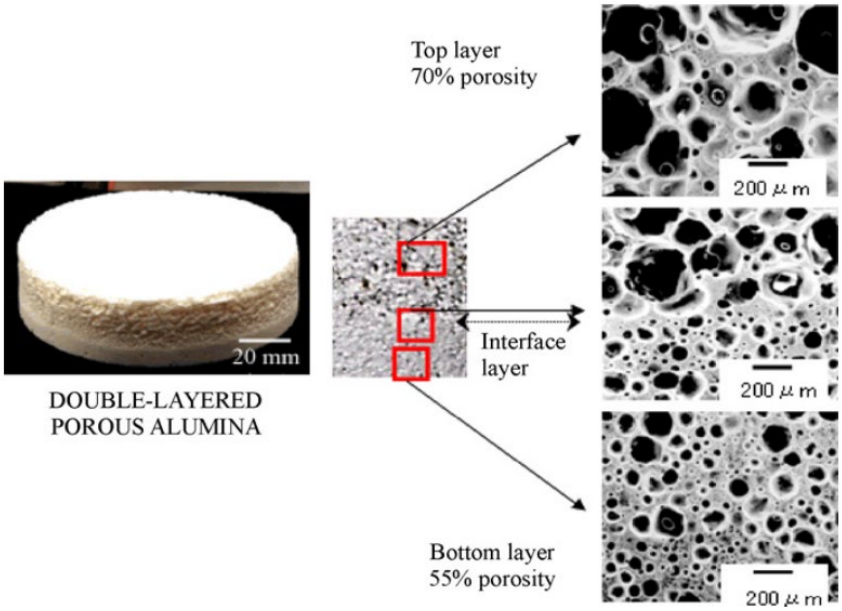

Fig. 12: Porous alumina filter with a double-layered structure fabricated by gel-casting [68].

2.4.2 Molten metal filters

One of the traditional applications of ceramic filters is in the casting of metals such as aluminium, iron or steel. Their aim is to remove non-metallic inclusions and other impurities from the molten metal to prevent defects and enhance the quality of the casting [61]. Larger particles are removed by surface filtration, removal of smaller particles is ensured by depth filtration and liquid inclusions can be captured by the intrinsic open micropores [69].

Ceramic foam filters (CFFs) have been shown to have high filtration efficiency and replication of polyurethane foams is typically used as a preparation technique for this application. The filters are used at high temperatures, so corrosion and thermal shock-resistant refractory materials are required. The material, filter size and pore density in pores per inch (ppi) vary according to the type of molten metal. The most common examples are summarised in Tab. 2. [70]

Tab. 2: Characteristics of commonly used molten metal filters [70].

Metal		Filter			
Type	**Temperature (°C)**	**Size (cm^2)**	**Pore density**	**Material**	**Preheating**
Aluminium	800	18–66	20–70 ppi (based on the required purity)	Al_2O_3	Yes
Iron	1400	35–185	10–25 ppi (based on the type of iron)	SiO_2-bonded SiC	No
Steel	1560	5–20	10–15 ppi (based on the type of steel)	Mg-stabilized ZrO_2	No

2.4.3 Water filters

Providing access to potable water remains a challenge, especially for people in developing countries. Point-of-use household water filters diminish the risk of diseases by removing bacteria, protozoans and viruses from unpurified or insufficiently disinfected water. Ceramic membranes with pores in the order of micrometres can often be made from low-cost, locally available materials (clay and organic pore former such as starch) and present an affordable solution to this problem. [71]

Ceramic membranes are also used for the treatment of wastewater produced by the industry to meet the acceptable discharge limits to nature and reduce the unfavourable effects of pollution on the environment. One of the major pollutants is oily wastewater, where the oily contaminants can be free-floating on the surface, dispersed, emulsified or dissolved and the separation strategy varies for each case depending on the droplet size and stability of the mixture. [72]

However, the industrial use of ceramic membranes for water treatment is limited due to the approximately ten times higher cost compared to polymeric membranes, which can be significantly reduced by using natural, low-cost materials [73, 74]. Nandi et al. [74] fabricated a membrane using kaolin, quartz, sodium carbonate, calcium carbonate, boric acid and sodium metasilicate, and estimated the cost of raw materials at $\$130/m^2$, respectively $\$200/m^2$ including manufacturing and shipping, a significant reduction compared to α-alumina tubular membranes ($\$500–1000/m^2$), making it closer to the cost of a polymeric membrane. In another work [73], they used local clay instead of kaolin and quartz and reduced the price of raw materials to $\$19/m^2$. In the same vein, Abbasi et al. [75] prepared mullite and mullite-alumina tubular membranes from kaolin clay and α-alumina powder by extrusion and studied the effects of operating conditions (temperature, pressure, oil concentration, flow rate) on their performance in MF. Extruded low-cost membranes were also studied by Kamoun et al. [76], who used Tunisian clay and cellulose fibres obtained from paper as pore-forming agent.

2.4.4 Oil filters

Generally, ceramic membranes have a moderate hydrophilic character due to the presence of hydroxyl groups on metal oxide surfaces, being the cause of the preferential forming of hydrogen bonds. However, surface technologies can be used to modify the wettability of the filter and enhance the oil flux by obtaining a (super)hydrophobic or (super)oleophilic character through a decrease of surface free energy. Chemicals like organophosphonic acids, steric acids, fatty acids, alkanethiols and organosilanes can be used for this purpose, the latter being the most commonly used. [77]

For instance, superhydrophobic-superoleophilic kaolin-based membranes with contact angles of 157° and 0°, respectively, were fabricated by Hubadillah et al. [78]. The increase of surface roughness and decrease in surface free energy was achieved through the organosilane-silica sol-gel method, which resulted in 99% separation efficiency for oil removal from water using the modified membrane, which can be seen in Fig. 13. Coating with organofunctional silanes was also applied for 3D printed silica membranes, where the optimal ratio between flux and separation efficiency as a function of membrane thickness and pore size, as well as the recovery and reusability of the coated membrane, was studied. [59]

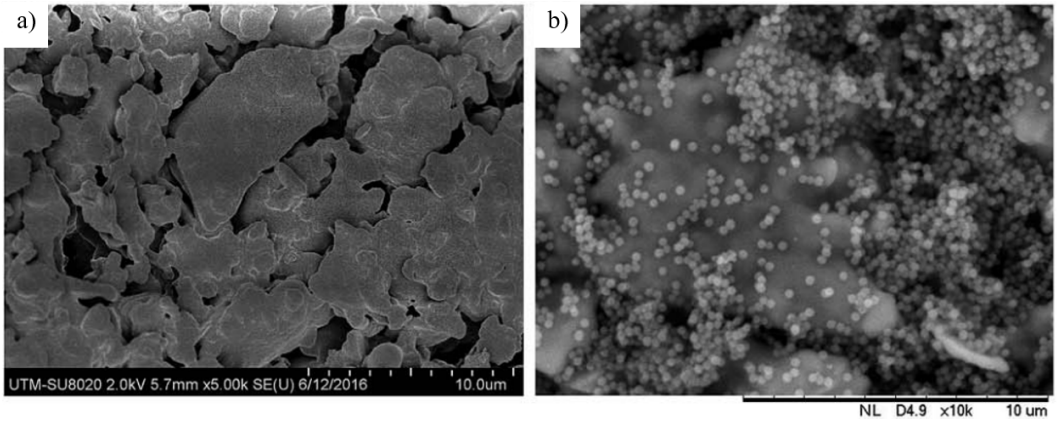

Fig. 13: SEM micrographs of a) a pristine and b) a modified superhydrophobic/superoleophilic membrane surface [78].

As an example of a ceramic filter used for the removal of solid particles from oil, a study of Nazarova et al. [79] can be cited. They prepared filters by the ceramic method from natural raw materials (bauxite, kaolinite, serpentinite, quartz sand, talc, alumina) by mixing them in the ratio of cordierite composition (pore size 5–70 µm, porosity 21–32 %). The filters were used to eliminate metal shavings from engine oil and after regeneration (mechanical surface cleaning and hydrochloric acid treatment), the productivity of filters was 100 % restored.

Research on ceramic filters used for electro-insulating oily liquid has not yet been carried out, most of the research conducted to this day dealt with the separation of water droplets from oil or water-oil emulsion separation, as described above.

2.5 Ceramic materials used in filtration

Material selection is based on the requirements of the specific application. The common properties for all the applications mentioned in Chapter 2.4 are sufficient mechanical strength, high temperature stability and resistance against corrosion and aggressive environments. For filters exposed to high temperatures (hot gas filters, DPFs and molten metal filters), thermal shock resistance and low coefficient of thermal expansion are additional important factors. Typical materials used for DPFs include silicon carbide, cordierite or mullite [64]. Silicon carbide is also commonly used in the foundry, as well as alumina and stabilized zirconia [70]. Concerning water and oil filtration, where the temperature of the fluid is not so elevated, the surface character (hydrophobicity/hydrophilicity) and the cost-effectiveness are also relevant criteria. Metal oxides like alumina, zirconia, silica or a combination of those are commonly used [80].

2.5.1 Alumina

Alumina (Al_2O_3) is one of the most important ceramic materials. It is characteristic for its hardness, strength, abrasion resistance and chemical inertness. The mechanical properties are superior to most oxides, typical values for dense polycrystalline alumina are listed in Tab. 3. However, the mechanical properties change significantly with the presence of porosity, for instance, an increase in porosity from 0 to 50 % results in a decrease of bending strength from 269 to 47 MPa. The melting temperature of alumina is 2054 °C, so it must be sintered at rather high temperatures above 1400 °C to obtain a dense solid. The sintering temperature can be lowered by adding other oxides to the powder, such as SiO_2, MgO, Cr_2O_3 and ZrO_2. [81]

Tab. 3: Typical properties of dense polycrystalline alumina at room temperature [82].

Density ($g \cdot cm^{-3}$)	Young's modulus (GPa)	Compressive strength (MPa)	Hardness (Knoop)	Fracture toughness ($MPa \cdot m^{-0.5}$)	Thermal expansion coeff. ($ppm \cdot °C^{-1}$)
3.85–3.99	380–410	3000–5000	15000–20000	3–6	6–9

Alumina is widely used for its good properties and versatility. Two phases of alumina, α (corundum) and γ, are commonly employed in MF, UF and NF processes as a substrate, the binding layer or even the active layer of the filter [80]. Alumina filters are chemically very inert and can be used in the pH range from 1 to 14, which implies not only the possibility of their use in harsh conditions but also the possibility of cleaning them chemically. Among the materials commonly used for membranes, alumina is the least hydrophilic [83].

2.5.2 Silica

Silica (SiO_2) exists in many various crystalline and non-crystalline forms. The main polymorphs formed at atmospheric pressure are α-quartz (thermodynamically stable at ambient conditions), β-quartz (formed at 573 °C), tridymite (formed at 867 °C) and cristobalite (formed at 1470 °C). Silica melts at 1723 °C, therefore the sintering temperatures and production cost are lower compared to other ceramic materials. [81]

Membranes from pure silica are usually employed in NF and RO processes, as their structure can be controlled on the nanometre scale. Silica has a high affinity with water, therefore its hydro-stability must be increased if a longer exposure to water is expected. [80]

2.5.3 Mullite

Mullite is the only stable intermediate crystalline phase in the Al_2O_3-SiO_2 system (Fig. 14) with stoichiometries ranging from relatively silica-rich ($3Al_2O_3 \cdot 2SiO_2$) to alumina-rich ($2Al_2O_3 \cdot SiO_2$). Mullite has a rather small coefficient of thermal expansion (5.1 $ppm \cdot °C^{-1}$), providing good thermal shock resistance. It also has superior temperature stability, hardness and creep resistance at high temperatures compared to α-alumina, so it is a good candidate for refractory applications. [81]

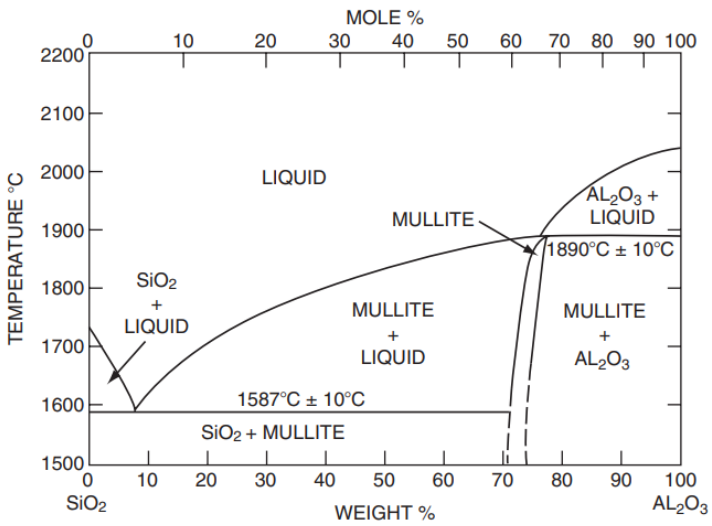

Fig. 14: Al_2O_3-SiO_2 binary phase diagram [84].

2.5.4 Kaolin clay

As mentioned in Chapter 2.4.3, the cost of ceramic filters and membranes fabricated from pure refractory oxides is often not competitive with the other solutions for the reason of expensive inorganic precursors and the requirement for a high sintering temperature. To reduce the production cost, filters can be fabricated from cheaper natural materials like clay, of which there are many different kinds varying in composition. Kaolin is the most common type of natural clay and is widely used for this purpose. It is mainly composed of the mineral kaolinite, described by the chemical formula $Al_2Si_2O_5(OH)_4$, and other oxides like Fe_2O_3 or TiO_2. [81]

Kaolin can be mixed with water and other additives to fabricate a ceramic slurry and then it can be processed directly by dry pressing, stiff plastic forming, soft plastic forming or casting [75, 81]. Another method of using kaolin is as a source of ceramic powder with crystalline mullite and silica-rich phase. This is carried out by heat treatment, the sequence of the reaction is represented in Fig. 15. [81] Above the eutectic temperature (1587 °C) an amorphous glassy phase of silica is predicted, however, the presence of some impurities (CaO, Na_2O or K_2O) can shift the phase transitions and vitrification of cristobalite to lower temperatures.

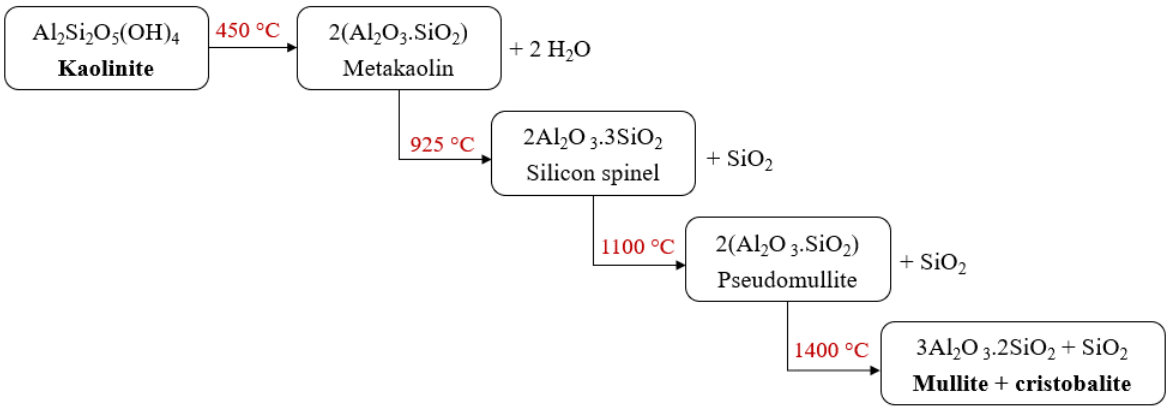

Fig. 15: Reaction scheme of kaolin calcination [81].

3 AIMS OF THE EXPERIMENTAL PART

The aim of the experimental part of this thesis was to prepare macroporous ceramic foams based on mullite and silica and evaluate their suitability for use in the filtration of electro-insulating oils. Filters were prepared using two methods; the replica template method, which uses polymeric foam as a template (see Chapter 2.3.3), and direct foaming, which consists of the fabrication of composite foams by incorporating ceramic particles directly into *in situ* blown polyurethane foam system (see Chapter 2.3.4).

The partial objectives of the work were as follows:

- Optimise the processing parameters for the preparation of foams with respect to their microstructure and handling strength,
- Evaluate the foams prepared with optimised processing parameters for their phase composition and microstructure,
- Perform scale-up experiments to meet the requirements for the size of the filter for the designed filtration device,
- Evaluate the mechanical strength and assess the suitability of the successfully scaled-up filters for filtration.

4 EXPERIMENTAL PART

4.1 Materials

The raw material used for the preparation of ceramic foams was Molochite™ (Imerys Minerals Ltd, United Kingdom), which was chosen to make the prepared filters competitive with the original paper filter solution. It is a relatively low-cost aluminosilicate powder produced by calcination of kaolin at 1500 °C; wide distribution of grain size 1–250 µm, median particle size d_{50} = 27 µm; theoretical density 2.7 g·cm^{-3}; chemical composition given in Tab. 4.

Tab. 4: Chemical composition (wt.%) of Molochite™ from the material data sheet, determined by XRF at 1000 °C.

	SiO_2	Al_2O_3	K_2O	FeO_2	MgO	Na_2O	CaO	TiO_2	LOI
wt.%	53.59	42.54	1.95	1.20	0.32	0.08	0.05	0.03	0.09

4.1.1 Replica template method

- Templates – commercial reticulated polyester-based polyurethane foams with open cell structure Bulpren S (Eurofoam, Czech Republic); two different pore sizes, 75 ppi and 90 ppi with average cell size 520–720 µm and 440–520 µm, respectively
- Binder – colloidal silica solution Granisol 30 (MINKO, Czech Republic); particle size 14 nm; density 1.18 g·cm^{-3}; pH 9.5; solid content 27.25 wt.% SiO_2, 0.27 wt.% Na_2O
- Dispersing agent – Dolapix CE64 (Zschimmer & Schwarz, Germany)
- Defoaming agent – n-Octanol $C_8H_{18}O$ (Lachema, Czech Republic)
- Deionized water

4.1.2 Direct foaming

- Polyol – phthalic anhydride-based aromatic polyester polyol Stepanpol® PS-2412 (Stepan Company, USA); density 1.2 g·cm^{-3}; max 0.15 wt.% water; hydroxyl number 230–250 mg KOH·g^{-1}
- Diisocyanate – solvent-free polymeric diphenylmethane-4,4'-diisocyanate (MDI), Lupranate® M10 (BASF, Germany); density 1.22 g·cm^{-3}; 32 wt.% NCO; functionality approximately 2.3
- Deionized water

4.2 Methodology

4.2.1 Replica template method

Each sample preparation step was optimised by performing a series of experiments on smaller samples (20x20x10 mm, 20x50x10 mm). Based on their results, presented in Chapter 5.1, processing parameters were selected to scale up and prepare filters with the required dimensions (cylinder ϕ 100 mm with an inner hole ϕ 27 mm, height 100 mm). The tested parameters, as well as the optimised parameters, are presented in each of the following subchapters.

Preparation of the suspension

An overview of the prepared suspensions (S1–S10) is given in Tab. 5. The optimal solid loading of the ceramic powder in the suspension was determined by gradually increasing its content (50–67 wt.%) and evaluating the ability of the suspension to coat the PU template. Once the solid loading was determined, three different methods of stirring and various formulations were tested:

- Overhead stirrer for 2 h at 300 rpm, presence of dispersing agent (0, 1, 1.5 and 2 wt.% on dry powder basis),
- Planetary ball mill for 3 h at 400 rpm (ratio of dry powder to zirconia balls 1:2), presence of dispersing agent (0 and 1 wt.% on dry powder basis), presence of defoaming agent (0 and 0.1 wt.% on dry powder basis),
- Overhead stirrer for 2 h at 300 rpm, application of ultrasound (alternating 20 min off/10 min on).

Given the wide particle size distribution of the raw ceramic powder, preparation of the suspension from a powder milled in a planetary ball mill was considered to reduce the particle size (0, 1, 2 and 3 h in water; ratio of dry powder to zirconia balls 1:4).

Tab. 5: Formulations of suspensions tested for the preparation by replica template method.

	Powder (wt.%)	Milling of the powder	Dispersing agent (*wt.%)	Defoaming agent (*wt.%)	Stirring method
S1	50–67	-	-	-	Overhead stirrer/10 min after increase
S2	63	-	-	-	Overhead stirrer/2 h
S3	63	-	1.5	-	Overhead stirrer/2 h
S4	63	-	2	-	Overhead stirrer/ 2 h
S5	60	-	2	-	Overhead stirrer/2 h
S6	63	-	-	-	Planetary ball mill/3 h
S7	63	-	-	0.1	Planetary ball mill/3 h
S8	63	3 h	-	0.1	Planetary ball mill/1 h
S9	63	3 h	-	-	Overhead stirrer/2 h
S10	63	2 h	-	-	Overhead stirrer/2 h + Ultrasound/40 min

*wt.% - weight percentage on dry powder basis

Based on the findings, which will be presented in Chapter 5.1.1, suspension S10 was selected for the preparation of final filters, therefore its preparation is described in more detail. The raw ceramic powder was wet-milled in a planetary ball mill using zirconia balls (ϕ 5 mm) for 2 h. Each jar was filled with 70 g of powder, 280 g of zirconia balls and 170 ml of deionized water. Subsequently, the water was removed through drying (85 °C, at least 24 h), and the powder was dry-milled on a roller ball mill with alumina balls (ϕ 20 mm) for 3 h to break the agglomerates formed during drying. Following this, the milled ceramic powder was added into a colloidal silica solution without any further additives to obtain a suspension with 63 wt.% of ceramic powder (72.9 wt.% solid loading including solids content in the binder). The beaker containing the suspension was then immersed in an ultrasonic bath and the suspension was stirred at 300 rpm for 2 h by an overhead stirrer. Ultrasound was intermittently applied in cycles of 20 min off and 10 min on.

Impregnation of PU foams with the suspension

The PU foams were immersed under compression into the suspension until completely soaked and then passed between two rotating metal rollers with a 3 mm gap to remove the excess slurry and homogenise the coating. The impregnated foams were left to dry under ambient conditions for at least 48 h.

Filling the hollow struts by infiltration

Part of the prepared samples was infiltrated with a less viscous suspension to improve the microstructure by filling the hollow struts present after the firing of the template (see Chapter 2.3.3, Improvement of mechanical strength).

For the infiltration, a suspension was prepared with 15 wt.% of milled ceramic powder in colloidal silica, stirred by a magnetic stirrer for 2 h. A pre-sintered ceramic body was placed into a desiccator, which was evacuated to 0.05 bar using a vacuum pump. Subsequently, the prepared suspension was applied via a tube system until the foams were fully submerged. After 10 min of holding time under reduced pressure, the foams were retrieved and the excess slurry was removed by applying compressed air.

Scale up

In order to achieve the desired dimensions and shape of the filter, it was necessary to carry out a process of scaling up. The preparation scheme of scaled-up filters is shown in Fig. 16. They were prepared as described above from disc-shaped PU foams with a cut-out centre (ϕ_{outer} 114 mm, ϕ_{inner} 30 mm, height 12 mm). Five impregnated foams were stacked on top of each other while still wet and gently pressed to bond the individual layers together. The resulting filter consisted of two so-prepared bodies (10 PU foams in total). Three different filters were prepared using this technique – two with a pore size of 90 ppi (hereinafter referred to as F90, F90+I) and one with a pore size of 75 ppi (F75+I). Filters F90+I and F75+I were infiltrated under reduced pressure, while filter F90 was left without infiltration.

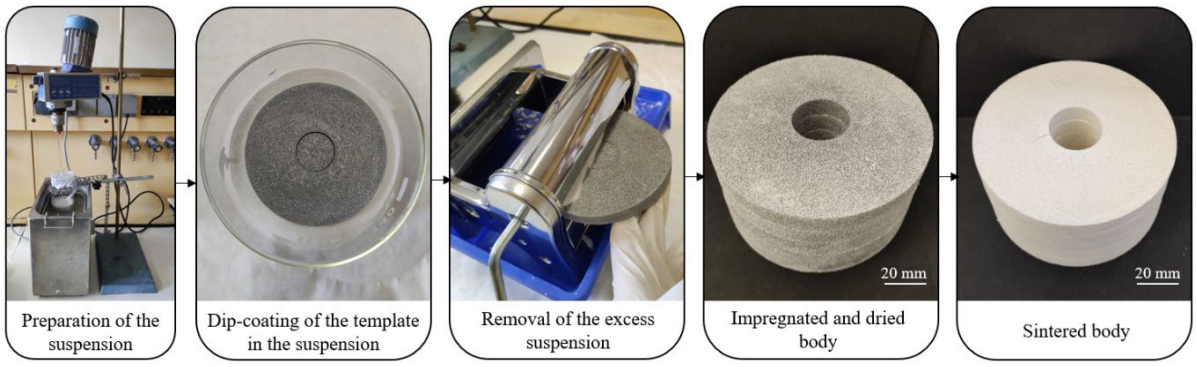

Fig. 16: Preparation of ceramic filters by the replica template method.

Heat treatment

Heat treatment of the foams consisted of two main steps:

- Firing of the organic components and PU template in a muffle furnace at 800 °C for 2 h with a slow heating rate (0.5–1 °C·min^{-1}),
- Sintering of the ceramic body in a high-temperature furnace at 1200, 1300, or 1400 °C for 2h with a heating rate of 4 °C·min^{-1}.

For the foams reinforced by infiltration, the first step was carried out up to 1100 or 1200 °C for 2 h to ensure sufficient handling strength for the infiltration process by pre-sintering the body. For the subsequent firing of the organic components after infiltration, an additional step of heat treatment at 800 °C for 1 h was incorporated.

Based on the results that will be discussed in Chapter 5.1.3, the heat treatment modes for the final filters F90, F90+I and F75+I were determined and are summarised in Tab. 6

Tab. 6: Heat treatment modes of the filters prepared by the replica template method.

Filter	Step	Heating	Dwell	Cooling
F90	Firing	20–600 °C, 0.5 °C·min^{-1} 600–800 °C, 1 °C·min^{-1}	800 °C/2 h	800–700 °C, 5 °C·min^{-1}
	Sintering	20–1400 °C, 4 °C·min^{-1}	1400 °C/2 h	1400–700 °C, 5 °C·min^{-1}
F90+I, F75+I	Firing, pre-sintering before infiltration	20–600 °C, 0.5 °C·min^{-1} 600–800 °C, 1 °C·min^{-1} 800–1100 °C, 3 °C·min^{-1}	1100 °C/2 h	1100–700 °C, 5 °C·min^{-1}
	Firing after infiltration	20–500 °C, 1 °C·min^{-1} 500–800 °C, 2 °C·min^{-1}	800 °C/1 h	800–700 °C, 5 °C·min^{-1}
	Sintering	20–1400 °C, 4 °C·min^{-1}	1400 °C/2 h	1400–700 °C, 5 °C·min^{-1}

4.2.2 Direct foaming

Ceramic foams prepared by the second method were obtained by firing the organic components from a composite foam, which was produced by incorporating ceramic particles directly into *in situ blown* polyurethane. By analogy, the process of optimisation of the processing parameters for the preparation of samples was carried out. Based on the optimised procedure, a scale-up experiment was performed.

Composite foams composition

To determine the optimal composition, different formulations of composite foams were tested (see Tab. 7). The composition of all foams was determined by fixing the I_{NCO} index to 1.05 (there is a 5 % excess of NCO groups in the system for complete reactions with all the OH groups of the precursors). The influence of the following parameters on the microstructure and handling strength of the foams was evaluated:

- The presence of deionized water (0, 1 and 2 wt.% to polyol),
- The weight ratio of ceramic powder to PU (1, 1.2, 1.6, 1.8, 2, 2.2), where the mass of PU is given by the sum of its precursors (polyol and MDI),
- Type of ceramic powder.

Three types of ceramic powder were tested – Molochite™, Molochite™ milled for 2 h (milling procedure identical to the one described in Chapter 4.2.1) and a mixture of Molochite™ and SiO_2. The SiO_2 powder was incorporated to achieve a similar chemical composition of ceramic foams as those prepared by the replica template method. It was obtained by calcination of silica sol, which was air-dried for 5 days, calcined in a muffle furnace at 700 °C for 1 hour and ground in a mortar afterwards.

Tab. 7: Formulations of composite foams tested for the preparation by direct foaming.

Composition	Powder (g)		H_2O (g)	Polyol (g)	MDI (g)	Powder/PU weight ratio
	Molochite™	SiO_2				
C1	5	-	-	3.15	1.85	1
C2	5	-	0.03	2.85	2.12	1
C3	5	-	0.05	2.61	2.34	1
C4	3.6	1.4	-	3.15	1.85	1
C5	8	-	-	3.15	1.85	1.6
C6	9	-	-	3.15	1.85	1.8
C7	10	-	-	3.15	1.85	2
C8	11	-	-	3.15	1.85	2.2
C9	6*	-	-	3.15	1.85	1.2

* powder milled for 2 h

Composite foams processing

The scheme of preparation is shown in Fig. 17. To prepare the composites, the given mass of ceramic powder was mixed with polyol (and deionized water) in a mortar and homogenised by mechanical stirring for 2 min. The MDI was then added and the homogenisation was carried out for another 1–2 min. If the powder/polyol ratio was higher than 1.8, the excess powder was added to the mortar in the second step of homogenisation. For selected samples, a prolonged time of processing (5, 10, 15, 20 and 25 min) before filling the mould was included. Every 3 min, an additional stirring for 20 s was employed to prevent the formation of large bubbles and reduce the pore size. The foam was then filled into a cylindrical mould and left to cure under ambient conditions for at least 24 h. After curing, the composite foam was cut into samples with a diameter of 20 mm and a height of 10 mm.

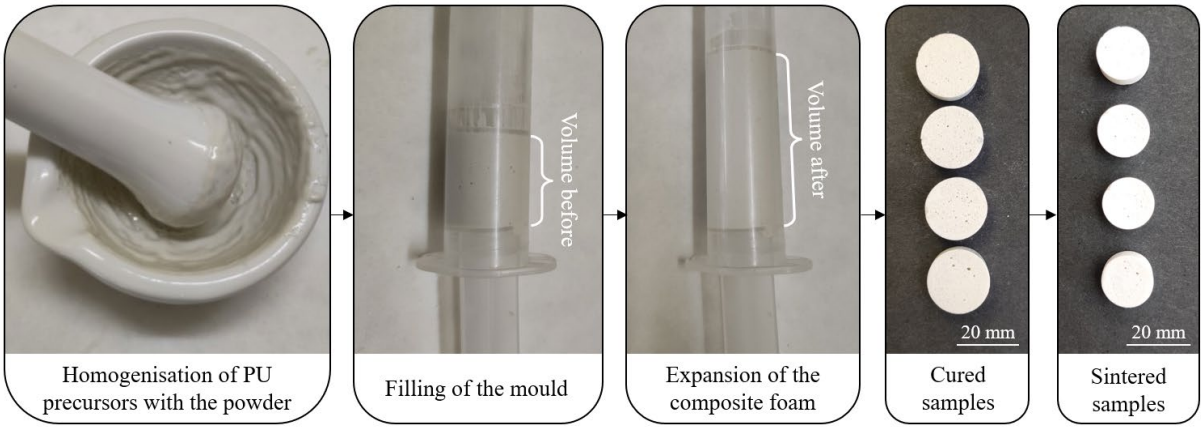

Fig. 17: Preparation of ceramic foams by the direct foaming.

Scale up

Based on the results discussed in Chapters 6.1.1 and 6.1.2, foams with composition referred to as C7 and C9 with a processing time of 20 min were chosen for scaling up. The foams were prepared as described above using a ten times higher quantity of reactants and filled into a cylindrical mould with a diameter of 92 mm.

Heat treatment

The cured samples were heat-treated in two steps:

- Firing the polyurethane and organic matter in a muffle furnace at 1000 °C for 1h with a slow heating rate of 0.5 °C·min^{-1},
- Sintering in a high-temperature furnace at 1200, 1300 or 1400°C for 2h (heating rate 5 °C·min^{-1}, cooling rate 10 °C·min^{-1}).

4.3 Characterisation of powders and foams

4.3.1 Particle size distribution

A laser particle size analyser LA-950 (HORIBA, Japan) was used to determine the size of particles in ceramic powder to evaluate the effect of milling on its particle size.

4.3.2 Thermogravimetric analysis

To set the right parameters for the first step of the heat treatment cycle, thermogravimetric analysis (TGA) was performed to determine the temperature of the removal of polyurethane and other organic components from the composite foams. The measurements were carried out by Setaram 96 Line TGA/DTA (Setaram, France) in an atmosphere of $N_2 + O_2$ between 20 and 1000 °C with a heating rate of 2 °C·min^{-1}.

4.3.3 Phase composition

The phase composition of the crushed sintered foams was evaluated using a Rigaku SmartLab 3kW X-ray powder diffractometer (Rigaku, Japan). Diffractometry was performed in Bragg-Brentano measurement mode between 10 and 90°. The evaluation was performed using the Rietveld refinement method.

4.3.4 Microstructure analysis

Morphology, microstructure

Morphology of the powders was observed via scanning electron microscope (SEM) LYRA 3 (Tescan, Czech Republic). SEM was also used to examine the morphology and microstructure of the sintered foams, both on fractured cross-sections and on polished ceramographic specimens. A digital stereo microscope MV 2000 HDMI (Top Optical, China) was used to evaluate the microstructure of the sintered foams at magnification below 50×.

Pore size

Pore size distribution of the sintered foams was determined by mercury intrusion porosimetry using PoreMaster 60 (Quantachrome, USA). Pore size was also investigated by image analysis. Due to the different nature of the pores in the bodies prepared by the replica template method and by direct foaming, the analysis procedure was different for the corresponding samples.

For the foams prepared using the replica template method, the cell size and the size of pores interconnecting the cells (windows) were determined from stereo microscope images. Considering that 3D objects might be captured at an angle in the 2D image, the largest dimension of the corresponding elliptical shape was measured, as illustrated in Fig. 18. The value was determined from 150 measurements.

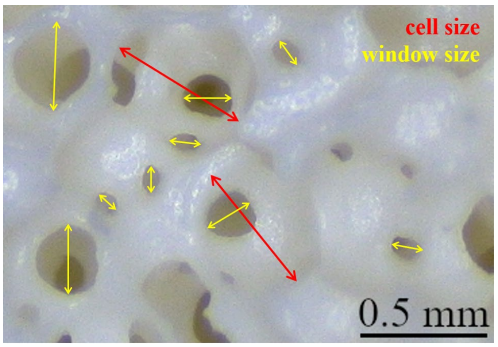

Fig. 18: Illustration of the image analysis of the foams prepared by the replica template method.

The pore size of samples prepared by direct foaming was determined by image analysis performed on SEM micrographs of polished ceramographic specimens using ImageJ software (National Institutes of Health, USA). The image analysis procedure is illustrated in Fig. 19. First, the image was converted to binary format through thresholding. Subsequently, the binary image was processed by the watershed algorithm to separate touching or overlapping spherical shapes. The areas of these shapes were measured and converted to equivalent diameter assuming each shape was circular. The analysis was performed on 3 images per sample and pores smaller than 5 µm were excluded from the evaluation.

The image analysis was done on 2D random sections, therefore a stereological correction factor was applied to the average circular pore size diameter in 2D (d_{circle}) to obtain the diameter of a spherical pore in 3D (d_{sphere}) according to the equation (3) [85]:

$$d_{sphere} = \frac{d_{circle}}{0.785} = 1.274 * d_{circle} \tag{3}$$

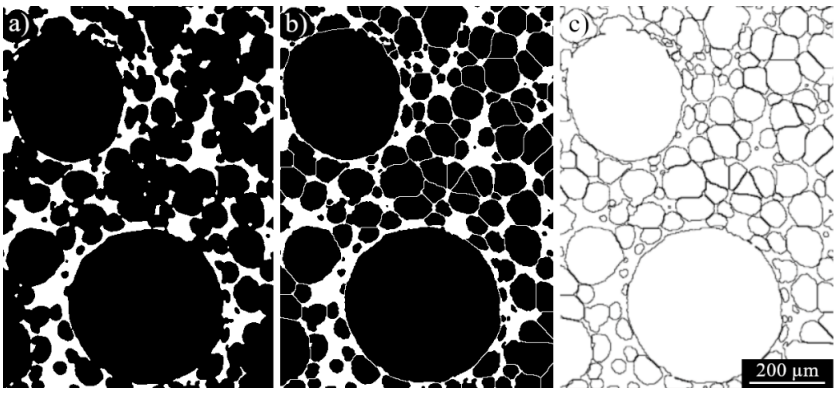

Fig. 19: Illustration of the image analysis of the foams prepared by direct foaming, a) SEM micrograph converted to binary format, b) applied watershed algorithm, c) identified particles.

Porosity

Porosity of the samples was determined using two methods according to ČSN EN ISO 18754 [86].

Method by measurement of geometric dimensions and mass was used to evaluate the porosity of all prepared samples. The porosity determined by this method is hereafter referred to as the "geometric porosity". The porosity P was determined by taking the mass of a dry sample m_1, its bulk volume V_b, theoretical density ρ_t and replacing in the equation (4):

$$P = 1 - \frac{m_1}{V_b * \rho_t} \cdot 100\ \% \tag{4}$$

The theoretical density ρ_t was determined as a weighted average of the densities of constituent materials, according to their ratio.

To verify the porosity obtained by the geometric method, the porosity of selected samples was also measured using the method by liquid displacement (Archimedes method). The impregnation of the sample with water for HPLC was carried out under reduced pressure (0.05 bar). The relative density ρ_{rel} was determined by replacing in the following equation:

$$\rho_{rel} = \frac{\rho_{H_2O}}{\rho_t} \cdot \frac{m_1}{m_3 - m_2} \cdot 100\ \% \tag{5}$$

where ρ_{H_2O} is the density of water at a given temperature, ρ_t is the theoretical density of the material, m_1 is the mass of a dry specimen, m_2 is the apparent mass and m_3 is the mass of the immersed specimen. The porosity P_a (ratio of the total volume of open pores to the bulk volume) is further determined according to the equation (6):

$$P_a = 1 - \rho_{rel} \tag{6}$$

4.3.5 Compressive strength

Compressive strength was determined for the samples prepared by the replica template method. The tests were performed on cylindrical specimens (ϕ 26.5 mm, height 31 mm) prepared from 3 PU foams of 12 mm height stacked on top of each other. A servo-electric testing system Instron 8862 (Instron, USA), equipped with a load cell Dynacell 100 kN (Instron, USA) to measure the applied load, and a displacement gauge sensor MTS 632.03C-21 (MTS, USA) with a gauge length of 4 mm to measure the displacement, was used for the loading of the specimens. A neoprene pad with a thickness of 3 mm was placed between the specimen and compression platen to fill irregularities and ensure an even distribution of the load on the surface of the specimen. The whole setup can be seen in Fig. 20. A constant displacement speed of 0.5 mm·min^{-1} was applied. The applied load and corresponding displacement were recorded and plotted, with the compressive strength determined as the maximum recorded stress value.

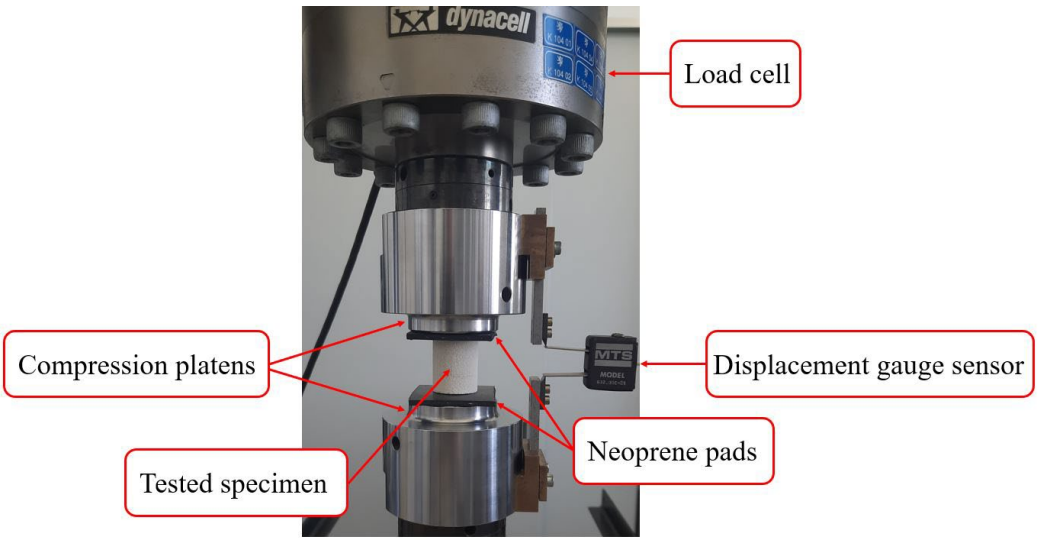

Fig. 20: Setup for the testing of compressive strength.

4.3.6 Filtration capacity

Within the framework of the project TAČR FW06010300, an experimental filtration unit was designed to test the prepared filters for their filtration capacity. A description of the unit is provided in Fig. 21. A one-way pump draws the contaminated oil from the tank into the filter via a high-pressure hydraulic hose. At the outlet of the filter, another hose is connected to drain the filtered oil into a second tank. The filtration process can be controlled through a display integrated into the electrical switchboard, and the flow can be manually regulated using ball valves. The pressure at the inlet and outlet of the filter is monitored by integrated flow meters.

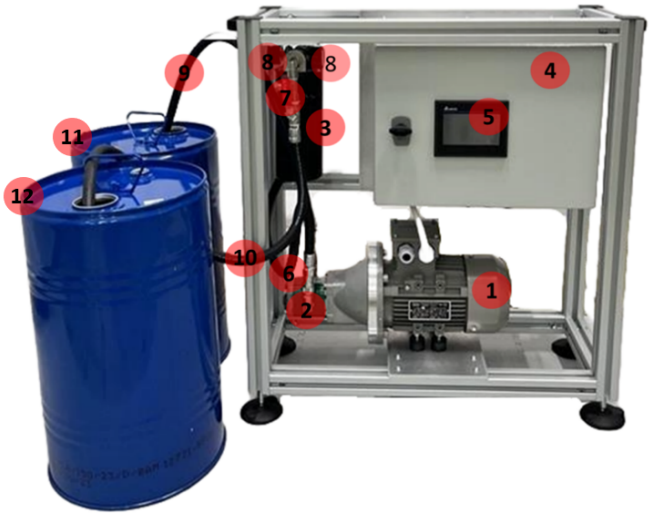

1: Three-phase asynchronous motor
2: One-way pump
3: Filter
4: Electrical switchboard
5: PLC display
6: Connecting hoses
7: Ball valve
8: Flow meters
9: Inlet hose (inlet to the filter)
10: Outlet hose (outlet from the filter)
11: Tank with contaminated oil
12: Tank with filtered oil

Fig. 21: Experimental filtration unit with a description.

The shape and dimensions of the ceramic filter were designed to resemble the currently used paper cartridge for filtration. Therefore, a cylinder with a diameter of 100 mm, an inner hole of 27 mm, and a height of 100 mm was set as the target for filter preparation.

For the testing of filtration capacity, the prepared filter was mounted in a custom-designed housing, as illustrated in Fig. 22. First, the filter was mounted through its central hole on a perforated tube (ϕ 26 mm) and secured with a threaded bottom cover. Then, the filter was fixed in place with a top cover and screwed to a flange using the thread in the central tube. The assembly thus prepared was then inserted into a cylindrical welded housing (ϕ 110 mm) and locked in place with screws. A valve was screwed onto the top of the flange, connected to both the oil inlet and outlet of the filtration unit. A schematic representation of the fluid flow through the filter is shown in Fig. 23.

Due to delays in the fabrication of the filtration unit as well as the filter housing, it was not possible to conduct the filtration tests of the prepared ceramic filters and evaluate their filtration capacity within the scope of this thesis. However, the suitability of porous ceramic foams prepared by the replica template method and direct foaming for filtration based on their microstructural properties is discussed in Chapters 5.2.4 and 6.2.2, respectively.

Fig. 22: Representation of the process of mounting the ceramic filter into the housing.

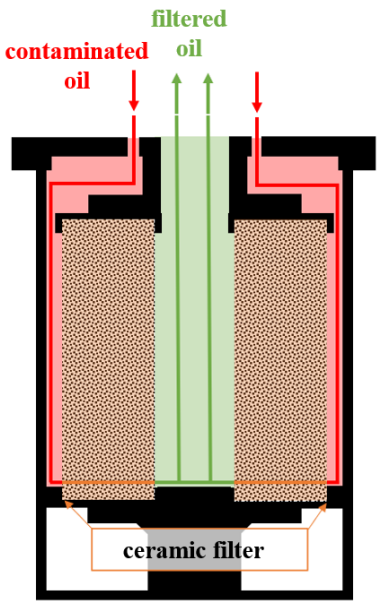

Fig. 23: Schematic representation of the fluid flow through the ceramic filter.

5 REPLICA TEMPLATE METHOD – RESULTS AND DISCUSSION

5.1 Optimisation of processing parameters

5.1.1 Preparation of the suspension

The first phase of optimisation of processing parameters was devoted to the preparation of the suspension. The influence of solid loading, additives (dispersing and/or defoaming agent), stirring method and powder particle size were evaluated in order to find a stable suspension with good adhesion to the PU template and optimal coating ability. Terms such as viscosity, shear-thinning behaviour, or thixotropy are used to describe the various suspensions, but it should be noted that no rheological measurements were performed, and these properties are stated based only on visual observations.

As a result of the first experiment with variable solid loading of the powder (S1), the optimal value was found to be 63 wt.%. With lower solid loading, the suspension was too fluid, did not adhere well to the PU foam and leaked onto the bottom of the template. On the contrary, when the solid loading exceeded 63 wt.%, the viscosity started to increase, and as a result, the suspension was unable to fully penetrate the foam and remained mostly on the surface.

However, the suspension (S2) tended to sediment so an addition of dispersing agent to stabilise it was considered. The presence of 1.5 wt.% of dispersing agent (S3) did not have any significant effect, so the amount was increased to 2 wt.% (S4). For this case, a strong shear-thinning behaviour with thixotropy was observed, which did not result in a homogeneous coverage of the foams. To decrease the viscosity of the suspension, the solid loading was lowered to 60 wt.% (S5), but the results were still not satisfactory due to a strong thixotropy.

Besides using a dispersing agent, another possible way to stabilise the dispersion of particles is by reducing their size, as described by Liang et al. [87] in their study on the case of kaolin. Therefore, a reduction in the powder particle size by planetary ball milling with zirconia balls was studied in the next step. Two approaches were compared – preparation of the suspension from raw powder, where the milling phase was conducted directly during stirring of the suspension with silica sol (S6, S7), and preparation from already milled powder with reduced particle size (S8–S10). Milling of the suspension had a positive effect on the dispersion of the particles in both cases. However, strong foaming of the suspension was observed (S6), which resulted in reduced weight of the applied suspension, leading to very high porosity (> 94 %) and poor handling strength of the sintered foams. The foaming phenomenon was partially suppressed by adding a defoaming agent (S7). However, better results were observed for the foam prepared from already milled powder (S8), a significant difference in microstructures of the sintered foams was observed as seen in Fig. 24. In the case of preparation directly in the planetary ball mill, the effect of milling was less effective, which resulted in rougher surface and reduced degree of sintering (linear shrinkage of 3.6±0.3 % for S7 compared to 8.2±0.8 % for S8, sintered at 1200 °C). Due to the slight foaming of all suspensions prepared in the planetary ball mill, the preparation from milled powder using an overhead stirrer (S9) was preferred. No sedimentation or foaming was observed, which helped to a homogeneous template coverage. Ultrasound was applied during stirring (S10) to prevent agglomeration of smaller particles with higher surface energy and to ensure more uniform particle dispersion overall. The foams prepared from suspension S10 presented the best results in terms of coverage of the PU foams and the microstructure, therefore this suspension was chosen for the following stage of experiments.

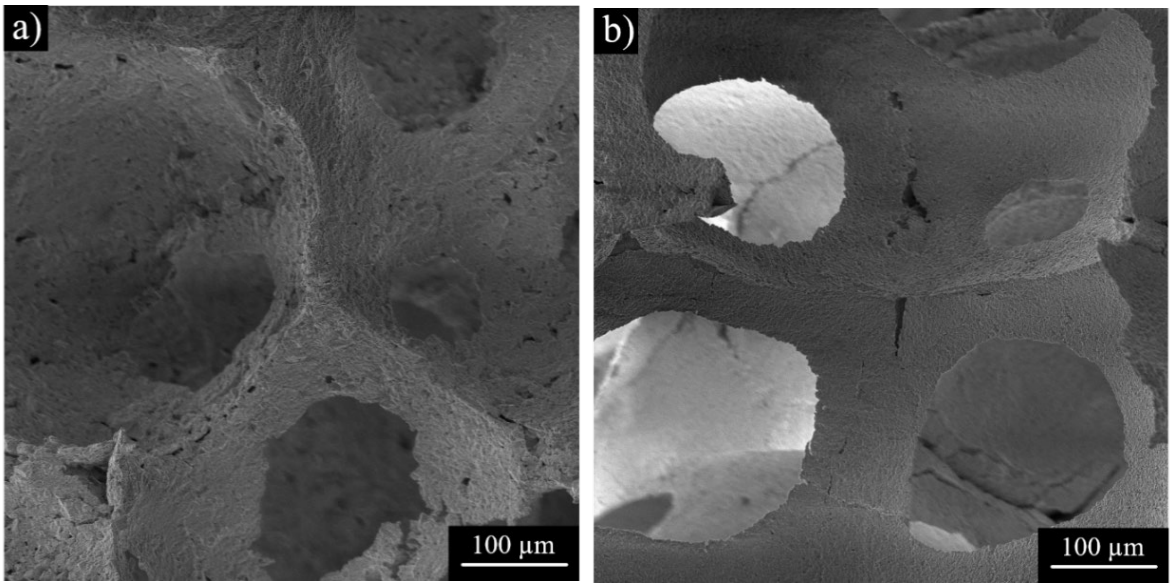

Fig. 24: SEM image of the microstructure of sintered foam from suspension prepared in a planetary ball mill from a) raw powder (S7), b) powder milled for 3 h (S8); sintered at 1300 °C.

The milling time of the powder was optimised with respect to the particle size. Milling the ceramic powder in water for 1, 2 and 3 h effectively reduced the particle size and in all cases contributed to the change from bimodal to a much narrower unimodal particle size distribution (Fig. 25). The median particle size decreased from 26.79 µm for the raw powder to 6.41, 5.14 and 4.08 µm, respectively. Since only a minor difference between particle size distributions was found for varying milling times, milling the powder for 2 h was chosen as the optimal compromise to ensure particle size reduction and decrease the processing time. SEM images of raw powder containing agglomerates (a) and powder milled for 2 h with finer particles (b) can be seen in Fig. 26.

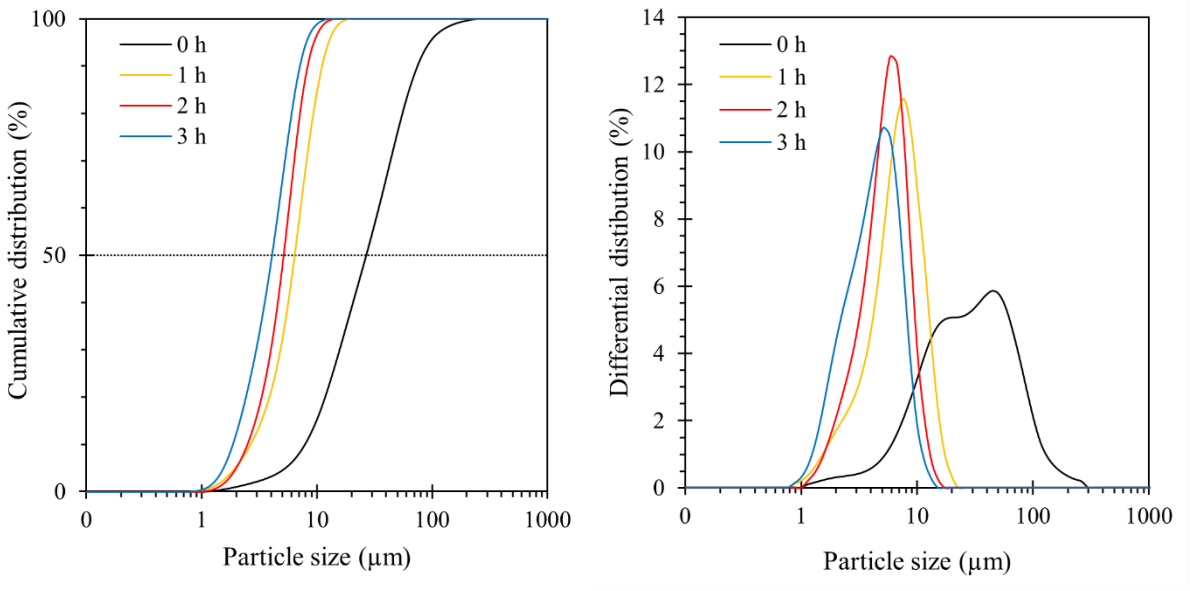

Fig. 25: Particle size distribution for powders with different time of milling.

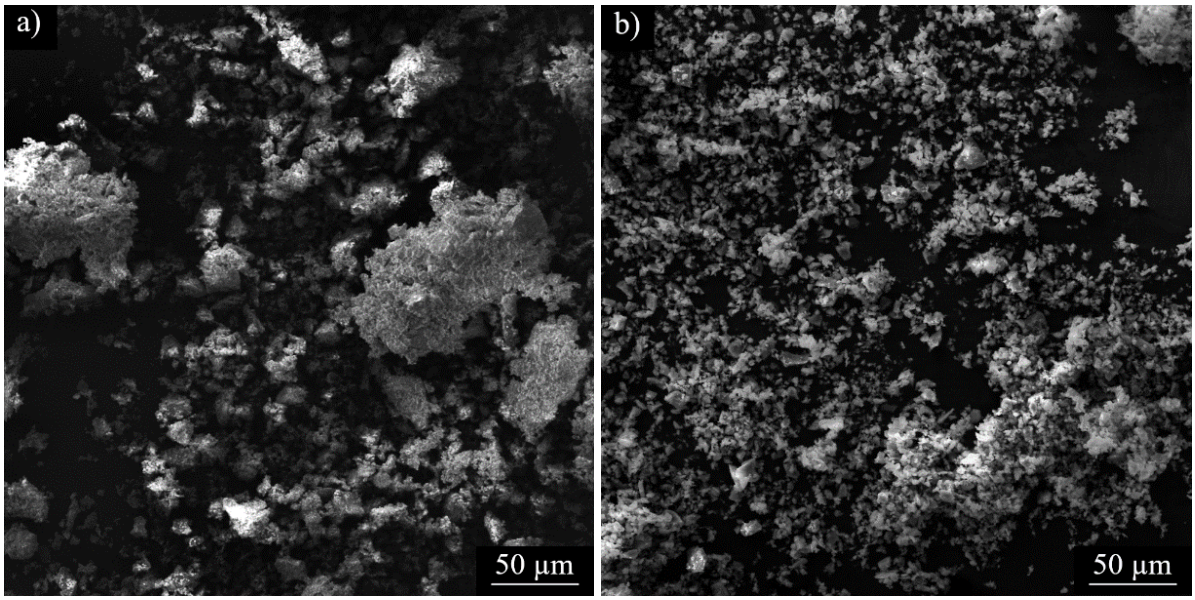

Fig. 26: SEM images of a) raw powder, b) powder milled for 2 h in water.

The microstructure of the foams prepared from milled powder was significantly improved compared to those prepared from raw powder, as it can be seen in Fig. 27. The sharp edges of the particles were rounded, and the intrinsic porosity was reduced due to a higher sintering activity of the finer particles, attributed to their higher surface energy [88]. The particle size distribution of the milled powder presented above (Fig. 25) suggests that the powder should be composed of particles smaller than 20 µm. However, it can be seen in Fig. 27b that larger particles were still occasionally present, which was probably caused by imperfect milling of the powder.

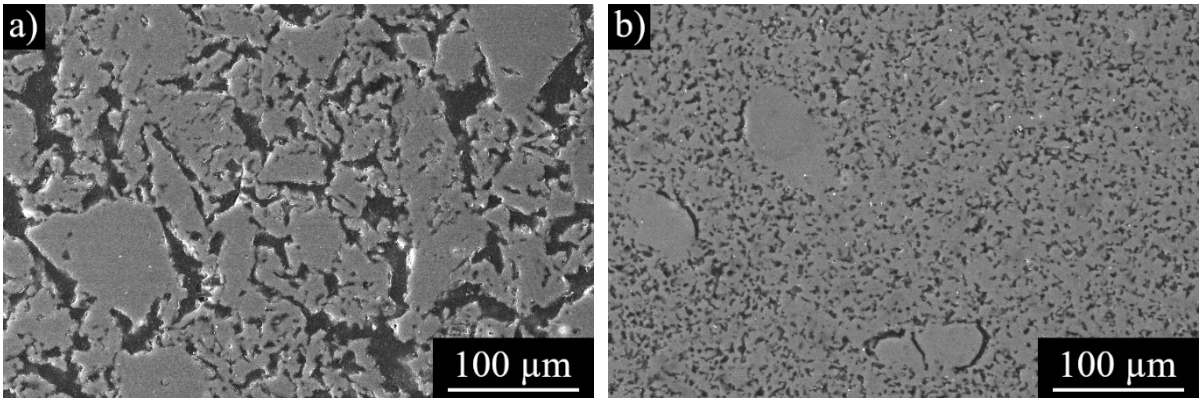

Fig. 27: SEM image of the microstructure of sintered foam from suspension prepared by an overhead stirrer from a) raw powder (S3), b) powder milled for 3 h (S9); sintered at 1200 °C

5.1.2 Impregnation of PU foams with the suspension

The aim was to prepare foam filters with the smallest possible pore size that the given processing technique could provide, in order to increase the filtration efficiency. Therefore, two types of commercial PU foams with the smallest pores, 75 and 90 ppi, were chosen as templates. The porosity of commercially available ceramic cellular filters prepared by the replica template method is typically between 70 and 90 %, depending on the pore count number of the template used and the supplier [89, 90].

This porosity range was confirmed as a target based on observations from experiments with varying impregnation rate. Foams with porosity under 70 % presented a high degree of sealed windows (i.e. the pores were not interconnected), which could negatively influence the permeability of the filter. With porosity above 90 %, the foam struts were too thin, as it can be seen in Fig. 28a, which resulted in worse mechanical strength and could lead to a collapse of the structure under fluid pressure. Foams with porosity around 80 % (see Fig. 28b) seemed to be a good trade-off between mechanical strength and degree of interconnectivity between cells. To achieve this porosity after sintering, the mass of the applied suspension was determined to be 17–19 times the mass of the PU template.

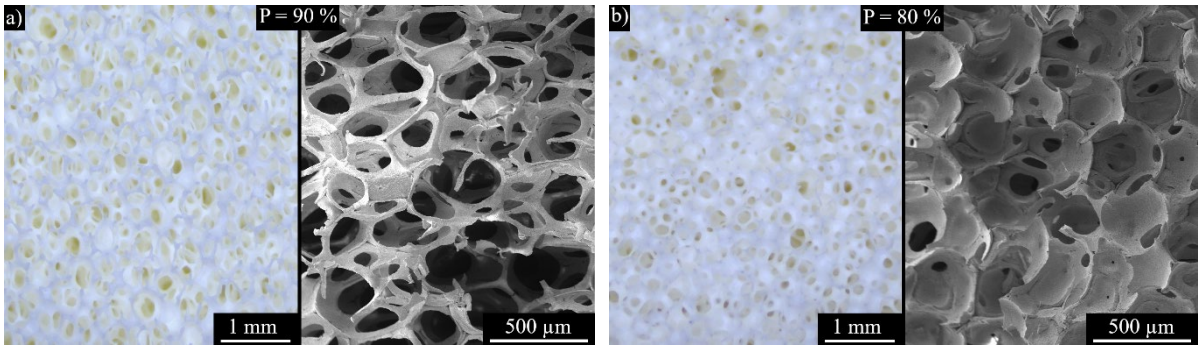

Fig. 28: SEM image of the foam (90 ppi) with porosity of a) 90 %, b) 80 %; sintered at 1300 °C.

5.1.3 Heat treatment

Several stages of mass loss during heating can be identified from the curves obtained by TGA in Fig. 29. The first stage, with 1 % mass loss between room temperature and 220 °C is associated with the elimination of adsorbed water. The evolution of the curve after 220 °C is linked to the typical three-staged decomposition of a polyester-based polyurethane foam template [91]. The first phase occurs between 220 and 280 °C, followed by a second stage up to 350 °C, and finally, a third stage with a complete PU decomposition at around 550 °C. However, only a part of the weight loss (7 %) corresponds to the mass of the polymeric template, the remainder (3 %) is due to the decomposition of organic matter in the silica sol present in the suspension. These two processes occur simultaneously, resulting in a slight difference in appearance when compared to PU decomposition curves.

The measured weight loss of 11 % (sample consisting of 7 wt.% PU) corresponds well to experimental values, where a weight loss of 10.4±0.9 % was observed for impregnated foams containing 6.9±0.7 wt.% of PU (in the dried state).

Based on the results, the first step of the heat treatment cycle was determined to involve a slow temperature increase of 0.5 $°C \cdot min^{-1}$ up to 600 °C to prevent cracking of the structure at the critical stage of firing the template [19]. Subsequently, the heating rate was increased to 1 $°C \cdot min^{-1}$ up to 800 °C to ensure sufficient handling strength of the body composed of loosely bound particles for transport to the high-temperature furnace.

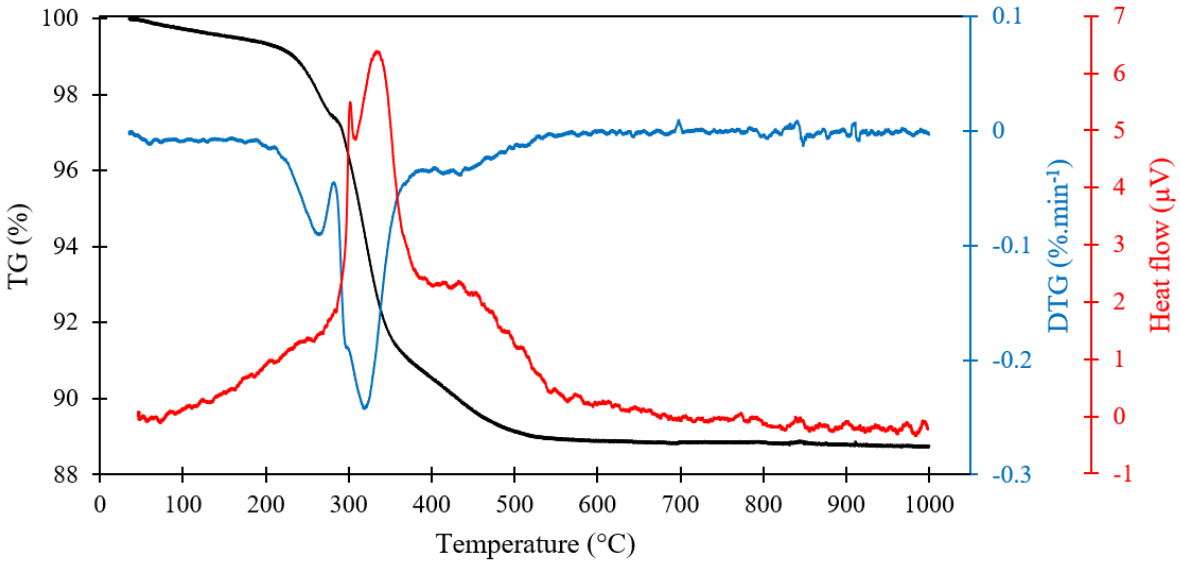

Fig. 29: TG analysis of reticulated PU foam coated by ceramic suspension.

The temperature of sintering was determined based on SEM images, pore size distribution and handling strength of the sintered solids. The evolution of microstructure with increasing sintering temperature is shown in Fig. 30. Individual non-sintered particles corresponding in size to the initial powder can be observed on the microstructure of the sample heat-treated at 1100 °C. The neck formation and bonding of the particles can be observed from 1200 °C, complemented by a progressive reduction of the intrinsic porosity with increasing temperature. The material sintered at 1400 °C seems to be densified.

However, it may be noted that the foam sintered at 1100 °C seems to have smaller pores between individual particles than the one sintered at 1200 °C. A possible reason may be the difference between their heat treatment cycles, where the heating rate was 2 °C·min^{-1} for sintering at 1100 °C, whereas for foams sintered at 1200 °C it was 4 °C·min^{-1}. Due to the longer heating time, the diffusion time was extended, and the particles could approach each other and reduce the microporosity.

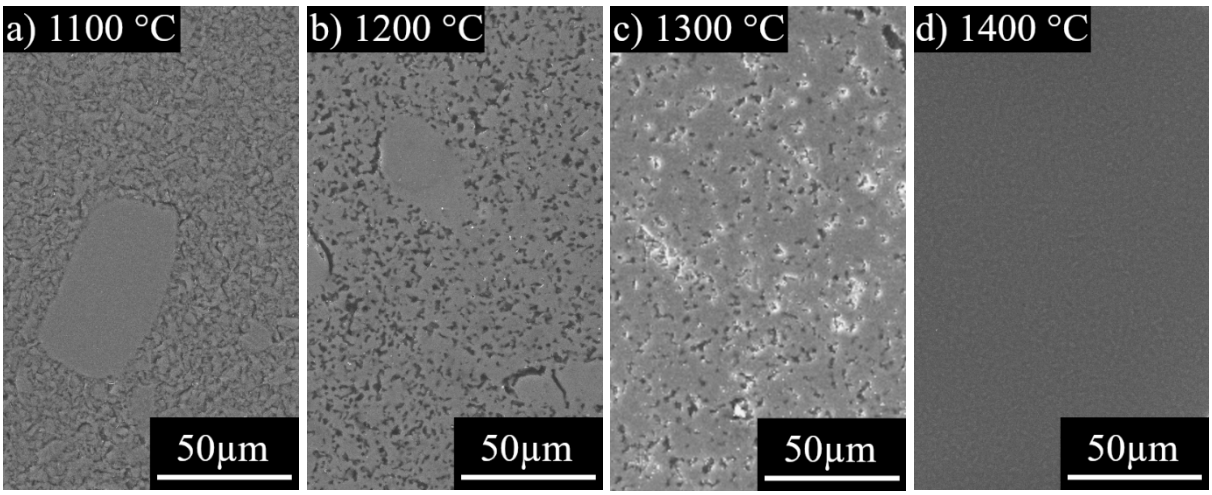

Fig. 30: SEM image of the microstructure of the foam sintered at a) 1100 °C, b) 1200 °C, c) 1300 °C, d) 1400 °C.

The dependence of linear shrinkage on temperature for both 75 and 90 ppi foams is represented in Fig. 31. A small shrinkage occurs already at 1000 °C, and further increases with the temperature. No significant difference was observed between 75 ppi and 90 ppi foams. The linear shrinkage for foams sintered at 1400 °C was 12.2±0.5 % for 90 ppi and 12.1±0.8 % for 75 ppi foams with the same impregnation rate.

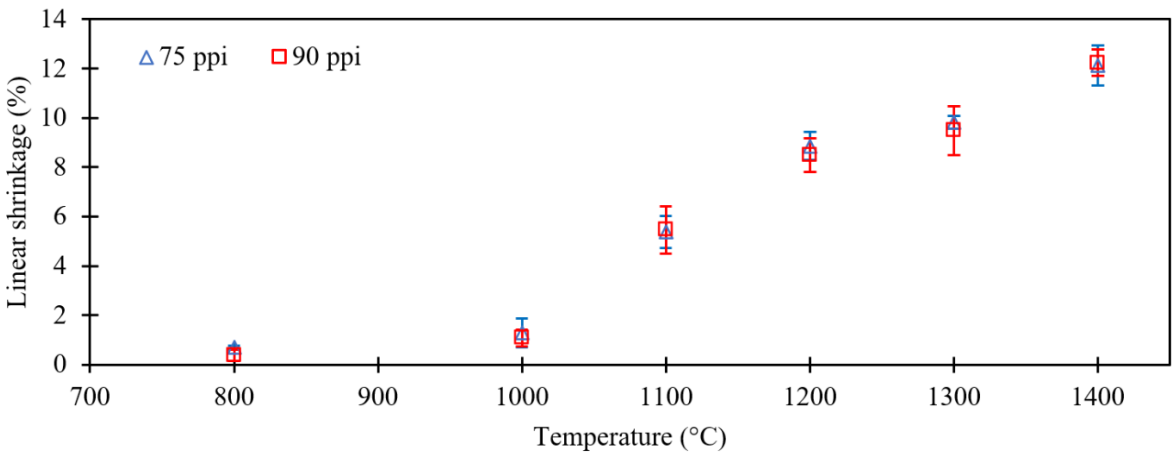

Fig. 31: Linear shrinkage as a function of sintering temperature.

The pore size distribution of 90 ppi foam sintered at 1100–1400 °C can be seen in Fig. 32. The distribution curves maintain a similar shape in all cases, featuring one significant peak at 211 µm, 211 µm, 200 µm and 190 µm, respectively, for increasing temperature. These peaks correspond to the size of the cell windows, i.e. macropores connecting individual cells. Their size decreases with the increasing temperature due to a higher shrinkage. From the detail of high-pressure porosimetry it can be seen that the concentration of pores under 5 µm is reduced for the foams sintered at 1300 and 1400 °C, suggesting that open pores between particles are closed at this temperature, marking the transition to the final stage of sintering at 1300 °C.

Although the results from mercury intrusion porosimetry show that open microporosity is no longer present in the structure sintered at 1300 °C, it can be seen from the SEM micrograph in Fig. 30c that intrinsic closed porosity is still present at this temperature and is reduced when temperature is raised to 1400 °C.

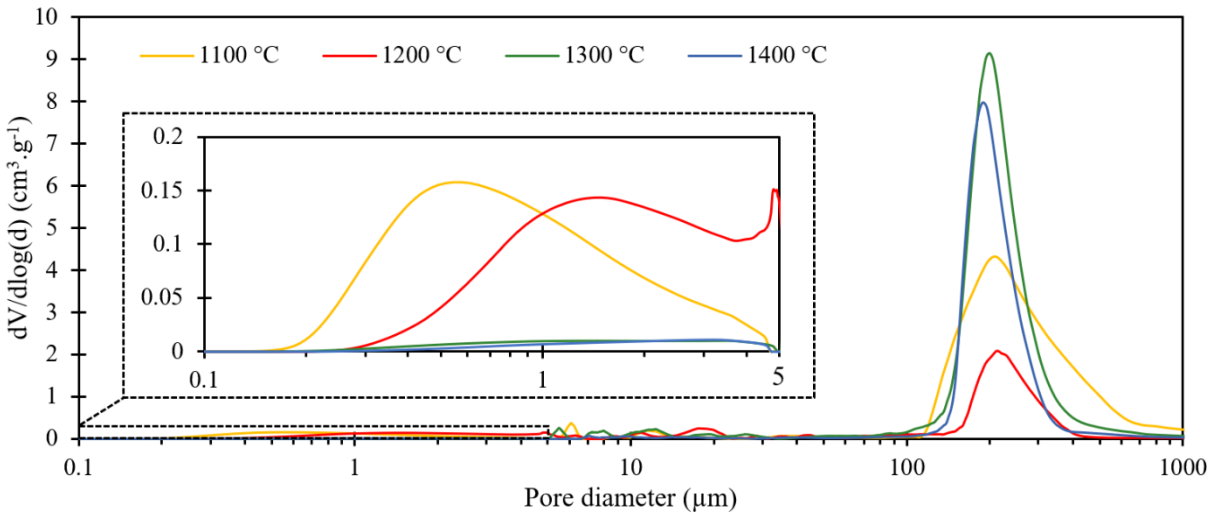

Fig. 32: Pore size distribution for 90 ppi foam sintered at different temperatures (1100–1400 °C), determined by mercury intrusion porosimetry.

The presence of microporosity decreases the mechanical strength of ceramics [92] and thus its removal is preferable. In addition, its presence, together with voids within the struts, is considered ineffective for the process of filtration, because their contribution to the fluid flow is negligible and it is the size of interconnected macropores that primarily influences filtration efficiency [93]. Based on these results, the temperature of 1400 °C was chosen for the sintering.

5.1.4 Filling the hollow struts by infiltration

Triangular voids that remain after burning out the polymeric template are considered as one of the disadvantages of foams prepared by the replica template method, as they act as stress concentrators and reduce their mechanical strength [18]. The presence of these voids is visible on the SEM micrographs of pre-sintered polished specimens shown in Fig. 33. The samples were pre-sintered at two different temperatures (1100 and 1200 °C) to ensure sufficient handling strength to prevent collapse of the structure during infiltration.

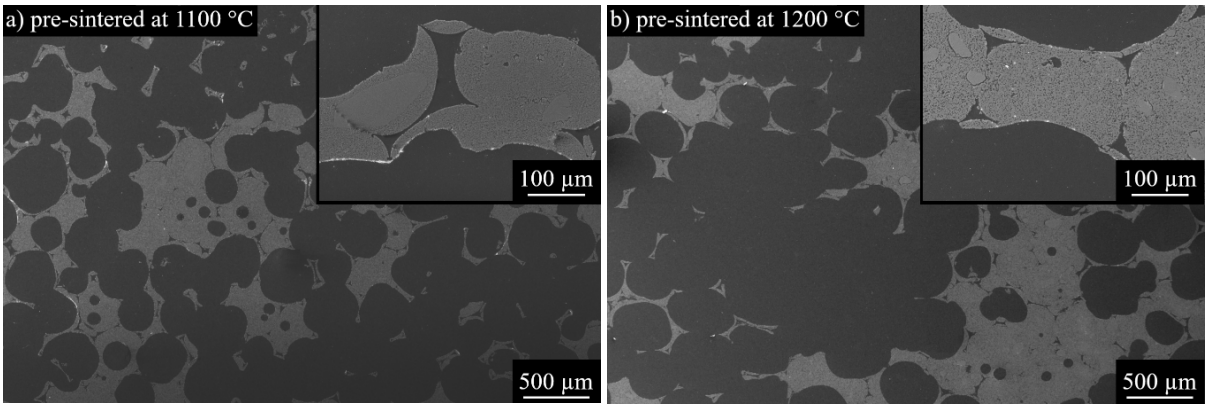

Fig. 33: SEM image of the microstructure (polished cross-section) of the foam pre-sintered at a) 1100 °C, b) 1200 °C.

The microstructure of the foams, infiltrated and sintered at 1300 and 1400 °C, can be seen in Fig. 34a–d. In both cases, partial filling of the hollow struts was observed after sintering at 1300 °C, which should positively affect the mechanical strength by rounding off sharp edges [42]. Some suspension also remained on the outer surface of the struts, however, decohesion of this layer from the substrate was observed in some areas. The solid loading (including the solid content in silica sol) of the suspension used for infiltration (37.8 wt.%) was significantly lower compared to that used for the preparation of the substrates (72.9 wt.%), potentially leading to the creation of these defects due to a different shrinkage rate and different composition of the suspension (higher percentage of SiO_2 in the suspension used for infiltration). Sintering at 1400 °C led to the sealing of the cavities, however, this effect was more pronounced for the foam pre-sintered at 1100 °C. It can be assumed, that foams pre-sintered at 1100 °C have a larger surface area and bigger cavities due to smaller shrinkage, allowing more suspension to get inside.

Therefore, the combination of pre-sintering at 1100 °C and sintering at 1400 °C after infiltration was adopted for selected ceramic foams, as the most significant improvement in microstructure was observed.

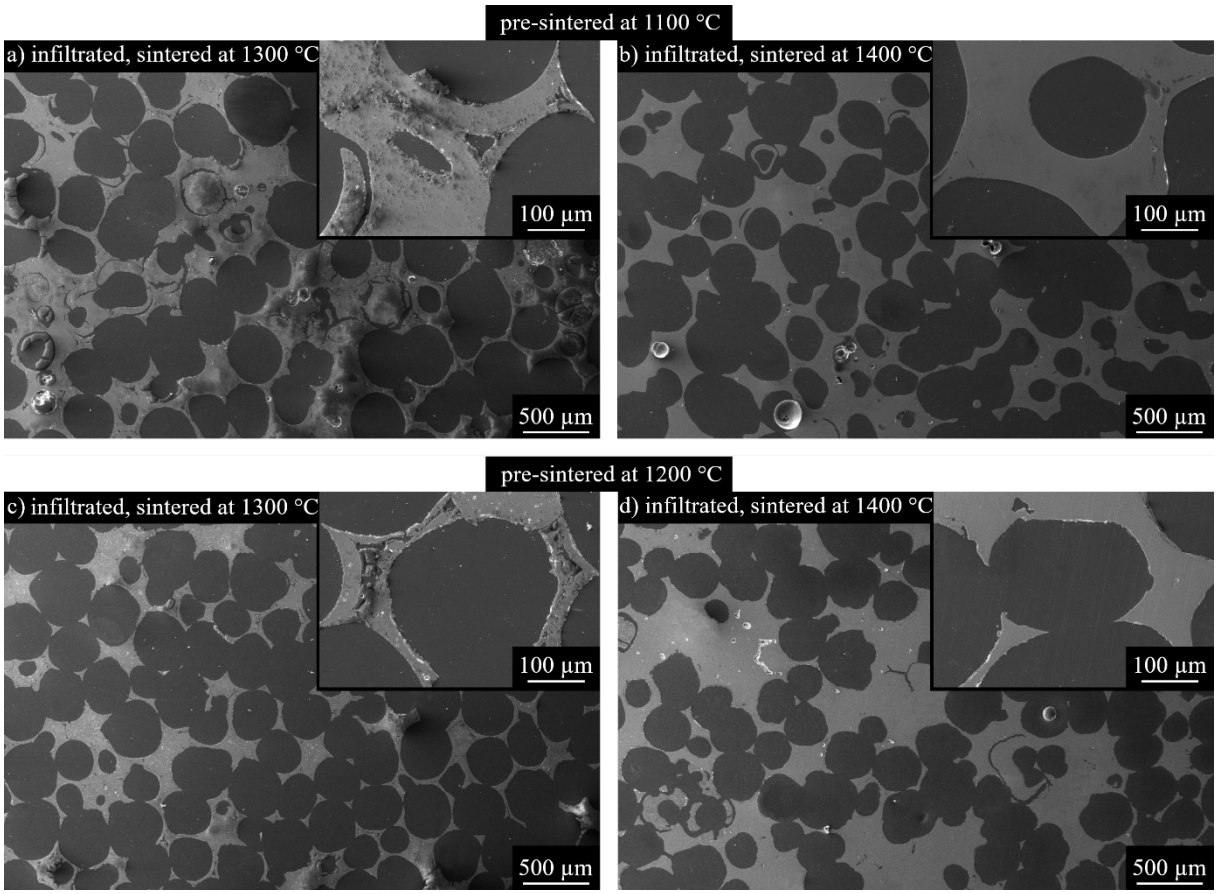

Fig. 34: SEM image of the microstructure (polished cross-section) of infiltrated foam pre-sintered at 1100 °C (a, b) and 1200 °C (c, d); sintered at 1300 °C (a, c) and 1400 °C (b, d).

5.1.5 Scale up

The scaled-up version of the filter is illustrated in Fig. 35a. It consists of two sintered bodies laid freely on each other. Each body is composed of 5 foams, connected by bonding layers (Fig. 35b), which were created by compressing the stacked impregnated wet foams to ensure the cohesion of the body.

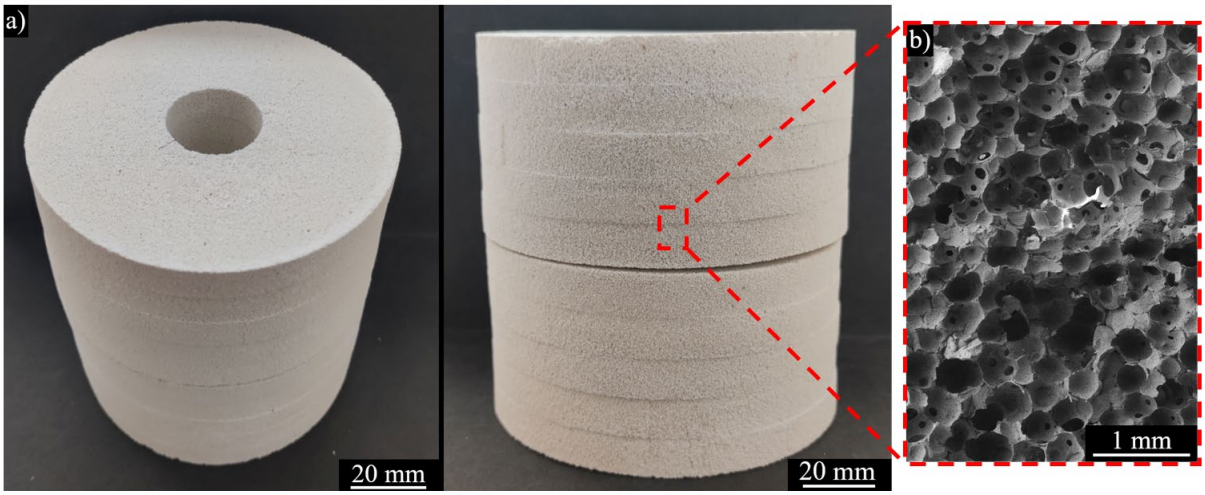

Fig. 35: a) Scaled-up filter composed of two bodies, b) detail of the bonding layer at the interface between the individual foams.

The formation of defects in the form of horizontal and vertical macroscopic cracks was more pronounced in the scaled-up samples. They could be observed already in dried impregnated foams (Fig. 36a), indicating that they were formed during the drying process and then expanded during sintering (Fig. 36b). In the drying phase, a significant concentration of water escapes from the binder and solidification shrinkage occurs [33], which could cause these type of defects. This theory is supported by the fact that cracks were mainly present in spots with a visibly larger amount of applied suspension, leading to a higher moisture gradient and an increased drying rate. To prevent cracking, it would be preferable to incorporate drying in a controlled atmosphere with a reduced drying rate.

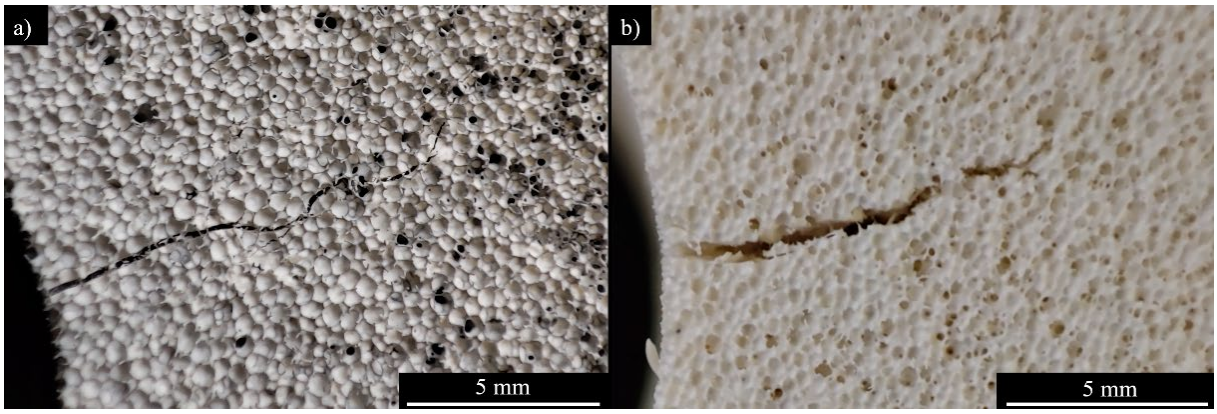

Fig. 36: Macroscopic crack present in the impregnated foam a) after drying, b) after sintering.

Based on the described optimisation process, the processing parameters of the final filters were determined. A total of three types of filters were prepared to compare the effect of pore size and infiltration on their performance. Hereafter in the text, they are referred to as F90 (90 ppi, without infiltration), F90+I (90 ppi, infiltrated) and F75+I (75 ppi, infiltrated). Their phase composition, microstructure and mechanical strength were evaluated and are discussed in the following chapter.

5.2 Characterisation of filters

5.2.1 Phase composition

The analysis of phase composition by X-ray diffraction (XRD) was performed for the filter without infiltration (F90), and with infiltration (F90+I). Infiltrated filters F90+I and F75+I were considered to be equivalent in terms of phase composition. The XRD patterns of the filter with and without infiltration can be seen in Fig. 37. Two crystalline phases were identified, both patterns present the same characteristic peaks corresponding to mullite and SiO_2 in the form of cristobalite. However, it can be noted, that the intensity of cristobalite peaks for the infiltrated foam is higher than for the foam without infiltration.

By quantitative phase analysis, it was determined that the proportion of crystalline phases present in the filter without infiltration corresponds to 93 % mullite and 7 % cristobalite. The infiltrated filter was shown to have a higher content of cristobalite (33 %), which is in agreement with the higher intensity of the cristobalite peaks. This result is consistent with the fact that the suspension used for infiltration had a higher content of SiO_2, thus increasing its overall percentage in the structure.

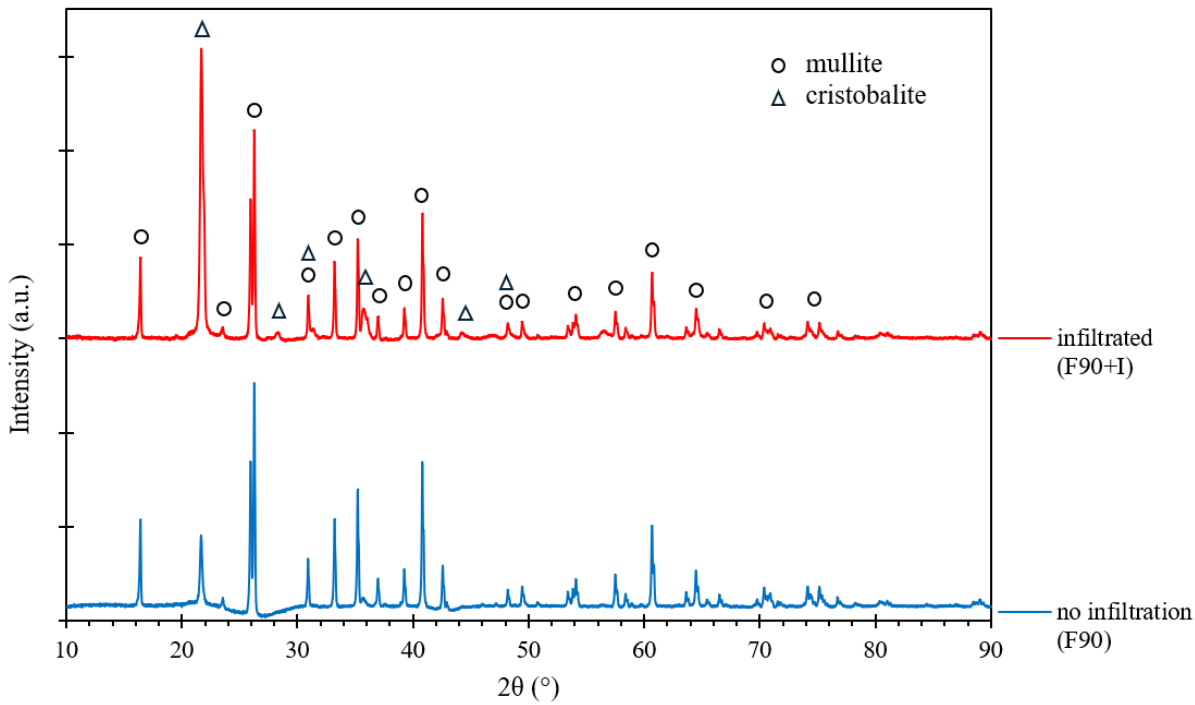

Fig. 37: XRD patterns of the filter without infiltration (F90) and filter with infiltration (F90+I).

Based on the composition of raw starting materials, the weight ratio of Al_2O_3/SiO_2 in the structure should be approximately 38/62 for the filter F90 and 34/66 for the filter F90+I. The starting raw material, Molochite^{TM}, is produced by calcination of kaolin above 1500 °C, and the manufacturer declares that it is composed of mullite and amorphous SiO_2, in unspecified proportions [94]. Although the patterns obtained by XRD analysis do not imply the presence of an amorphous phase (no broad peaks, high measured crystallinity), it should be noted that the weight fraction of crystalline phases may be overestimated when using the Rietveld method to evaluate XRD patterns [95]. Due to the high percentage of SiO_2 in the starting material, the presence of an amorphous phase of SiO_2 in the structure cannot be excluded with certainty. An additional analysis would be necessary for further quantification, for example, XRD with an internal standard.

5.2.2 Microstructure analysis

The morphology and microstructure of the filters at three different magnifications can be seen in Fig. 38–40. The structure is highly porous and reproduces the form of the PU template. Good interconnectivity between cells is evident for filters F90 and F90+I, while filter F75+I (Fig. 40b–c) shows a larger number of sealed windows. However, the image taken at lower magnification (Fig. 40a) shows that this is rather a local phenomenon, as most cells remain visibly interconnected.

Infiltration led to the filling of the strut voids (Fig. 39c), which are present in the case of the filter without infiltration (Fig. 38c) The infiltration process also influenced the surface morphology, as the infiltrated filters have visibly rougher surface due to the suspension applied on the initial structure.

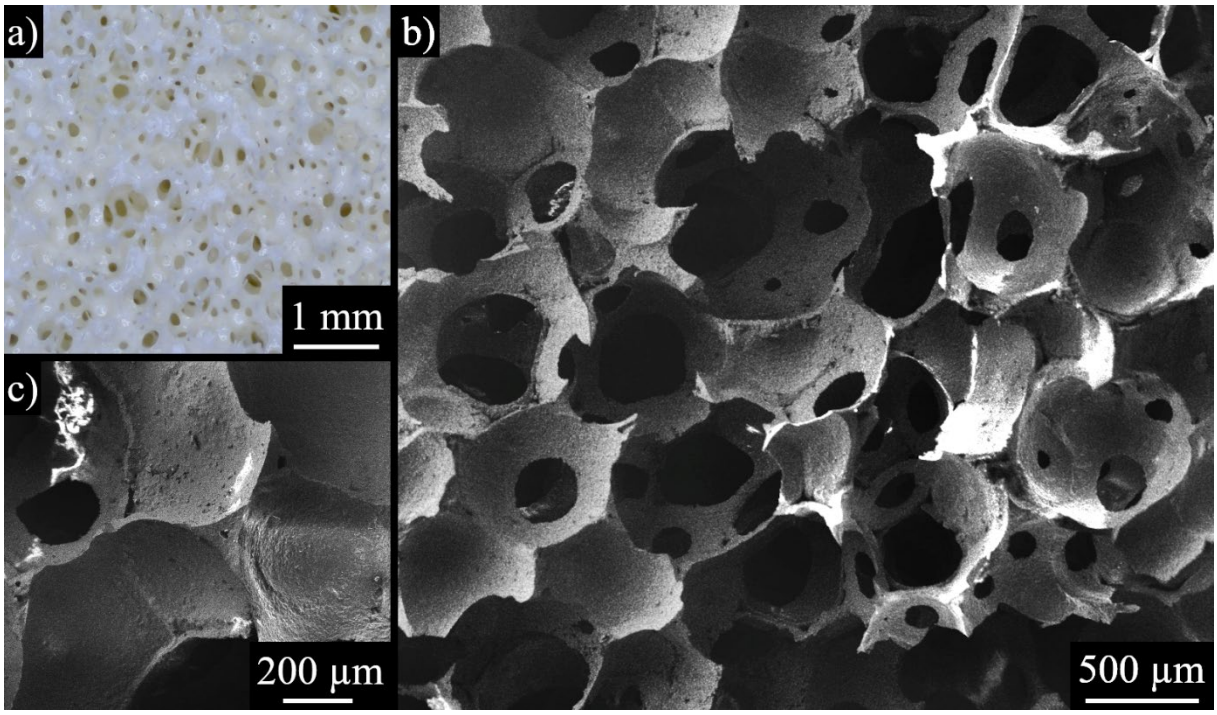

Fig. 38: Microstructure of the filter F90; a) stereomicroscope, b) SEM image of a fractured cross-section, c) detail of the hollow strut.

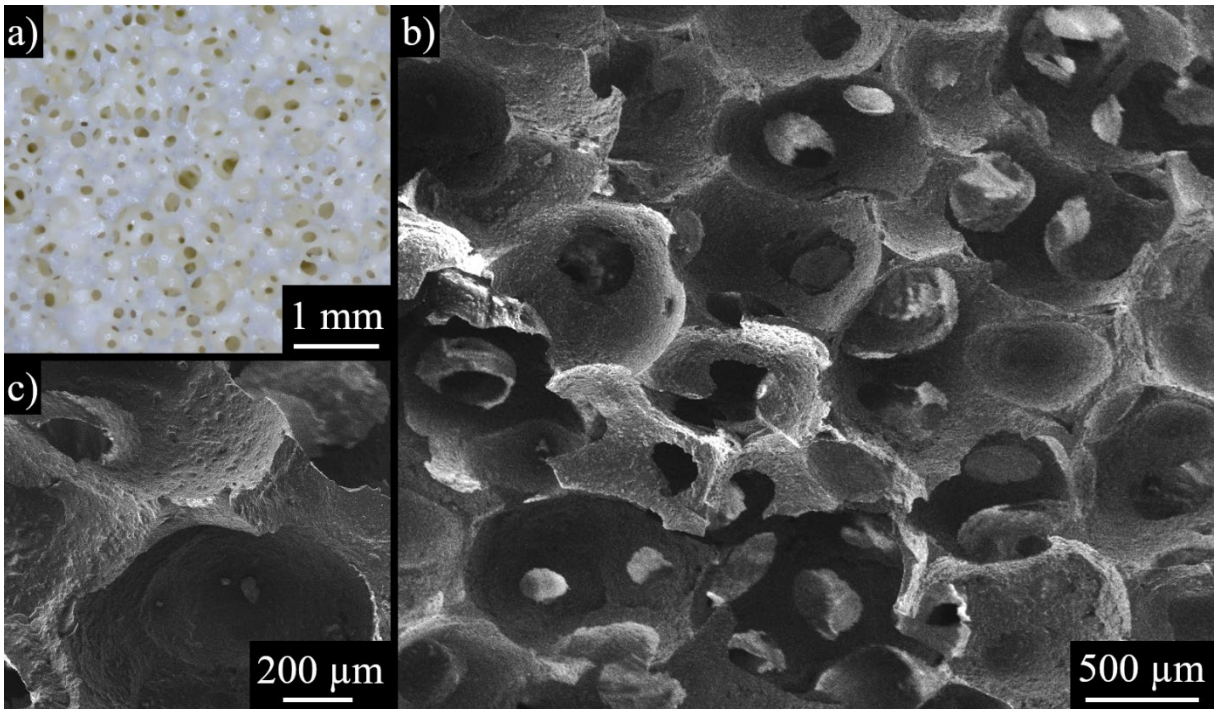

Fig. 39: Microstructure of the filter F90+I; a) stereomicroscope, b) SEM image of a fractured cross-section, c) detail of the dense strut.

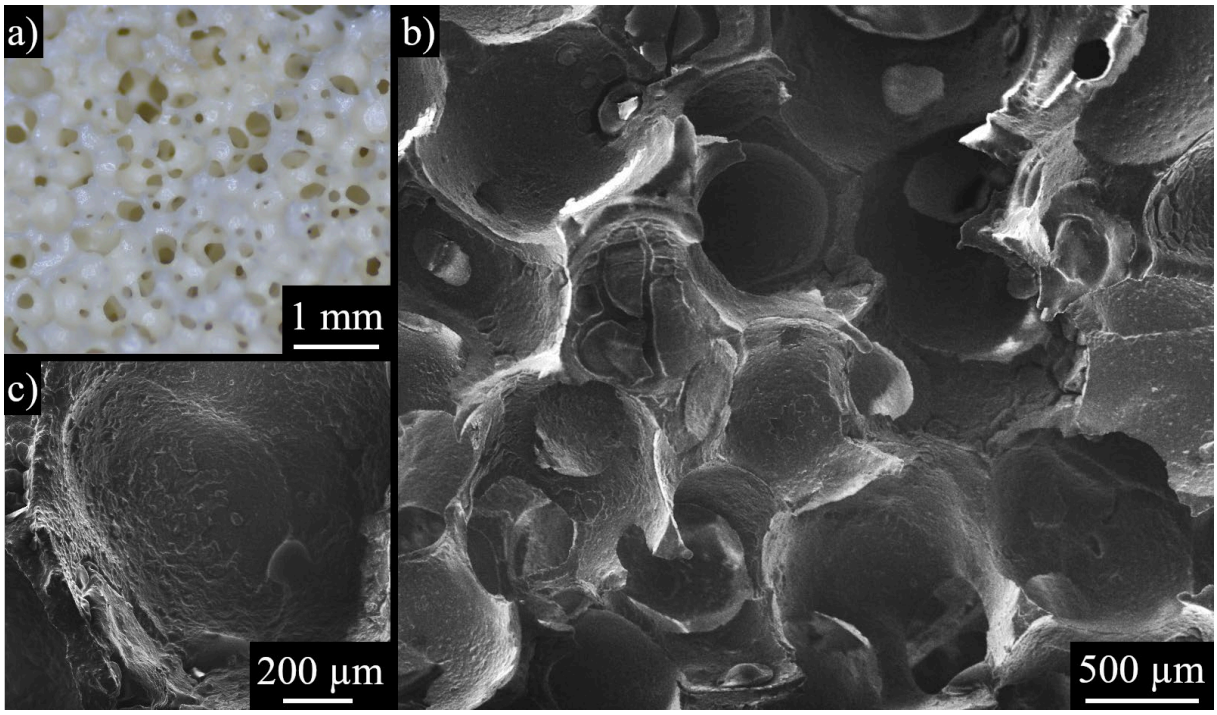

Fig. 40: Microstructure of the filter F75+I; a) stereomicroscope, b) SEM image of a fractured cross-section, c) detail of the sealed window.

The porosity of the prepared filters, along with their average cell size and window size (pores between cells), is detailed in Tab. 8. Porosity ranges between 70 and 78 %, which corresponds to the set target. Filters with filled struts have lower porosity due to the mass increase by infiltration, with the value for 90 ppi being slightly lower due to the higher mass of suspension applied compared to 75 ppi filters (by infiltration the mass increased by 47±8 % compared to 31±2 %).

The ppi number refers to the template used. Ceramic foam prepared by its replication has the same characteristics but the cell size is reduced by the thickness of the applied ceramic suspension and shrinkage after sintering. As the cell size of the template declared by the manufacturer is 440–520 µm for 90 ppi, and 520–720 µm for 75 ppi, the measured values are in agreement with this statement.

The infiltration process led to a slightly smaller cell size and pore size, which can be explained by the increased thickness of the strut due to the second layer of suspension applied.

Tab. 8: Characteristics of prepared filters.

Filter	Porosity (%)		Cell size (µm)	Window size (µm)
F90	77.9±0.5		395±56	125±43
	Before reinforcement (1100 °C)	After reinforcement (1400 °C)		
F90+I	83.4±1.0	70.6±0.3	392±62	124±41
F75+I	82.7±0.6	72.7±0.2	562±57	226±133

The pore size distribution obtained by mercury intrusion porosimetry (Fig. 41) confirms the trend of reducing pore size by infiltration. The distribution for 90 ppi filters is unimodal in the range measured by low-pressure porosimetry with peaks around 190 (F90) and 167 µm (F90+I). Mercury intrusion porosimetry measures the largest entrance of an interconnected open pore [96], which in this case can be interpreted as the window size connecting the

individual cells. The values determined by mercury intrusion porosimetry are however higher than the ones determined by image analysis. The image analysis was performed on 2D images of a 3D foam structure, which could lead to inaccuracy in the measurement of pore size due to potential distortions. The pores might appear smaller than they actually are, as they could be rotated or positioned at different depths within the foam. Therefore, the results obtained by mercury intrusion porosimetry seem to be more relevant. They are also more representative given to the measurement principle on which mercury intrusion porosimetry is based, since the intrusion of a liquid under pressure into a porous structure is a process comparable to filtration.

Filter F75+I exhibited a bimodal pore size distribution with less pronounced peaks around 165 and 519 µm. The window size measured by image analysis indicated above has a rather large scatter of values, which could indicate that the pore size distribution is wide, as it can be seen from the results obtained by mercury intrusion porosimetry. The wide pore size distribution could be limiting for filtration as it could reduce its efficiency [97].

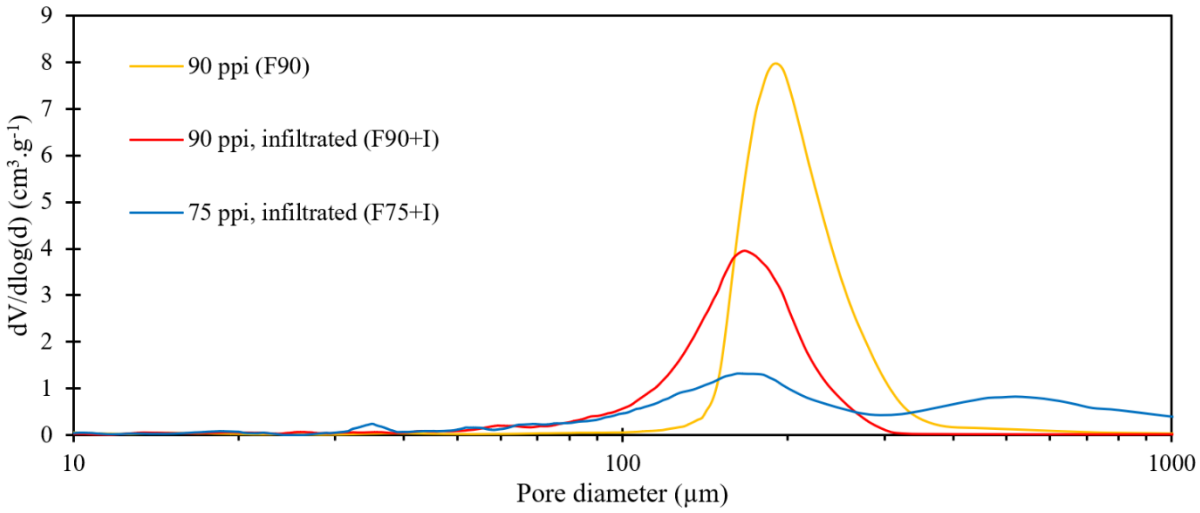

Fig. 41: Pore size distribution of the prepared filters, determined by mercury intrusion porosimetry.

5.2.3 Compressive strength

The influence of infiltration, porosity and pore size on the compressive strength was investigated. A typical stress-strain curve is shown in Fig. 42a, the curves of all but one tested sample had the same character. The strain response to increasing load was linear until the maximum value of compressive stress was reached, at this point, the sample began to crack. The direction of propagation of the macroscopic crack cannot be clearly defined; some propagated parallel to the axis of loading (see Fig. 42b) some perpendicular to it or at an angle of 45°. The fracture mechanism suggests that the failure was not associated with the failure of individual struts, but rather with the propagation of a macroscopic crack through the specimen due to the accumulation of critical damage, as is common in bulk material. This behaviour was ensured by neoprene pads, which distributed the load evenly over the specimen surface and prevented premature failure due to local stress concentration.

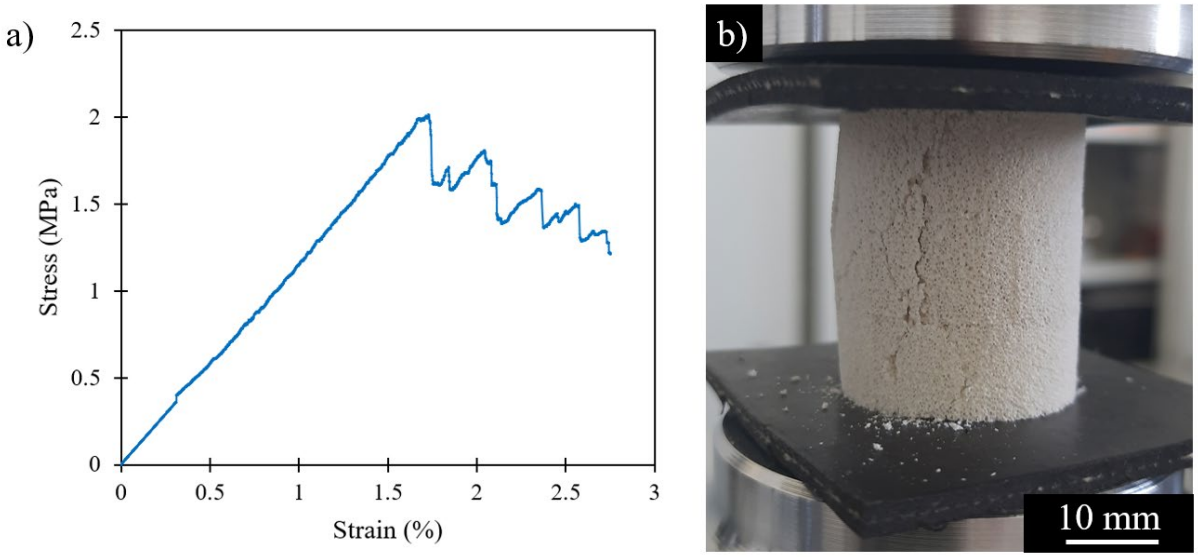

Fig. 42: a) Typical stress-strain curve, b) macroscopic crack propagating through the volume of the specimen.

Due to the lack of material, only 5–6 samples were prepared for each set representing the given filter. Therefore, no reliable statistical statements can be made, but a certain trend was present, as can be seen from the results in Fig. 43.

The measured compressive strengths ranged from 1.35 to 2.42 MPa for samples F90 (porosity 80.0–76.8 %), 1.28 to 1.70 MPa for samples F90+I (porosity 76.3–69.8 %) and 0.61 to 1.17 MPa for samples F75+I (porosity 78.5.79–68.8 %). The compressive strength decreased with increasing porosity for all cases, which is a typical phenomenon for porous ceramics [92]. At the same porosity, the compressive strength was higher for foams with 90 ppi compared to 75 ppi, which is consistent with the fact that foams with bigger cells usually exhibit lower mechanical strength [98].

The results indicate that the reinforcement strategy was not effective since all infiltrated foams have lower strength than those without infiltration. Several factors could have contributed to this surprising result.

First of all, the infiltrated foams have a higher content of SiO_2 in the form of cristobalite, as discussed above in Chapter 5.2.1. This fact could be critical for the strength of the foams, despite the usual positive effect of infiltration in terms of reduced porosity and void-filling. Ceramic materials containing mullite and cristobalite can tend to crack during cooling from the sintering temperature, as explained in the study of Sato et al. [99]. There is a big mismatch of thermal expansion coefficient between mullite and cristobalite, which can cause thermal stresses and lead to cracking at rather high temperatures (650–750 °C). In addition to that, the β-α phase transformation of cristobalite at around 250 °C is accompanied by a large volume contraction, which can lead to the creation of tensile stresses inside the structure and lower the mechanical strength of the material. The mechanical strength could be also decreased by the presence of a brittle SiO_2 phase, potentially amorphous, between the grains [98, 100].

Another factor could be the presence of more critical defects, as infiltrated foams are more susceptible to their creation during preparation. During infiltration, the foams pre-sintered at 1100 °C are prone to damage due to the low mechanical strength of the incompletely sintered body. They also undergo two drying processes of the suspension, which have been shown to be critical for crack formation in the structure.

It was also noticed that the foams without infiltration exhibited partial void sealing due to shrinkage after sintering, reducing the negative effect of triangular stress concentrators.

However, to give a more precise explanation, a larger statistical set of values, and further analysis of fracture surfaces and microstructure would be required.

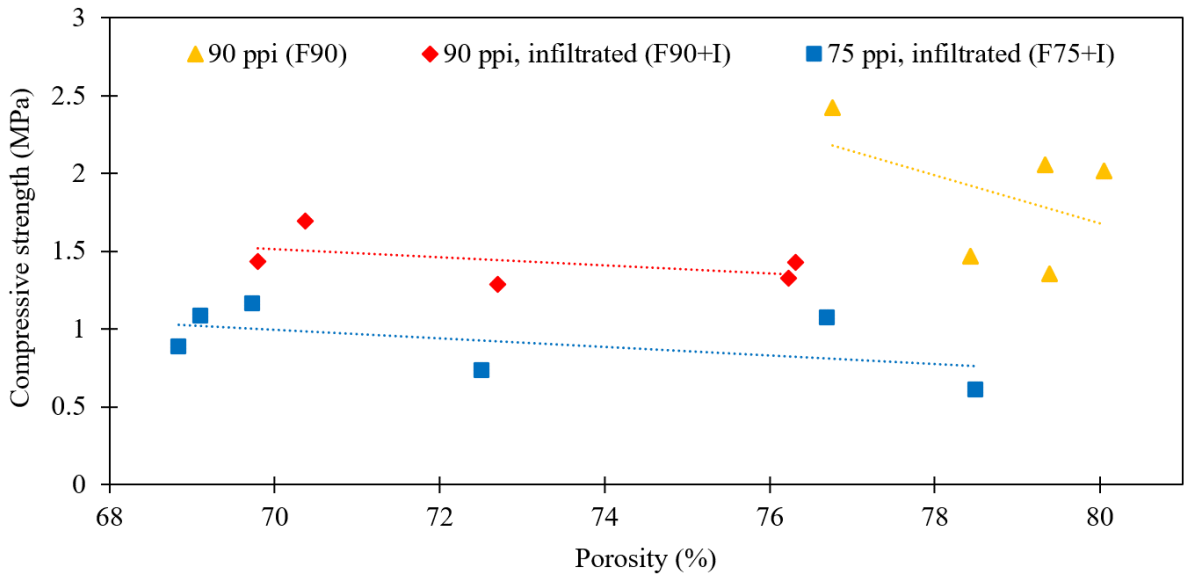

Fig. 43: Compressive strength as a function of porosity.

5.2.4 Filtration capacity

Due to delays in the fabrication of the filtration unit, it was not possible to test the prepared filters for their filtration capacity as part of this work. However, the suitability of the prepared foams for filtration can be discussed based on their microstructural properties. As it was already mentioned, the key properties of a filter with high efficiency are the following:

- Porous structure with interconnected pores, to allow the fluid flow,
- Unimodal and narrow pore size distribution, tailored to the size of contaminants, to ensure the efficiency of filtration,
- Sufficient mechanical strength, to withstand the pressure of the fluid. [60]

Based on the determined properties, filter F90 (90 ppi, no infiltration) and F90+I (90 ppi, infiltrated) seem to be the most suitable candidates, as they both meet the essential requirements of porous ceramics usable in filtration. They have an open porous structure with interconnected pores, unimodal pore size distribution and sufficient mechanical strength, with a value slightly higher for the filter without infiltration. The filter F75+I exhibited a wide size distribution and lower mechanical strength, which could negatively influence its performance.

As mentioned in Chapter 2.1.2, the filtration process of an electro-insulating oil usually consists of multiple steps where the liquid passes through filters with different pore sizes from coarse to fine, each designed to remove a different type of contamination. The size of contaminants is usually on the scale of units to hundreds of microns [101]. Given the relatively big pore size achievable by the replica template method, it is envisaged to employ the filters prepared by this technique in the first step of filtration to ensure the removal of the largest particles from the service-aged oil. A detail of the coarse particles present in the mechanically contaminated oil can be seen in Fig. 44.

Another possibility is that they could serve as a macroporous support for a membrane with smaller pores. The interest in using macroporous foam as a support is to provide sufficient mechanical strength and minimise the pressure drop due to the larger pore size while ensuring high filtration efficiency through the active layer of the membrane. Foams with similar characteristics have been successfully employed as macroporous supports in the study of Park et al. [67]. They used porous cordierite foams with a porosity of 80 %, pore size of 100–200 µm and mechanical strength of 2.7–2.9 MPa as supports for a membrane and achieved a removal efficiency of 99.99 % for particles of 0.5–10 µm.

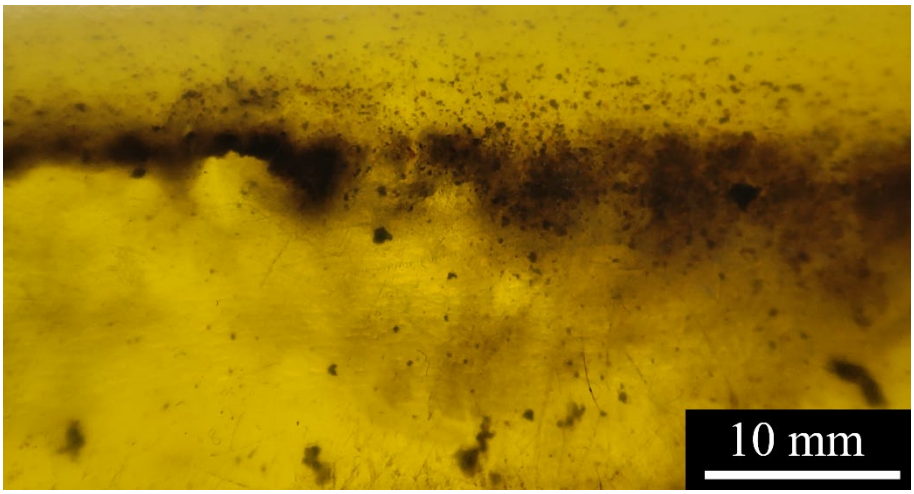

Fig. 44: Detail of large particles present in the mechanically contaminated electro-insulating oil.

The filtration device being developed within the project TAČR FW06010300, of which this thesis is a part, aims to purify the oil using a single filter rather than a series of individual filters. Given the wide size distribution of the particles to be removed from the oil, the fabrication of a hierarchical filter is proposed as a potential solution. Although the prepared filters will be tested separately to determine their individual filtering capacities, it is likely that, in the final design, the foams prepared by the replica template method will constitute only one layer of the hierarchical filter.

6 DIRECT FOAMING – RESULTS AND DISCUSSION

Porous foams prepared by the replica template method are limited in terms of minimal pore size by the properties of the replicated template, and by the presence of hollow struts and defects created during its firing. To propose an alternative and prepare filters with smaller pore size and dense struts, the preparation by direct foaming based on polyurethane (PU) foam system was investigated.

6.1 Optimisation of processing parameters

6.1.1 Composite foams composition

For optimisation of the processing parameters, the influence of composition and processing time of the composite foams on their microstructure and handling strength was investigated. An overview of the samples prepared during this study is given in Tab. 9, along with porosities of the corresponding ceramic foams obtained after sintering at 1200 °C.

Tab. 9: Overview of samples prepared as part of the optimisation of the composition.

Sample	Powder (g)		H_2O (g)	Polyol (g)	MDI (g)	Powder/PU weight ratio	Geometric porosity (%)	Archimedes porosity (%)
	Molochite™	SiO_2						
C1	5	-	-	3.15	1.85	1	88.2	-
C2	5	-	0.03	2.85	2.12	1	90.4	-
C3	5	-	0.05	2.61	2.34	1	91.5	-
C4	3.6	1.4	-	3.15	1.85	1	-	-
C5	8	-	-	3.15	1.85	1.6	86.7	86.4
C6	9	-	-	3.15	1.85	1.8	86.0	84.8
C7	10	-	-	3.15	1.85	2	83.0	82.0
C8	11	-	-	3.15	1.85	2.2	80.6	80.1
C9	6*	-	-	3.15	1.85	1.2	81.1	-

* powder milled for 2 h

For the first set of experiments, the ratio between ceramic powder and PU was fixed to 1 and the influence of added water (samples C2, C3) and SiO_2 powder (C4) were studied.

Water acts as a blowing agent by reacting with isocyanate groups to form CO_2 according to equation (2) (see Chapter 2.3.4). The addition of water resulted in increased porosity and a more homogeneous microstructure (Fig. 45b–c) compared to the sample without water (Fig. 45a). However, both samples with added water exhibited poor handling strength and fell apart at the slightest application of force.

Poor handling strength was also the limiting factor of the sample with increased SiO_2 content (Fig. 45d). It fell apart immediately after sintering, thus its porosity could not be measured. However, considering the porosity of the composite foam before heat treatment it can be assumed, that its porosity after sintering would exceed 90 %.

Based on these results, subsequent experiments were conducted without the addition of water or SiO_2 powder.

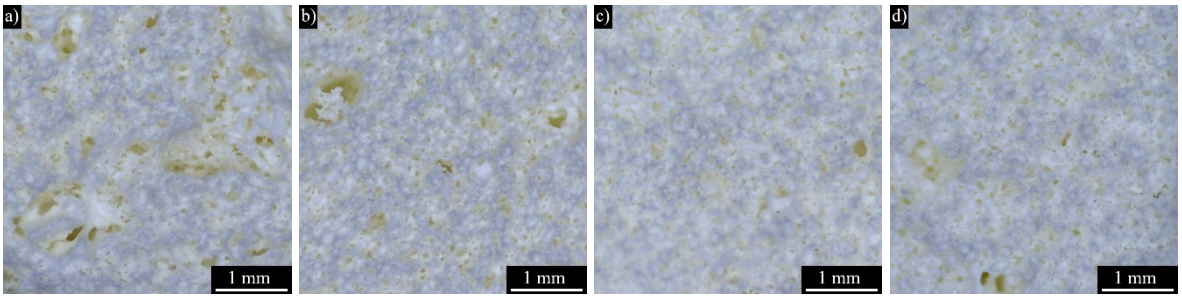

Fig. 45: Microstructure of samples with an equal ratio of powder and PU with a) 0 wt.% H_2O (C1), b) 1 wt.% H_2O (C2), c) 2 wt.% H_2O (C3), d) 0 wt.% H_2O, 14 wt.% SiO_2 (C4); sintered at 1200 °C.

Due to a relatively poor handling strength of the sintered foams with an equal ratio of powder and PU, an increase in powder loading was considered for the next stage of optimisation. Therefore, samples with powder/PU ratio varying from 1.6 to 2.2 were prepared (C5–C8) and the corresponding microstructures obtained after sintering can be seen in Fig. 46.

Higher powder loading increased the viscosity of the mixture, which made its processability more difficult. When the ratio was higher than 2, the mixture could not properly fill the mould due to the high viscosity, which resulted in an incorporation of irregular pores into the structure. Furthermore, the foaming ability was also affected and a lower final volume was observed with increased powder loading (the increase in volume by foaming went from 262 % to 227 % for samples C5–C8). Increasing the powder to PU ratio from 1 to 2.2 increased the rigidity of the foams and reduced the porosity from 88.2 to 80.6 %. To verify the values of porosity determined by the geometric method, the Archimedes method was used, and comparable values were obtained (see Tab. 9).

A powder/PU ratio of 2 was identified as the limit for achieving a homogeneous incorporation of powder with PU precursors while achieving increased strength.

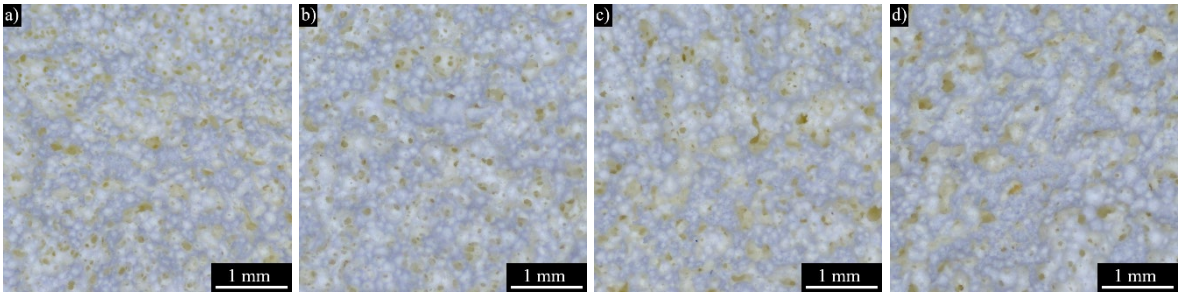

Fig. 46: Microstructure of samples with increasing powder/PU ratio, a) 1.6 (C5), b) 1.8 (C6), c) 2 (C7), d) 2.2 (C8); sintered at 1200 °C.

Due to the large particle size of the initial raw powder, a preparation from milled powder with finer particles was also considered (C9). The characteristics of the milled powder are presented in Chapter 5.1.1.

The above-described optimisation of powder to PU ratio is adapted for the use of raw Molochite™ powder. The larger specific area of the milled powder with finer particles made it difficult to incorporate it homogeneously with PU precursors. Therefore, its quantity had to be reduced and the limit ratio for obtaining a defect-free structure was found to be 1.2.

The change in the microstructure of the foam prepared by direct foaming due to the reduction in powder particle size (Fig. 47) is similar to that prepared by the replica template method (Fig. 27). There is a visible reduction of larger particles with sharp edges, which enhanced their sintering activity.

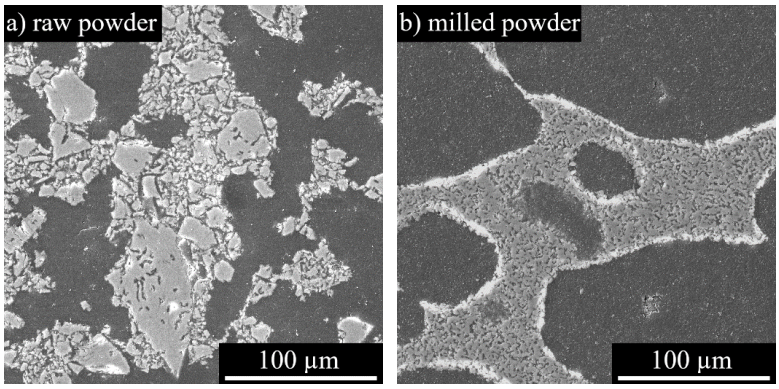

Fig. 47: SEM image of the microstructure of the sample prepared from a) raw powder (C7), b) milled powder (C9); sintered at 1200 °C.

Based on the discussed results, foams with compositions referred to as C7, prepared from raw powder, and C9, prepared from milled powder, were chosen for the next stage of experiments. Although the use of milled powder improved the microstructure, the foam from raw powder was kept in the evaluation due to the possibility of higher powder loading.

6.1.2 Composite foams processing

In this set of experiments, in addition to the initial 2 min homogenisation, the mixture was allowed to foam freely in the air before filling the mould. At the same time, the mixture was stirred every 3 min for 20 s to prevent excessive bubble growth.

The change in processing time did not have any significant influence on the linear shrinkage of the foams after sintering. However, the gradual breaking of the nucleated bubbles had a significant effect on the microstructure, as it can be seen from Fig. 48.

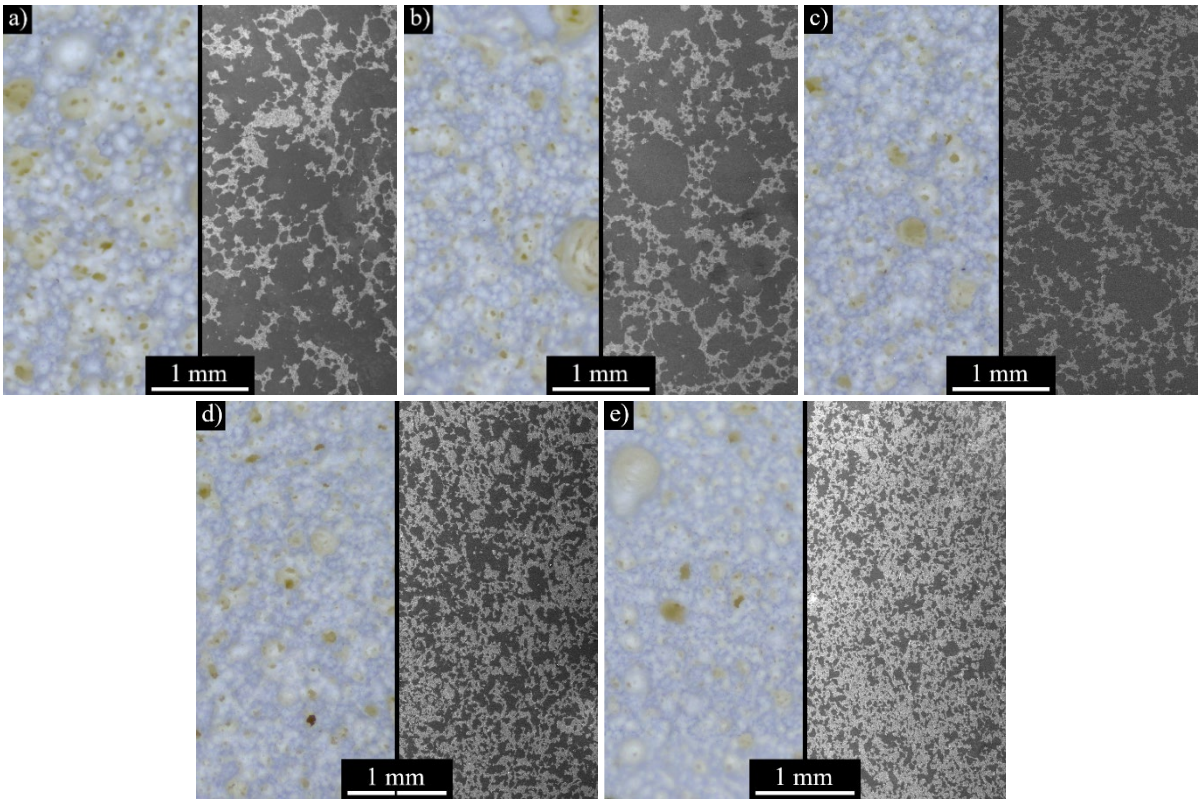

Fig. 48: Influence of processing time on the microstructure of the sample C7 (stereo microscope and SEM polished cross-section), a) 5 min, b) 10 min, c) 15 min, d) 20 min, e) 25 min; sintered at 1200 °C.

From the micrographs in Fig. 48, a reduction in pore size and porosity with increasing processing time is evident. The corresponding values of porosity are given in Tab. 10.

The foam processed for 25 min started to solidify before the mould filling which led to an incorporation of irregular pores. Therefore, the processing time of 20 min was determined to be the limit. At the same time, it was chosen as the optimum because the pore size and porosity were reduced, therefore a higher mechanical strength can be expected.

Tab. 10: Influence of processing time on porosity for sample C7, sintered at 1200 °C.

Processing time (min)	**5**	**10**	**15**	**20**	**25**
Archimedes porosity (%)	84.8	77.7	77.6	74.7	71.3

6.1.3 Heat treatment

Ceramic foams were obtained by burning out the PU from composite foams. The curves obtained by TGA of composite foam containing 67 wt.% of ceramic powder (sample C7) are plotted in Fig. 49. Three stages of mass loss corresponding to the decomposition of PU can be identified. The appearance of the curves and position of exothermic peaks corresponds well with the decomposition of rigid PU foams in the air atmosphere, as reported by Jiao et al. [102]. The measured mass loss of 35 % corresponds approximately to the amount of PU in the composite (33 %). The difference was probably caused by a slightly different ratio of powder to PU in the analysed sample. The experimentally measured mass loss for samples with 67 wt.% of PU was 33.0±0.6 %.

Although the decomposition of PU is completed at around 580 °C, due to its relatively high proportion in the composite foam, the first step of heat treatment was carried out up to 1000 °C. This temperature was chosen to ensure sufficient handling strength and to avoid a collapse of the structure composed of non-sintered ceramic particles after the PU was burned out.

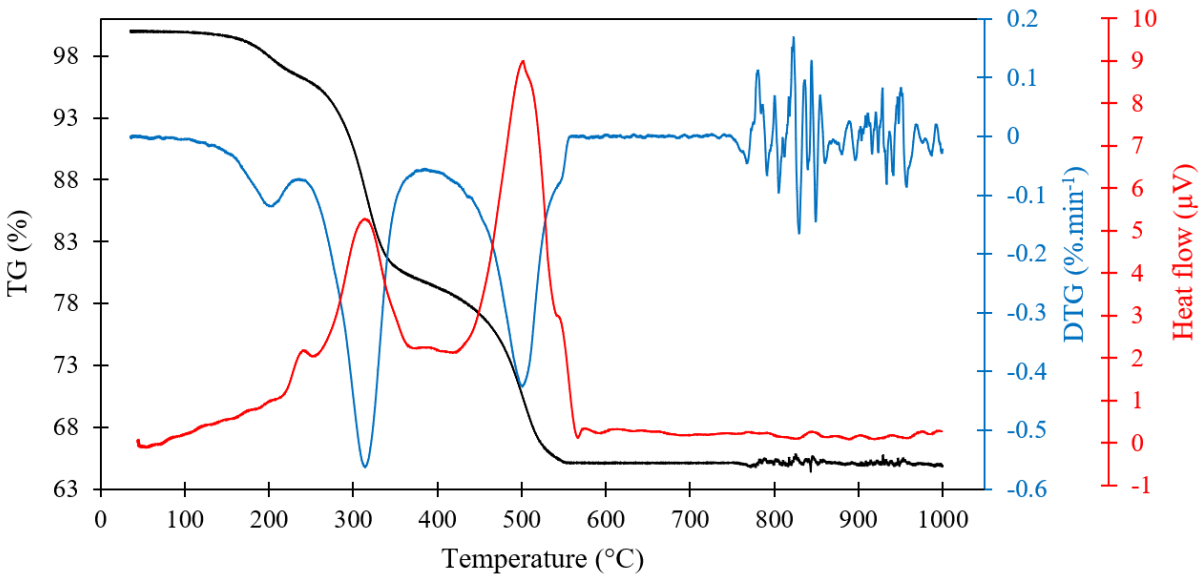

Fig. 49: TG analysis of composite foam prepared by direct foaming.

After firing the PU from the composite, the next heat treatment step consisted of sintering to densify the material. The evolution of microstructure with the increasing sintering temperature for the samples from raw and milled powder is illustrated in Fig. 50 and Fig. 51, respectively.

At 1200 °C, the individual coarse particles of the raw powder can be distinguished. The necks formed between the particles are visible at 1300 °C, and further growth can be observed at 1400 °C. However, it can be seen that even at this temperature, the material is still not fully densified and there is a lot of microporosity between the necked particles.

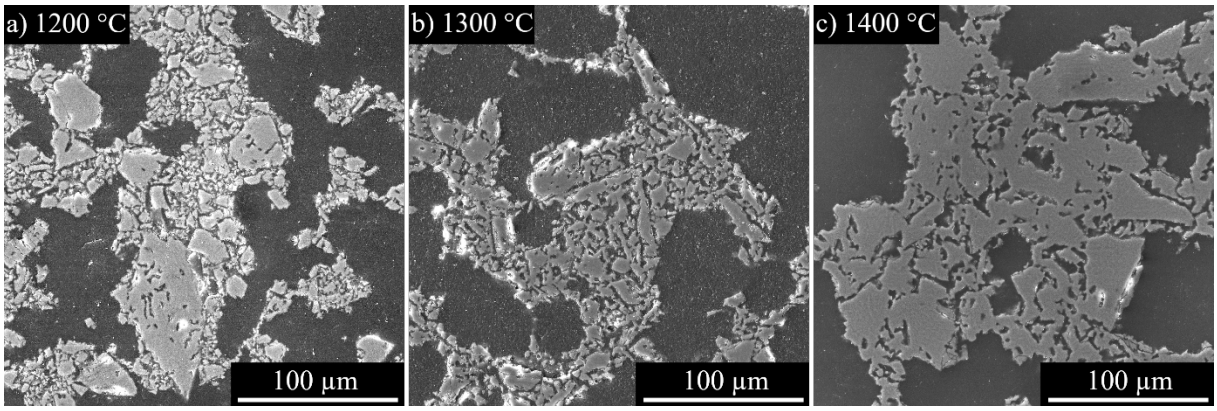

Fig. 50: SEM image of the microstructure (polished cross-section) of sample C7 (raw powder) sintered at a) 1200 °C, b) 1300 °C, c) 1400 °C.

In contrast, the microstructure obtained from milled powder consists of finer particles, which, as already mentioned, increases their sintering activity. Therefore, densification can be observed already at 1400 °C, as can be seen in Fig. 51c.

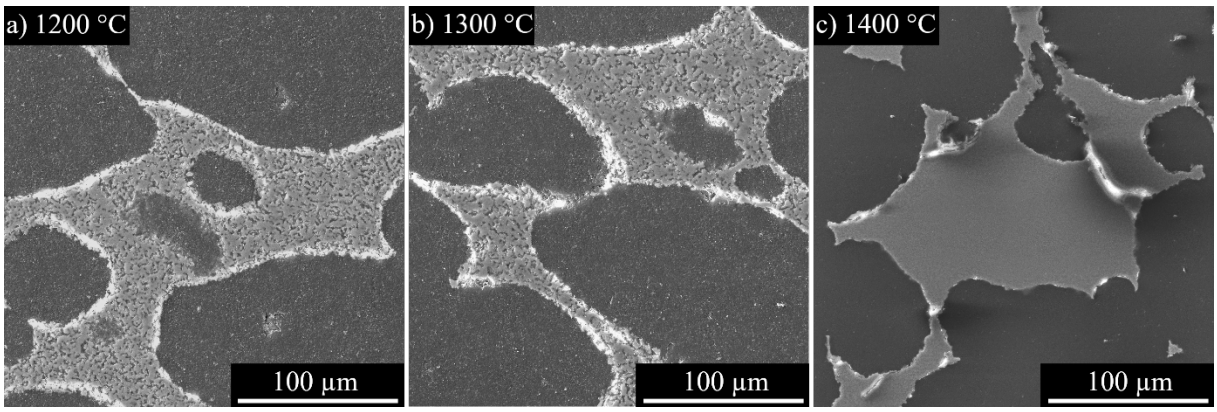

Fig. 51: SEM image of the microstructure (polished cross-section) of sample C9 (milled powder) sintered at a) 1200 °C, b) 1300 °C, c) 1400 °C.

6.1.4 Scale up

To evaluate the possibility of using the prepared foams for filtration, a scale-up experiment was performed. However, the preparation of composite foam in a larger volume presented several complications, as it can be seen in Fig. 52. The first issue was the presence of irregular large pores resulting from the difficulty in controlling their size during foaming. This was followed by the presence of macroscopic cracks, and last but not least, the creation of a cavity inside the body. A possible explanation is that, due to the large volume, the foamed body cured at a slower rate, progressively from the outside to the inside. Unstable bubbles may have

therefore coalesced, and eventually formed a cavity inside the body. This process could be implied by the different microstructure of the foam when observed from the exterior and interior of the hollow body, as shown in Fig. 52b. On the external side, which was in contact with the air, the same microstructure as for foams prepared in smaller volumes can be observed, consisting of smaller pores relatively homogeneously distributed. In contrast, on the inner side, this character was lost, and a rather dense structure with randomly distributed large pores was present.

To limit bubble coalescence, the foam could be perhaps stabilised by a catalyst, which is often used to maintain the balance between the crosslinking and foaming reactions [103]. However, further exploration of this solution was beyond the scope of this thesis.

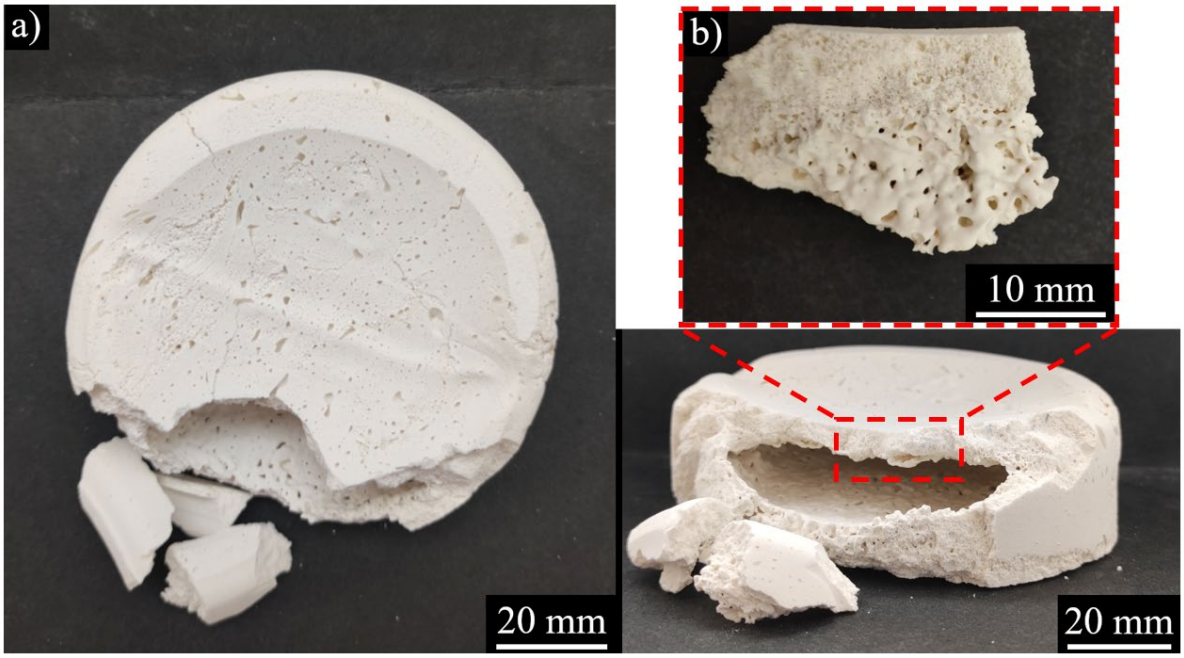

Fig. 52: a) Scaled-up version of sample C7, b) detail of the wall with two different morphologies.

For the reason of poor control over the resulting structure, direct foaming was found to be unsuitable for the preparation of large-sized filters. Even though the scale-up process was not successful, the phase composition and microstructure of two selected samples, C7 and C9, were analysed for their potential use on a smaller scale.

6.2 Characterisation of filters

6.2.1 Phase composition

To determine the phase composition of the foams sintered at 1400 °C, an analysis of the pattern obtained by X-ray diffraction (Fig. 53) was performed. The retrieved pattern corresponds to the pattern of mullite, which was the only crystalline phase identified by the quantitative analysis. Compared to the foams prepared by the replica template method, the foams prepared by direct foaming contained less SiO_2 due to the absence of silica sol binder.

The phase composition of the sintered foam is the same as that of the initial ceramic powder, indicating that no phase transformation occurred during heat treatment. Since the powder was obtained by calcination of kaolin above 1500 °C, this was to be expected.

However, the weight ratio of Al_2O_3/SiO_2 in the starting ceramic powder is approximately 45/55 (neglecting the content of minor oxide phases), indicating a higher content of SiO_2 than

in mullite. The manufacturer declares the presence of an amorphous SiO_2 in the starting powder Molochite™ [94], therefore, it may also be present in the sintered foam, but due to its amorphous nature, it was not detected by XRD. Further analysis would be necessary to confirm this statement.

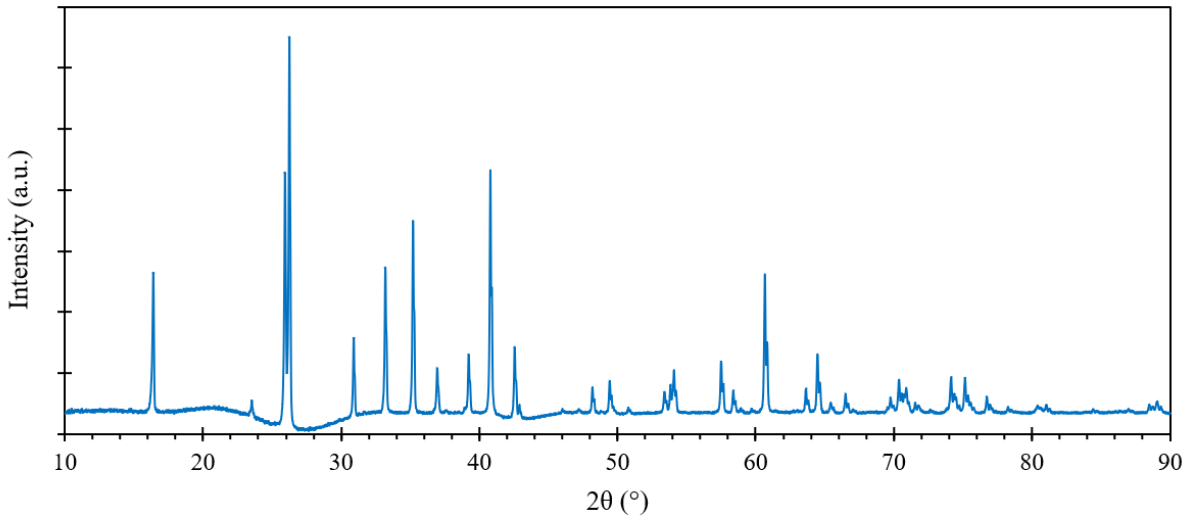

Fig. 53: XRD pattern of the foam prepared by direct foaming, corresponding to the pattern of mullite.

6.2.2 Microstructure analysis

The morphology and microstructure of the foam from the raw powder can be seen in Fig. 54. Due to the high powder loading and coarser sharper particles in the composite foam, the circular character of pores was partially lost. In addition to the pores formed by the release of CO_2, microporosity between grains resulting from sintering can also be observed in the detail of the microstructure in Fig. 50c. As it was mentioned before, the microporosity in the presence of macropores is not usually effective in the filtration process and its presence could negatively influence the mechanical strength of the foams.

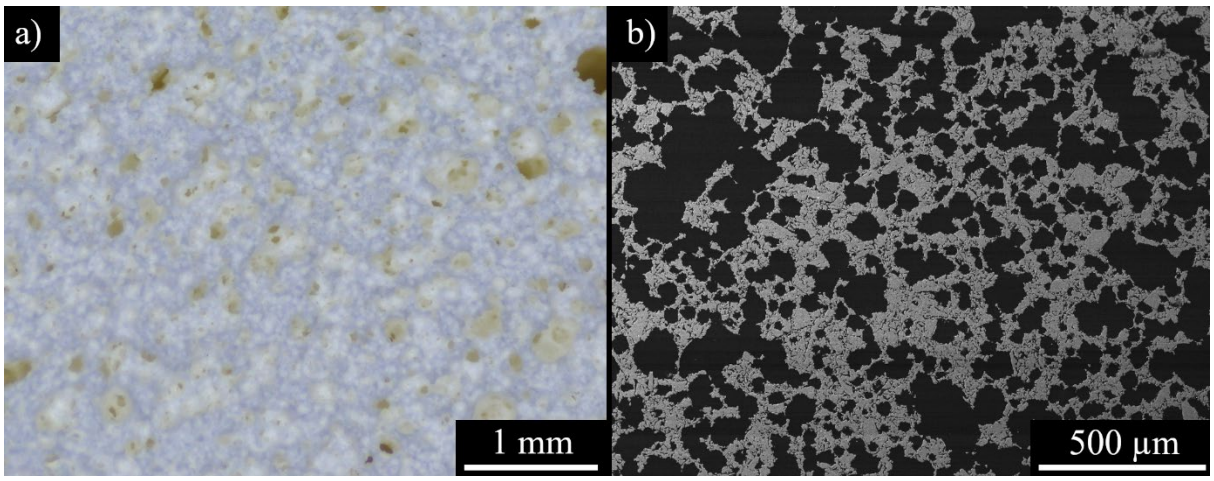

Fig. 54: Microstructure of the sample C7 (raw powder); a) stereomicroscope, b) SEM polished cross-section; sintered at 1400 °C.

Compared to the sample from raw powder, the foam from milled powder consists of pores with more pronounced circular shape. Just by visual observation of the micrograph in Fig. 55b, it can be stated that it also has a higher porosity due to the lower powder loading.

The objects visible inside some larger circular pores are most likely artefacts created while cutting the larger body into smaller samples – to achieve a flat surface, the sample was sanded on a sandpaper and the separated particles probably filled the pores. These artefacts were removed before evaluating the pore size by image analysis.

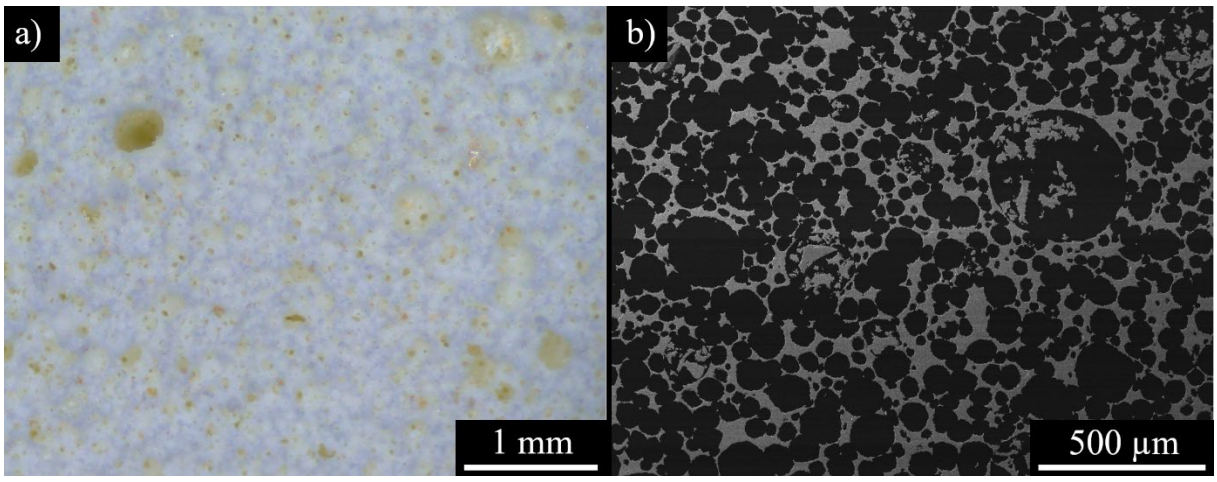

Fig. 55: Microstructure of the sample C9 (milled powder); a) stereomicroscope, b) SEM polished cross-section; sintered at 1400 °C.

Based on the procedure described in the experimental part of the work, the pore size was evaluated by image analysis. For clarity, the measured values were summarised into a histogram with intervals of 15 µm, given in Fig. 56, together with the distribution of pore size in terms of their percentage of the total pore volume. For both samples, the majority of pores were determined to be in the range of 5–200 µm, with a few larger irregular pores present locally. The highest number of pores for both samples was found to be between 35 and 50 µm. When considering the volume of the pores of the given size, the distribution peak shifts to the right, as pores with larger diameter have a more significant contribution to the volume fraction.

For both samples, the pores were evaluated over the same area of 10 mm^2, so the visibly higher number of measured pores in the sample from milled powder indicates its higher porosity, which was confirmed by the experimentally measured value of 73.2±0.6 % compared to 68.8±0.8 % for the sample from raw powder.

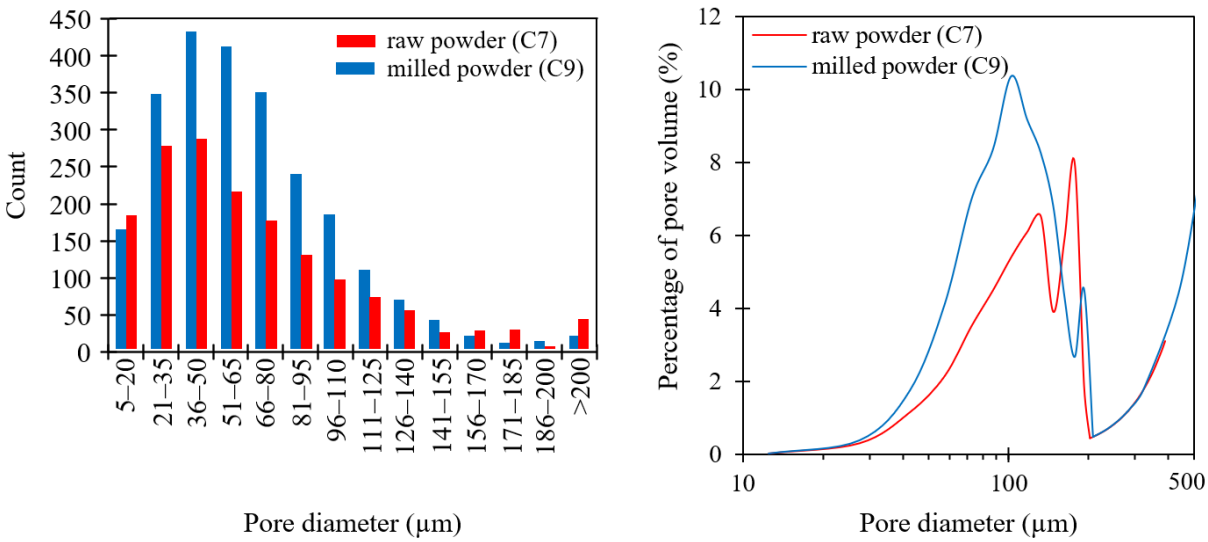

Fig. 56: Pore size distribution determined by image analysis in terms of the count of pores and the percentage of the total pore volume.

The curve of pore size distribution determined by mercury intrusion porosimetry is plotted in Fig. 57. It can be seen that the peaks are around 40 and 60 µm for the samples from milled and raw powder, respectively. These values are lower than those determined by image analysis, where the peaks are present around 100 and 110 µm (see Fig. 56), which can be explained by the fact that mercury intrusion porosimetry detects the largest entrance to an open pore [96], while image analysis captures the spherical diameter of it. The diameter of a spherical pore is not necessarily equal to the size of the interconnection between pores. Given the function of the porous network for filtration purposes, the indication of the size of the interconnection between pores is more relevant.

The detail from high-pressure porosimetry confirms the higher amount of micropores present in the sample prepared from raw powder, as it can be observed on the micrograph in Fig. 50c.

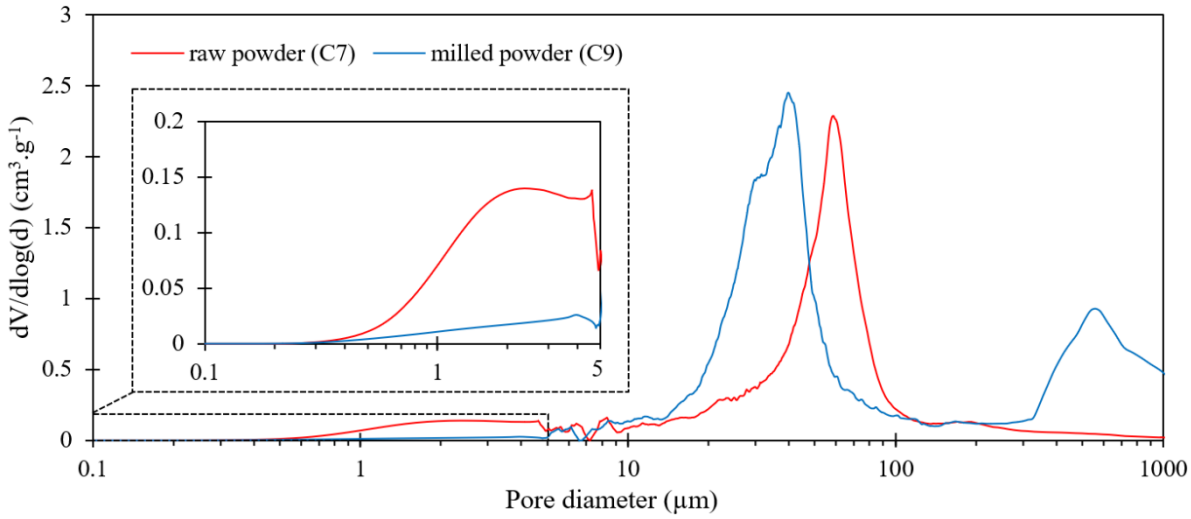

Fig. 57: Pore size distribution determined by mercury intrusion porosimetry.

The prepared foams were evaluated based on their phase composition and microstructure. Microstructural analysis revealed that the foams have a macroporous open structure, with spherical pores, approximately 5–200 µm in diameter, connected by interconnections smaller than 100 µm, and with locally embedded irregular pores. Given the difficulty in controlling the resulting structure to obtain a narrower pore size distribution, along with the inability to prepare filters on a larger scale, direct foaming was assessed as unsuitable for the preparation of filters for electro-insulating liquids according to the set requirements.

7 CONCLUSION

In the present thesis, the preparation of macroporous ceramic filters based on mullite and silica was studied in the context of their potential use in the filtration of electro-insulating liquids in distribution transformers. The filters were prepared from a relatively low-cost kaolin-based ceramic powder, using two methods: the replica template method and direct foaming.

The first method studied was the replica template method. It involved optimising the ceramic suspension, foam processing and heat treatment to improve the microstructure, porosity and handling strength of the filters. The best results were obtained from the suspension prepared from milled powder, which improved microstructure and sinterability. The heat treatment involved firing the polymeric template at 800 °C and sintering at 1400 °C to densify the structure. The resulting filters had an open interconnected porous structure derived from the polymeric template, with a porosity of approximately 80 %, a unimodal pore size distribution of 150–350 µm and compressive strength up to 2.4 MPa. The identified phases were mullite and cristobalite. Infiltrating a part of the filters with a silica-rich suspension led to filling the hollow struts and reducing the porosity and pore size but also resulted in a lower compressive strength of 0.6–1.7 MPa, likely due to defects and internal stresses caused by the differential thermal expansion between mullite and silica during heat treatment. Future studies should focus on optimising the infiltration process, perhaps by modifying the silica content or the heat treatment profile.

The second method studied was direct foaming using polyurethane foam system, both from raw ceramic powder and milled powder. Higher powder loading resulted in lower porosity and improved handling strength of the foams, as well as incorporating a 20 min processing time before the mould filling. After firing the organic matter and sintering at 1400 °C, filters from milled powder showed better densification. These filters had a similar open interconnected porous structure as those prepared by the replica template method, however, the porosity and pore size were decreased to 68–73 % and 5–100 µm, respectively. The reduction in pore size suggests an enhanced filtration efficiency for finer particles.

Scaling up the filters to the dimensions required by the filtration device revealed that direct foaming was unsuitable due to the instability of the foam and poor control over the final structure, which likely results from the inherent limitations of the foaming process in maintaining uniformity over large scales. However, filters prepared by the replica template method were successfully scaled up and are ready for the testing of their filtration capacity.

The aim of this master's thesis, to fabricate ceramic filters that can be potentially used in the filtration of electro-insulating liquids, was achieved. Filters prepared by the replica template method meet the structural requirements for filtration due to their open interconnected pores with unimodal pore size distribution and sufficient mechanical strength. Based on the pore size achievable by this method, they seem to be suitable candidates for use in the first stage of filtration of electro-insulating liquids to remove coarse particles from the contaminated oil. Future research will focus on exploring other methods of preparing ceramic filters with smaller pore sizes, which could enable the development of a multi-stage filtration system, where a ceramic filter with varying porosities could fully replace the currently used paper filter and offer a more sustainable alternative.

REFERENCES

[1] *Global EV Outlook 2024* [online]. Paris: IEA. 2024. Available at: https://www.iea.org/reports/global-ev-outlook-2024

[2] CHEN, Y., N. WANG, O. OLA, Y. XIA and Y. ZHU. Porous ceramics: Light in weight but heavy in energy and environment technologies. *Materials Science and Engineering: R: Reports* [online]. 2021, **143**, 100589. ISSN 0927796X. Available at: doi:10.1016/j.mser.2020.100589

[3] FUKUSHIMA, M. and T. OHJI. Macroporous ceramics for the sustainable development goals (SDGs): Review. *International Journal of Applied Ceramic Technology* [online]. 2023, **20**(2), 660–680. ISSN 1546-542X, 1744-7402. Available at: doi:10.1111/ijac.14261

[4] ISSAOUI, M. and L. LIMOUSY. Low-cost ceramic membranes: Synthesis, classifications, and applications. *Comptes Rendus Chimie* [online]. 2019, **22**(2–3), 175–187. ISSN 16310748. Available at: doi:10.1016/j.crci.2018.09.014

[5] ČSN EN 60422. *Minerální izolační oleje v elektrických zařízeních – Návod pro kontrolu a údržbu*. Ed. 2.0. Geneva: Úřad pro technickou normalizaci, metrologii a státní zkušebnictví, 2013.

[6] ROUSE, T.O. Mineral insulating oil in transformers. *IEEE Electrical Insulation Magazine* [online]. 1998, **14**(3), 6–16. ISSN 0883-7554. Available at: doi:10.1109/57.675572

[7] FOFANA, I. 50 years in the development of insulating liquids. *IEEE Electrical Insulation Magazine* [online]. 2013, **29**(5), 13–25. ISSN 0883-7554. Available at: doi:10.1109/MEI.2013.6585853

[8] CIGRE. *Life management techniques for power transformers*. Paris: CIGRE. 2003.

[9] *IEEE Guide for Acceptance and Maintenance of Insulating Mineral Oil in Electrical Equipment* [online]. USA: IEEE. 2016. Available at: doi:10.1109/IEEESTD.2006.371041

[10] *IEEE Guide for the Reclamation of Mineral Insulating Oil and Criteria for Its Use* [online]. USA: IEEE. 1985. Available at: doi:10.1109/IEEESTD.2015.7328235

[11] MICAFLUID AG. *Oil purifications systems - Oil Treatment Plants*. Schlieren: Micafluid AG. 2020.

[12] SALVI, S. and A. P. PARANJAPE. Study of Transformer Oil Filtration Machine. 2017, **4**(4), 2471–2472. ISSN 2395 -0056.

[13] SCHEFFLER, M. and P. COLOMBO, eds. *Cellular Ceramics: Structure, Manufacturing, Properties and Applications* [online]. 1st ed. B.m.: Wiley, 2005 [accessed. 2023-11-29]. ISBN 978-3-527-31320-4. Available at: doi:10.1002/3527606696

[14] SING, K. S. W. Reporting physisorption data for gas/solid systems with special reference to the determination of surface area and porosity (Recommendations 1984). *Pure and Applied Chemistry* [online]. 1985, **57**(4), 603–619. ISSN 1365-3075, 0033-4545. Available at: doi:10.1351/pac198557040603

[15] ROUQUEROL, J., D. AVNIR, C. W. FAIRBRIDGE, D. H. EVERETT, J. M. HAYNES, N. PERNICONE, J. D. F. RAMSAY, K. S. W. SING and K. K. UNGER. Recommendations for the characterization of porous solids (Technical Report). *Pure and Applied Chemistry* [online]. 1994, **66**(8), 1739–1758. ISSN 1365-3075, 0033-4545. Available at: doi:10.1351/pac199466081739

[16] COLOMBO, P., C. VAKIFAHMETOGLU and S. COSTACURTA. Fabrication of ceramic components with hierarchical porosity. *Journal of Materials Science* [online]. 2010, **45**(20), 5425–5455. ISSN 0022-2461, 1573-4803. Available at: doi:10.1007/s10853-010-4708-9

[17] OHJI, T. and M. FUKUSHIMA. Macro-porous ceramics: processing and properties. *International Materials Reviews* [online]. 2012, **57**(2), 115–131. ISSN 0950-6608, 1743-2804. Available at: doi:10.1179/1743280411Y.0000000006

[18] COLOMBO, P. Conventional and novel processing methods for cellular ceramics. *Philosophical Transactions of the Royal Society A: Mathematical, Physical and Engineering Sciences* [online]. 2006, **364**(1838), 109–124. ISSN 1364-503X, 1471-2962. Available at: doi:10.1098/rsta.2005.1683

[19] STUDART, A. R., U. T. GONZENBACH, E. TERVOORT and L. J. GAUCKLER. Processing Routes to Macroporous Ceramics: A Review. *Journal of the American Ceramic Society* [online]. 2006, **89**(6), 1771–1789. ISSN 0002-7820, 1551-2916. Available at: doi:10.1111/j.1551-2916.2006.01044.x

[20] FUKUSHIMA, M., Y. ZHOU, H. MIYAZAKI, Y. YOSHIZAWA, K. HIRAO, Y. IWAMOTO, S. YAMAZAKI and T. NAGANO. Microstructural Characterization of Porous Silicon Carbide Membrane Support With and Without Alumina Additive. *Journal of the American Ceramic Society* [online]. 2006, **89**(5), 1523–1529. ISSN 0002-7820, 1551-2916. Available at: doi:10.1111/j.1551-2916.2006.00931.x

[21] DUDINA, D., B. BOKHONOV and E. OLEVSKY. Fabrication of Porous Materials by Spark Plasma Sintering: A Review. *Materials* [online]. 2019, **12**(3), 541. ISSN 1996-1944. Available at: doi:10.3390/ma12030541

[22] YANG, J-F., G-J. ZHANG and T. OHJI. Porosity and microstructure control of porous ceramics by partial hot pressing. *Journal of Materials Research* [online]. 2001, **16**(7), 1916–1918. ISSN 0884-2914, 2044-5326. Available at: doi:10.1557/JMR.2001.0262

[23] EOM, J-H., Y-W. KIM and S. RAJU. Processing and properties of macroporous silicon carbide ceramics: A review. *Journal of Asian Ceramic Societies* [online]. 2013, **1**(3), 220–242. ISSN 2187-0764. Available at: doi:10.1016/j.jascer.2013.07.003

[24] WANG, H., I. SUNG, X. LI and D. KIM. Fabrication of Porous SiC Ceramics with Special Morphologies by Sacrificing Template Method. *Journal of Porous Materials* [online]. 2004, **11**(4), 265–271. ISSN 1380-2224. Available at: doi:10.1023/B:JOPO.0000046353.24308.86

[25] FUKASAWA, T., M. ANDO, T. OHJI and S. KANZAKI. Synthesis of Porous Ceramics with Complex Pore Structure by Freeze-Dry Processing. *Journal of the American Ceramic Society* [online]. 2001, **84**(1), 230–232. ISSN 0002-7820, 1551-2916. Available at: doi:10.1111/j.1151-2916.2001.tb00638.x

[26] DEVILLE, S. Freeze-Casting of Porous Ceramics: A Review of Current Achievements and Issues. *Advanced Engineering Materials* [online]. 2008, **10**(3), 155–169. ISSN 1438-1656, 1527-2648. Available at: doi:10.1002/adem.200700270

[27] SCHWARTZWALDER, K. and A. V. SOMERS. Method of Making Porous Ceramic Articles. US Patent 3,090,094.

[28] FAURE, R., F. ROSSIGNOL, T. CHARTIER, C. BONHOMME, A. MAÎTRE, G. ETCHEGOYEN, P. DEL GALLO and D. GARY. Alumina foam catalyst supports for industrial steam reforming processes. *Journal of the European Ceramic Society* [online]. 2011, **31**(3), 303–312. ISSN 09552219. Available at: doi:10.1016/j.jeurceramsoc.2010.10.009

[29] GÓMEZ-MARTÍN, A., M.P. ORIHUELA, J.A. BECERRA, J. MARTÍNEZ-FERNÁNDEZ and J. RAMÍREZ-RICO. Permeability and mechanical integrity of porous biomorphic SiC ceramics for application as hot-gas filters. *Materials & Design* [online]. 2016, **107**, 450–460. ISSN 02641275. Available at: doi:10.1016/j.matdes.2016.06.060

[30] AKPINAR, S., I.A. ALTUN and K. ONEL. Effects of SiC addition on the structure and properties of reticulated porous mullite ceramics. *Journal of the European Ceramic Society* [online]. 2010, **30**(13), 2727–2734. ISSN 09552219. Available at: doi:10.1016/j.jeurceramsoc.2010.05.005

[31] HE, X., B. SU, Z. TANG, B. ZHAO, X. WANG, G. YANG, H. QIU, H. ZHANG and J. YANG. The comparison of macroporous ceramics fabricated through the protein direct foaming and sponge replica methods. *Journal of Porous Materials* [online]. 2012, **19**(5), 761–766. ISSN 1380-2224, 1573-4854. Available at: doi:10.1007/s10934-011-9528-z

[32] VOIGT, C., C. G. ANEZIRIS and J. HUBÁLKOVÁ. Rheological Characterization of Slurries for the Preparation of Alumina Foams via Replica Technique. *Journal of the American Ceramic Society* [online]. 2015, **98**(5), 1460–1463. ISSN 0002-7820, 1551-2916. Available at: doi:10.1111/jace.13522

[33] FEY, T., U. BETKE, S. RANNABAUER and M. SCHEFFLER. Reticulated Replica Ceramic Foams: Processing, Functionalization, and Characterization. *Advanced Engineering Materials* [online]. 2017, **19**(10), 1700369. ISSN 1438-1656, 1527-2648. Available at: doi:10.1002/adem.201700369

[34] TULLIANI, J. M., L. MONTANARO and C. BORELLO. Open-pore mullite foams for diesel particulate filtration. In: *4th European Ceramic Society Conf.* 1995, p. 493–500.

[35] GÓMEZ, S. Y., O. A. ALVAREZ, J. A. ESCOBAR, J. B. RODRIGUES NETO, C. R. RAMBO and D. HOTZA. Relationship between Rheological Behaviour and Final Structure of Al 2 O 3 and YSZ Foams Produced by Replica. *Advances in Materials Science and Engineering* [online]. 2012, **2012**, 1–9. ISSN 1687-8434, 1687-8442. Available at: doi:10.1155/2012/549508

[36] PU, X., X. LIU, F. QIU and L. HUANG. Novel Method To Optimize the Structure of Reticulated Porous Ceramics. *Journal of the American Ceramic Society* [online]. 2004, **87**(7), 1392–1394. ISSN 0002-7820, 1551-2916. Available at: doi:10.1111/j.1151-2916.2004.tb07745.x

[37] ZHU, X., D. JIANG, S. TAN and Z. ZHANG. Improvement in the Strut Thickness of Reticulated Porous Ceramics. *Journal of the American Ceramic Society* [online]. 2001, **84**(7), 1654–1656. ISSN 0002-7820, 1551-2916. Available at: doi:10.1111/j.1151-2916.2001.tb00895.x

[38] DRESSLER, M., S. REINSCH, R. SCHADRACK and S. BENEMANN. Burnout behavior of ceramic coated open cell polyurethane (PU) sponges. *Journal of the European Ceramic Society* [online]. 2009, **29**(16), 3333–3339. ISSN 09552219. Available at: doi:10.1016/j.jeurceramsoc.2009.07.025

[39] RANNABAUER, S, G-M. SÖFFKER, M. SCHEUNEMANN, U. BETKE and M. SCHEFFLER. Increased Mechanical Stability and Thermal Conductivity of Alumina Reticulated Porous Ceramics (RPC) by Nanoparticle Infiltration Processing. *Advanced Engineering Materials* [online]. 2017, **19**(10), 1700211. ISSN 1438-1656, 1527-2648. Available at: doi:10.1002/adem.201700211

[40] JUN, I-K., Y-H. KOH, J-H. SONG, S-H. LEE and H-E. KIM. Improved compressive strength of reticulated porous zirconia using carbon coated polymeric sponge as novel template. *Materials Letters* [online]. 2006, **60**(20), 2507–2510. ISSN 0167577X. Available at: doi:10.1016/j.matlet.2006.01.031

[41] YOSHIHISA, K. and F. MASASHI. Ceramic foam. British Patent 2 168 337.

[42] JUN, I-K., Y-M. KONG, S-H. LEE, H-E. KIM, H-W. KIM and K. C. GORETTA. Reinforcement of a Reticulated Porous Ceramic by a Novel Infiltration Technique. *Journal of the American Ceramic Society* [online]. 2006, **89**(7), 2317–2319. ISSN 0002-7820, 1551-2916. Available at: doi:10.1111/j.1551-2916.2006.00997.x

[43] VOGT, U.F., M. GORBAR, P. DIMOPOULOS-EGGENSCHWILER, A. BROENSTRUP, G. WAGNER and P. COLOMBO. Improving the properties of ceramic foams by a vacuum infiltration process. *Journal of the European Ceramic Society* [online]. 2010, **30**(15), 3005–3011. ISSN 09552219. Available at: doi:10.1016/j.jeurceramsoc.2010.06.003

[44] SALVINI, V. R., B. LUCHINI, C. G. ANEZIRIS and V. PANDOLFELLI. Innovation in ceramic foam filters manufacturing process. *International Journal of Applied Ceramic Technology* [online]. 2019, **16**(1), 378–388. ISSN 1546-542X, 1744-7402. Available at: doi:10.1111/ijac.13062

[45] FUJI, M., T. KATO, F-Z. ZHANG and M. TAKAHASHI. Effects of surfactants on the microstructure and some intrinsic properties of porous building ceramics fabricated by gelcasting. *Ceramics International* [online]. 2006, **32**(7), 797–802. ISSN 02728842. Available at: doi:10.1016/j.ceramint.2005.06.003

[46] BINKS, B. P. Particles as surfactants—similarities and differences. *Current Opinion in Colloid & Interface Science* [online]. 2002, **7**(1–2), 21–41. ISSN 13590294. Available at: doi:10.1016/S1359-0294(02)00008-0

[47] GONZENBACH, U. T., A. R. STUDART, E. TERVOORT and L. J. GAUCKLER. Ultrastable Particle-Stabilized Foams. *Angewandte Chemie International Edition* [online]. 2006, **45**(21), 3526–3530. ISSN 1433-7851, 1521-3773. Available at: doi:10.1002/anie.200503676

[48] WOOD, L. L., P. MESSINA and K. C. FRISCH. Method of preparing porous ceramic structures by firing a polyurethane foam tha is impregnated with inorganic material. 3833386.

[49] PINTO, M. L. Formulation, Preparation, and Characterization of Polyurethane Foams. *Journal of Chemical Education* [online]. 2010, **87**(2), 212–215. ISSN 0021-9584, 1938-1328. Available at: doi:10.1021/ed8000599

[50] COLOMBO, P. and J. R. HELLMANN. Ceramic foams from preceramic polymers. *Materials Research Innovations* [online]. 2002, **6**(5–6), 260–272. ISSN 1432-8917, 1433-075X. Available at: doi:10.1007/s10019-002-0209-z

[51] TOMITA, T., S. KAWASAKI and K. OKADA. A Novel Preparation Method for Foamed Silica Ceramics by Sol-Gel Reaction and Mechanical Foaming. *Journal of Porous Materials* [online]. 2004, **11**(2), 107–115. ISSN 1380-2224. Available at: doi:10.1023/B:JOPO.0000027366.90408.1f

[52] EKA PUTRI, S., A. AHMAD, I. RAYA, R. TRIANDI TJAHJANTO, H. NATSIR, P. TABA and H. KARIM. A REVIEW OF THE DEVELOPMENT OF THE GEL CASTING METHOD FOR POROUS CERAMIC FABRICATION. *RASAYAN Journal of Chemistry* [online]. 2023, **16**(01), 48–60. ISSN 09741496, 09760083. Available at: doi:10.31788/RJC.2023.1616975

[53] BARG, S., D. KOCH and G. GRATHWOHL. Processing and Properties of Graded Ceramic Filters. *Journal of the American Ceramic Society* [online]. 2009, **92**(12), 2854–2860. ISSN 0002-7820, 1551-2916. Available at: doi:10.1111/j.1551-2916.2009.03301.x

[54] ZHANG, F., Z. LI, M. XU, S. WANG, N. LI and J. YANG. A review of 3D printed porous ceramics. *Journal of the European Ceramic Society* [online]. 2022, **42**(8), 3351–3373. ISSN 09552219. Available at: doi:10.1016/j.jeurceramsoc.2022.02.039

[55] DU, W., X. REN, Z. PEI and C. MA. Ceramic Binder Jetting Additive Manufacturing: A Literature Review on Density. *Journal of Manufacturing Science and Engineering* [online]. 2020, **142**(4), 040801. ISSN 1087-1357, 1528-8935. Available at: doi:10.1115/1.4046248

[56] SING, S. L., W. Y. YEONG, F. E. WIRIA, B. Y. TAY, Z. ZHAO, L. ZHAO, Z. TIAN and S. YANG. Direct selective laser sintering and melting of ceramics: a review. *Rapid Prototyping Journal* [online]. 2017, **23**(3), 611–623. ISSN 1355-2546. Available at: doi:10.1108/RPJ-11-2015-0178

[57] MINAS, C., D. CARNELLI, E. TERVOORT and A. R. STUDART. 3D Printing of Emulsions and Foams into Hierarchical Porous Ceramics. *Advanced Materials* [online]. 2016, **28**(45), 9993–9999. ISSN 0935-9648, 1521-4095. Available at: doi:10.1002/adma.201603390

[58] HUANG, K., H. ELSAYED, G. FRANCHIN and P. COLOMBO. 3D printing of polymer-derived SiOC with hierarchical and tunable porosity. *Additive Manufacturing* [online]. 2020, **36**, 101549. ISSN 22148604. Available at: doi:10.1016/j.addma.2020.101549

[59] JONHSON, W., X. XU, K. BIAN, Y. XUN, Y. H. TAN, Z. CHEN, D. ZHANG and J. DING. 3D-Printed Hierarchical Ceramic Architectures for Ultrafast Emulsion Treatment and Simultaneous Oil–Water Filtration. *ACS Materials Letters* [online]. 2022, **4**(4), 740–750. ISSN 2639-4979, 2639-4979. Available at: doi:10.1021/acsmaterialslett.2c00147

[60] LIU, R., T. XU and C. WANG. A review of fabrication strategies and applications of porous ceramics prepared by freeze-casting method. *Ceramics International* [online]. 2016, **42**(2), 2907–2925. ISSN 02728842. Available at: doi:10.1016/j.ceramint.2015.10.148

[61] HAMMEL, E.C., O.L.-R. IGHODARO and O.I. OKOLI. Processing and properties of advanced porous ceramics: An application based review. *Ceramics International* [online]. 2014, **40**(10), 15351–15370. ISSN 02728842. Available at: doi:10.1016/j.ceramint.2014.06.095

[62] ZUO, X., S. ZHANG, G. MA, Y. LV and P. LI. Analysis of ceramic membrane fouling behavior and cleaning technology. *E3S Web of Conferences* [online]. 2020, **194**, 04048. ISSN 2267-1242. Available at: doi:10.1051/e3sconf/202019404048

[63] HEIDENREICH, S. Hot gas filtration – A review. *Fuel* [online]. 2013, **104**, 83–94. ISSN 00162361. Available at: doi:10.1016/j.fuel.2012.07.059

[64] ADLER, J. Ceramic Diesel Particulate Filters. *International Journal of Applied Ceramic Technology* [online]. 2005, **2**(6), 429–439. ISSN 1546-542X, 1744-7402. Available at: doi:10.1111/j.1744-7402.2005.02044.x

[65] ISOBE, T., Y. KAMESHIMA, A. NAKAJIMA, K. OKADA and Y. HOTTA. Gas permeability and mechanical properties of porous alumina ceramics with unidirectionally aligned pores. *Journal of the European Ceramic Society* [online]. 2007, **27**(1), 53–59. ISSN 09552219. Available at: doi:10.1016/j.jeurceramsoc.2006.02.030

[66] LIU, R., J. YUAN and C. WANG. A novel way to fabricate tubular porous mullite membrane supports by TBA-based freezing casting method. *Journal of the European Ceramic Society* [online]. 2013, **33**(15–16), 3249–3256. ISSN 09552219. Available at: doi:10.1016/j.jeurceramsoc.2013.06.005

[67] PARK, J. K., J. S. LEE and S. I. LEE. Preparation of Porous Cordierite Using Gelcasting Method and its Feasibility as a Filter. *Journal of Porous Materials* [online]. 2002, **9**(3), 203–210. ISSN 13802224. Available at: doi:10.1023/A:1020939018359

[68] TAKAHASHI, M., R. L. MENCHAVEZ, M. FUJI and H. TAKEGAMI. Opportunities of porous ceramics fabricated by gelcasting in mitigating environmental issues. *Journal of the European Ceramic Society* [online]. 2009, **29**(5), 823–828. ISSN 09552219. Available at: doi:10.1016/j.jeurceramsoc.2008.07.030

[69] CHAKRABORTY, S., R. J. O'MALLEY and L. BARTLETT. Ceramic Foam Filter Micropores as Sites for Liquid Inclusion Retention. *International Journal of Metalcasting* [online]. 2022, **16**(1), 20–34. ISSN 1939-5981, 2163-3193. Available at: doi:10.1007/s40962-021-00585-9

[70] OLSON, R. A. and L. C. B. MARTINS. Cellular Ceramics in Metal Filtration. *Advanced Engineering Materials* [online]. 2005, **7**(4), 187–192. ISSN 1438-1656, 1527-2648. Available at: doi:10.1002/adem.200500021

[71] SIMONIS, J. J. and A. K. BASSON. Evaluation of a low-cost ceramic micro-porous filter for elimination of common disease microorganisms. *Physics and Chemistry of the Earth, Parts A/B/C* [online]. 2011, **36**(14–15), 1129–1134. ISSN 14747065. Available at: doi:10.1016/j.pce.2011.07.064

[72] MAGGAY, I. V., Y. CHANG, A. VENAULT, G. V. DIZON and C-J. WU. Functionalized porous filtration media for gravity-driven filtration: Reviewing a new emerging approach for oil and water emulsions separation. *Separation and Purification Technology* [online]. 2021, **259**, 117983. ISSN 13835866. Available at: doi:10.1016/j.seppur.2020.117983

[73] JANA, S., M. K. PURKAIT and K. MOHANTY. Preparation and characterization of low-cost ceramic microfiltration membranes for the removal of chromate from aqueous solutions. *Applied Clay Science* [online]. 2010, **47**(3–4), 317–324. ISSN 01691317. Available at: doi:10.1016/j.clay.2009.11.036

[74] NANDI, B.K., R. UPPALURI and M.K. PURKAIT. Preparation and characterization of low cost ceramic membranes for micro-filtration applications. *Applied Clay Science* [online]. 2008, **42**(1–2), 102–110. ISSN 01691317. Available at: doi:10.1016/j.clay.2007.12.001

[75] ABBASI, M., M. MIRFENDERESKI, M. NIKBAKHT, M. GOLSHENAS and T. MOHAMMADI. Performance study of mullite and mullite–alumina ceramic MF membranes for oily wastewaters treatment. *Desalination* [online]. 2010, **259**(1–3), 169–178. ISSN 00119164. Available at: doi:10.1016/j.desal.2010.04.013

[76] KAMOUN, N., M. A. RODRÍGUEZ and F. JAMOUSSI. Ceramic filters for oil emulsion treatments. *Desalination and Water Treatment* [online]. 2016, **57**(58), 28071–28076. ISSN 1944-3994, 1944-3986. Available at: doi:10.1080/19443994.2016.1182080

[77] USMAN, J., M. H. OTHMAN, A. F. ISMAIL, M. A. RAHMAN, J. JAAFAR, Y. O. RAJI, A. O. GBADAMOSI, T. H. EL BADAWY and K. A. M. SAID. An overview of superhydrophobic ceramic membrane surface modification for oil-water separation. *Journal of Materials Research and Technology* [online]. 2021, **12**, 643–667. ISSN 22387854. Available at: doi:10.1016/j.jmrt.2021.02.068

[78] HUBADILLAH, S. K., P. KUMAR, M H. DZARFAN OTHMAN, A. F. ISMAIL, M. A. RAHMAN and J. JAAFAR. A low cost, superhydrophobic and superoleophilic hybrid kaolin-based hollow fibre membrane (KHFM) for efficient adsorption–separation of oil removal from water. *RSC Advances* [online]. 2018, **8**(6), 2986–2995. ISSN 2046-2069. Available at: doi:10.1039/C7RA13206A

[79] NAZAROVA, E. A., D. S ALIMOVA, V. I. MIKHAYLOV, E. F. KRIVOSHAPKINA and P. V. KRIVOSHAPKIN. Macroporous ceramic filters from mineral raw materials for machine oils filtration. *Ceramics International* [online]. 2019, **45**(7), 8767–8773. ISSN 02728842. Available at: doi:10.1016/j.ceramint.2019.01.201

[80] HE, Z., Z. LYU, Q. GU, L. ZHANG and J. WANG. Ceramic-based membranes for water and wastewater treatment. *Colloids and Surfaces A: Physicochemical and Engineering Aspects* [online]. 2019, **578**, 123513. ISSN 09277757. Available at: doi:10.1016/j.colsurfa.2019.05.074

[81] SHACKELFORD, J. F. and R. H. DOREMUS, eds. *Ceramic and Glass Materials* [online]. Boston, MA: Springer US, 2008 [accessed. 2024-03-30]. ISBN 978-0-387-73361-6. Available at: doi:10.1007/978-0-387-73362-3

[82] CARTER, C. B. and M. G. NORTON. *Ceramic materials: science and engineering*. New York: Springer, 2007. ISBN 978-0-387-46271-4.

[83] ABADI, S. R. H., M. R. SEBZARI, M. HEMATI, F. REKABDAR and T. MOHAMMADI. Ceramic membrane performance in microfiltration of oily wastewater. *Desalination* [online]. 2011, **265**(1–3), 222–228. ISSN 00119164. Available at: doi:10.1016/j.desal.2010.07.055

[84] KLUG, F. J., S PROCHAZKA and R. DOREMUS. Alumina-Silica Phase Diagram in the Mollite Region. *Journal of the American Ceramic Society* [online]. 1987, **70**(10), 750–759. ISSN 0002-7820, 1551-2916. Available at: doi:10.1111/j.1151-2916.1987.tb04875.x

[85] LOCK, P. A, X. JING, R. W. ZIMMERMAN and E. M. SCHLUETER. Predicting the permeability of sandstone from image analysis of pore structure. *Journal of Applied Physics* [online]. 2002, **92**(10), 6311–6319. ISSN 0021-8979, 1089-7550. Available at: doi:10.1063/1.1516271

[86] ČSN EN ISO 18754. *Jemná keramika (speciální keramika, speciální technická keramika) - Stanovení hustoty a zdánlivé pórovitosti*. Praha: Úřad pro technickou normalizaci, metrologii a státní zkušebnictví. 2022.

[87] LIANG, Xiulin, Qiang LI and Ying FANG. Preparation and Characterization of Modified Kaolin by a Mechanochemical Method. *Materials* [online]. 2023, **16**(8), 3099. ISSN 1996-1944. Available at: doi:10.3390/ma16083099

[88] ZENG, Li, Hong-juan SUN, Tong-jiang PENG and Wen-miao ZHENG. The sintering kinetics and properties of sintered glass-ceramics from coal fly ash of different particle size. *Results in Physics* [online]. 2019, **15**, 102774. ISSN 22113797. Available at: doi:10.1016/j.rinp.2019.102774

[89] APPOLONI, C. R., C. P. FERNANDES, M. D. D. M. INNOCENTINI and A. MACEDO. Ceramic foams porous microstructure characterization by X-ray microtomography. *Materials Research* [online]. 2004, **7**(4), 557–564. ISSN 1516-1439. Available at: doi:10.1590/S1516-14392004000400008

[90] HASSANABADI, M., T. BERTO, S. AKHTAR and R. E. AUNE. Hydraulic Characterization of Ceramic Foam Filters Used in Aluminum Filtration. *Materials* [online]. 2023, **16**(7), 2805. ISSN 1996-1944. Available at: doi:10.3390/ma16072805

[91] SHUFEN, L., J. ZHI, Y. KAIJUN, Y. SHUQIN and W. K. CHOW. Studies on the Thermal Behavior of Polyurethanes. *Polymer-Plastics Technology and Engineering* [online]. 2006, **45**(1), 95–108. ISSN 0360-2559, 1525-6111. Available at: doi:10.1080/03602550500373634

[92] PECQUEUX, F., F. TANCRET, N. PAYRAUDEAU and J.M. BOULER. Influence of microporosity and macroporosity on the mechanical properties of biphasic calcium phosphate bioceramics: Modelling and experiment. *Journal of the European Ceramic Society* [online]. 2010, **30**(4), 819–829. ISSN 09552219. Available at: doi:10.1016/j.jeurceramsoc.2009.09.017

[93] BEAR, J. *Dynamics of fluids in porous media*. Repr. New York: Dover [u.a.], 1988. Dover books on physics and chemistry. ISBN 978-0-486-65675-5.

[94] MOLOCHITE™. *IMERYS* [online]. 2024. Available at: https://www.imerys.com/product-ranges/molochite

[95] MADSEN, I. C., N. V. SCARLETT and A. KERN. Description and survey of methodologies for the determination of amorphous content via X-ray powder diffraction. *Zeitschrift für Kristallographie* [online]. 2011, **226**(12), 944–955. ISSN 0044-2968. Available at: doi:10.1524/zkri.2011.1437

[96] GIESCHE, H. Mercury Porosimetry: A General (Practical) Overview. *Particle & Particle Systems Characterization* [online]. 2006, **23**(1), 9–19. ISSN 0934-0866, 1521-4117. Available at: doi:10.1002/ppsc.200601009

[97] SHARMA, M. M. and Y. C. YORTSOS. A network model for deep bed filtration processes. *AIChE Journal* [online]. 1987, **33**(10), 1644–1653. ISSN 0001-1541, 1547-5905. Available at: doi:10.1002/aic.690331008

[98] LEE, S., J-H. HA, J. LEE and I-H. SONG. Enhanced mechanical strength of talc-containing porous kaolin prepared by a replica method. *Journal of the Korean Ceramic Society* [online]. 2021, **58**(1), 123–133. ISSN 1229-7801, 2234-0491. Available at: doi:10.1007/s43207-020-00073-6

[99] SATO, T., Y. SAWABE, Y. OHYA, M. SUGAI and Z. NAKAGAWA. Cracking in a Cristobalite-Containing Mullite Body during Cooling. *Journal of the Ceramic Society of Japan* [online]. 2000, **108**(1256), 345–349. ISSN 0914-5400, 1882-1022. Available at: doi:10.2109/jcersj.108.1256_345

[100] ZHU, J. and H. YAN. Microstructure and properties of mullite-based porous ceramics produced from coal fly ash with added Al2O3. *International Journal of Minerals, Metallurgy, and Materials* [online]. 2017, **24**(3), 309–315. ISSN 1674-4799, 1869-103X. Available at: doi:10.1007/s12613-017-1409-2

[101] CIGRE. *Effect of particles on transformer dielectric strength*. Paris: CIGRE. 2000.

[102] JIAO, L., H. XIAO, Q. WANG and J. SUN. Thermal degradation characteristics of rigid polyurethane foam and the volatile products analysis with TG-FTIR-MS. *Polymer Degradation and Stability* [online]. 2013, **98**(12), 2687–2696. ISSN 01413910. Available at: doi:10.1016/j.polymdegradstab.2013.09.032

[103] TANG, Xinyue, Zaijuan ZHANG, Xiaoyan ZHANG, Wenlong HUO, Jingjing LIU, Shu YAN and Jinlong YANG. Design and formulation of polyurethane foam used for porous alumina ceramics. *Journal of Polymer Research* [online]. 2018, **25**(6), 136. ISSN 1022-9760, 1572-8935. Available at: doi:10.1007/s10965-018-1535-1